

Disequilibrium river networks dissecting the western slope of the Sierra Nevada, California, USA, record significant late Cenozoic tilting and associated surface uplift

Helen W. Beeson[†] and Scott W. McCoy

Department of Geological Sciences and Engineering, University of Nevada, Reno, Nevada 89557, USA

ABSTRACT

The timing, rates, and spatial patterns of elevation change in the Sierra Nevada, California, USA, have long been the subject of vigorous debate owing to their importance in constraining the tectonic history of western North America and models of orogenesis. Here we present a systematic analysis of multiple measures of fluvial geomorphology along the entire length of the range and interpret these observations using 1-D and 2-D landscape evolution modeling based on the stream power fluvial erosion rule with the rate parameter calibrated from a large data set of millennial-scale erosion rates. We demonstrate that westward-draining rivers in the Sierra Nevada are in a disequilibrium state and that this state is consistent with the transient fluvial response expected from significant down-to-the-west tilting in the last 11 m.y. Assuming rigid-block tilting and using multiple independent measures of tilt magnitude, we find that the magnitude of surface uplift from late Cenozoic tilting appears to have been similar along strike and likely resulted in ~500–1300 m of surface uplift at the crest (0.3–0.8° tilt) from the Yuba through the Stanislaus rivers (~39.2–38.2°N) and 1000–1400 m of surface uplift at the crest (0.6–0.9° tilt) from the Tuolumne River south through the Kings River (~38.2–36.4°N). We show that the transient fluvial response to tilting in the northern Sierra is heavily modulated by heterogeneous lithology and drainage area exchange in a manner that reconciles the high spatial variability in basement incision observed in numerous prior studies. However, we find that heterogeneous lithology alone cannot explain both the tran-

sient state and observed patterns in channel steepness, which seem to require late Cenozoic changes in tectonic forcing. Beyond the regional implications of a short-lived rapid pulse of late Cenozoic surface uplift along the entire length of the range, our results demonstrate that a range-wide approach in which river networks are analyzed both in planform and profile can elucidate tectonic histories despite heterogeneous lithology and ongoing changes in network topology.

INTRODUCTION

The Sierra Nevada is an ~80–100-km-wide, ~600-km-long range striking northwest-southeast through eastern California (Fig. 1) that first developed as a magmatic arc from the Late Triassic through the Late Cretaceous (Bateman and Wahrhaftig, 1966). The modern range is strongly asymmetric in cross-section with a gentle western slope rising to a steep eastern escarpment (Fig. 1). Deeply incised canyons dissect the gentle western slope and separate broad interfluves that define a distinct low-relief upland surface (Figs. 1 and 2B). This broad-scale morphology and apparent rejuvenation of river incision led early observers to hypothesize that much of the range-crest elevation had been obtained through recent westward tilting of a rigid block of crust about a horizontal axis parallel to and located at the western range front (Gilbert, 1883; LeConte, 1886; Lindgren, 1911; Matthes, 1930; Fig. 1D). A vigorous debate still exists today as to whether the modern elevation of the Sierra Nevada, which increases southward along the crest from ~2000 m to ~4400 m (Fig. 1D), is indeed predominately a result of late Cenozoic surface uplift or whether the Sierra has been a topographic feature as high or higher than the modern Sierra since the Late Cretaceous.

Our goal in this paper is to answer the question: To what degree do river networks dissecting the Sierra Nevada record timing, magnitude, and

spatial patterns of surface uplift, especially the debated episode in the late Cenozoic? To do so we analyze quantitative metrics of river geomorphology in the Sierra Nevada in a spatially complete and systematic manner and interpret these results using a calibrated stream power model framework, an approach that has been used to constrain tectonic histories in a multitude of other similar detachment-limited river systems (Gailleton et al., 2021; Kirby and Whipple, 2001, 2012; Lague, 2014; Lavé and Avouac, 2000; Mitchell and Yanites, 2019b; Whipple, 2004; Wobus et al., 2006). By including all major river basins draining the western slope of the Sierra from the Feather River in the north to the Tehachapi River in the south we seek to quantify range-wide patterns in fluvial geomorphology that could further support arguments for or against late Cenozoic surface uplift. We use an ensemble of methods, each with different assumptions, to further constrain the timing, magnitude, and spatial patterns of surface uplift along the range.

STATE OF PLAY IN THE DEBATE OVER LATE CENOZOIC UPLIFT

A multitude of studies have argued for significant (>1 km) late Cenozoic surface uplift, but each required methods or assumptions that have been questioned or were limited to isolated localities. Studies using Cenozoic river deposits as evidence for late Cenozoic surface uplift have argued: (1) for significant river incision into basement rock below the base of Mio-Pliocene volcanics (Wakabayashi, 2013; Wakabayashi and Sawyer, 2001); (2) that modern gradients of preserved Eocene-Oligocene alluvial paleochannel deposits are much steeper than modern alluvial stream gradients (Christensen, 1966; Lindgren, 1911; Wakabayashi and Sawyer, 2001); and (3) that a strong relationship exists between paleochannel azimuth and modern gradient of preserved paleochannel deposits consistent with

Helen W. Beeson  <https://orcid.org/0000-0001-6386-5560>

[†]hbeeson@nevada.unr.edu

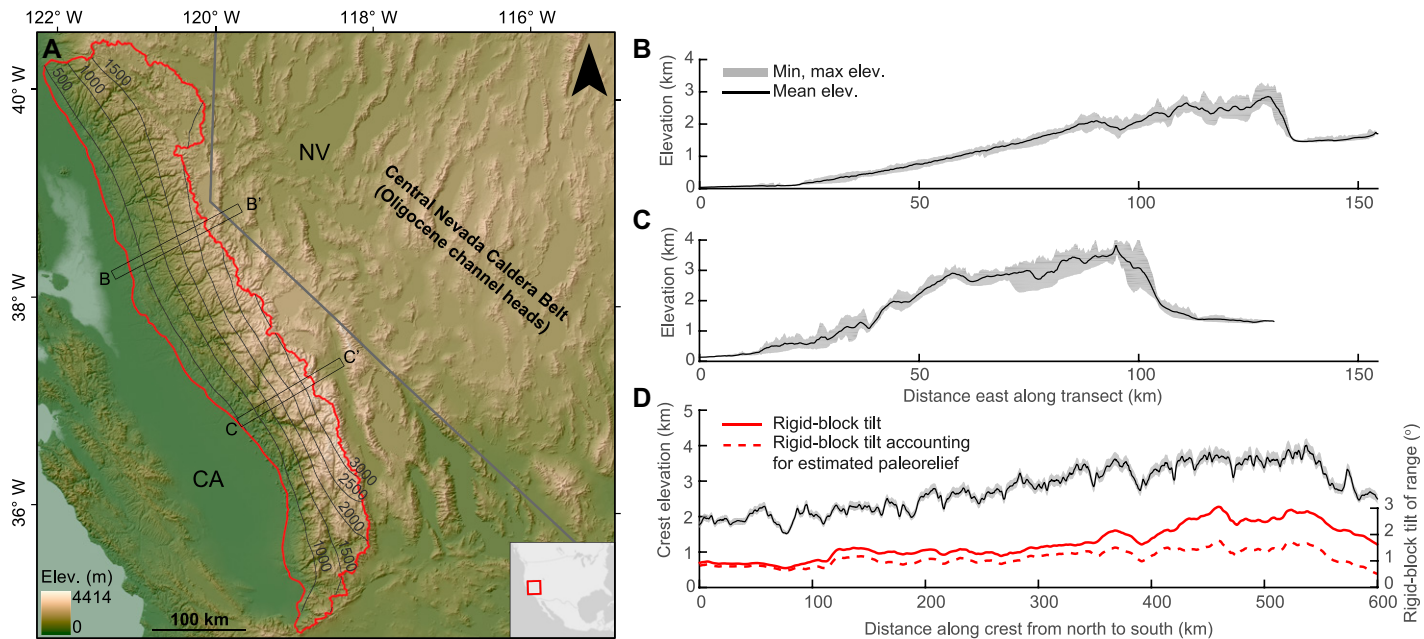


Figure 1. Digital elevation model (DEM) of eastern California and western Nevada, USA, and characteristic elevation profiles. (A) The extent of the western Sierra Nevada is enclosed by a red line with the western boundary demarcating the mountain front as identified with a slope threshold that generally separates bedrock units from alluvium. Black lines show 500 m contours of elevation after smoothing DEM with a 20 km² moving-window mean filter. State lines, shown in gray, of California (CA) and Nevada (NV) for reference. Inset shows location of the Sierra Nevada relative to North America. Black rectangles enclose 10 km wide swath elevation profiles B–B' and C–C' displayed in B and C. Mean elevation along the profile is shown in black and gray encompasses the elevation range. These profiles show the characteristic asymmetric cross-sectional shape of the Sierra in the northern (B) and southern (C) portions of the range. (D) North-south oriented 10-km-wide swath elevation (elev.) profile centered on the Sierra Nevada crest shown in black and gray. The magnitude of down-to-the-west rigid-block tilt of the range is shown with red lines as estimated by assuming modern crest elevations result purely from a single rigid-block tilting event (solid line) or allowing for pre-tilt crest elevation equal to published values of paleorelief (dashed line) as shown in Figure 18.

a westward tilt (Jones et al., 2004; Lindgren, 1911; Wakabayashi, 2013; Yeend, 1974). These studies rely on the assumptions that the primary cause of river incision is a response to surface uplift, that the river network planform geometry has been static since the Eocene, that paleochannel gradient can be accurately reconstructed, or that the Eocene river deposits reflect preserved portions of a smoothly graded river profile at a particular point in time. However, the modern river network is in a different configuration than the Eocene-Oligocene network (Henry et al., 2012 and references within) and Eocene river deposits may reflect a time-transgressive disequilibrium braided river system, with a highly variable gradient that may reflect underlying lithology rather than uplift rates (Cassel and Graham, 2011; Gabet, 2014, 2020a).

Other studies have used large knickzones in river profiles in the southern Sierra to argue for the presence of uplifted relict surfaces that can be used to estimate the magnitude of late Cenozoic surface uplift (Clark et al., 2005; Pelletier, 2007). However, extrapolating uplift timing and magnitude from modern longitudinal river profiles relies on the assumption that channel steepness

above knickzones reflect past equilibrated conditions, which might not be the case if nonuniform uplift and/or planform changes in river basin geometry perturb channel steepness (Beeson et al., 2017; Willett et al., 2014). It has also been suggested that knickpoints in the granitic terrain of the southern Sierra reflect differential bedrock weathering rather than tectonics (Wahrhaftig, 1965). Still other studies estimate tilt magnitude and surface uplift at the range crest from tilted late Cenozoic sedimentary and volcanic deposits preserved near the mountain front (Huber, 1981; Unruh, 1991; Wakabayashi and Sawyer, 2001) by assuming an initial inclination at time of deposition and perfect rigid-block rotation to extrapolate the measured tilt angle to the crest. Both deviation from rigid-block rotation resulting from internal deformation or non-tectonic differential rock uplift due to isostatic response to erosion and depositional loading would introduce error to these estimates (Small and Anderson, 1995). Lastly, incision below dated tiered cave deposits provides evidence of a pulse of late Cenozoic incision, which has been interpreted to be a response to surface uplift (Stock et al., 2005, 2004) but tiered caves have only been dated in

the southern Sierra, specifically the Kings and Kaweah river basins.

More recent arguments that the Sierra Nevada has been a high topographic feature throughout the Cenozoic, with <500 m of late Cenozoic uplift, have been supported using a variety of geochemical data. Variations in (U-Th)/He cooling ages along constant elevation profiles suggests relief of 1–2 km in the early Cenozoic southern Sierra, which by comparison to modern ranges of similar relief permit an estimated paleoelevation in excess of 4 km (House et al., 2001, 1998). Similarly, stable isotope paleoaltimetry (Cassel et al., 2009b, 2012a, 2014; Crowley et al., 2008; Mix et al., 2016; Mulch et al., 2006, 2008) and paleobotany (Hren et al., 2010) data sets have been used to argue that the elevation of the western slope of the Sierra has remained largely unchanged from the Eocene through modern time. Both stable isotope paleoaltimetry and the paleobotanical work by Hren et al. (2010) rely on the assumption that atmospheric flows pass over high topography, but modern atmospheric flows in the Sierra have been shown to largely flow around instead of over portions of the range with elevations in excess of 2.5 km (Lechner and

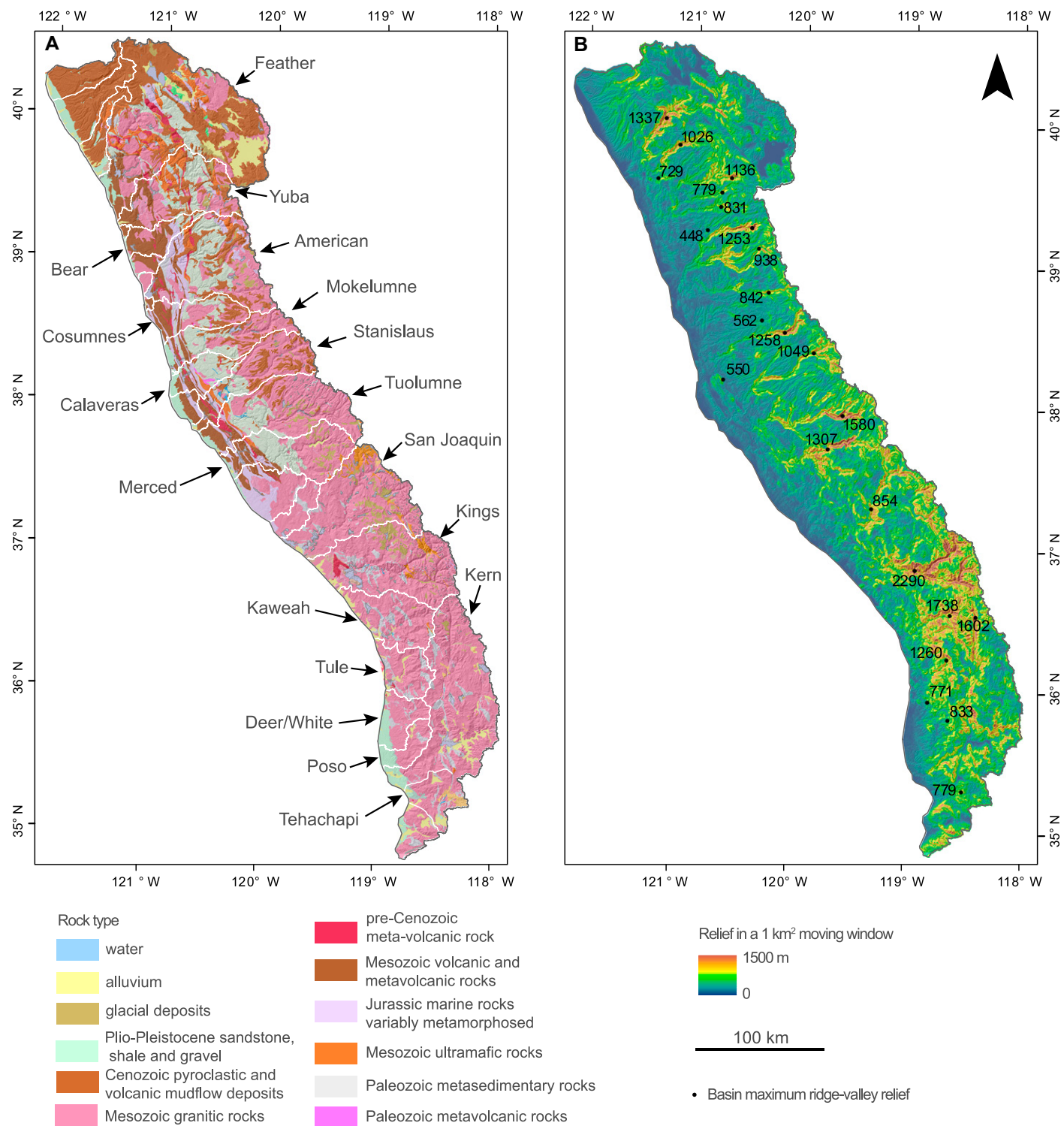


Figure 2. (A) Simplified geologic map at 1:500,000 scale showing major rock types (Ludington et al., 2005) of the western slope of the Sierra Nevada, California, USA. White lines delineate drainage basins. (B) Map of relief calculated within a 1 km² moving window for the western slope of the Sierra Nevada. Black dots show the locations and adjacent numbers report magnitude in meters of maximum ridge-valley relief in each basin, calculated by subtracting the river elevation from the ridge elevation as shown in Figure 11 and Figure S9 (see text footnote 1).

Galewsky, 2013). This observation was demonstrated more generally in computational studies (Galewsky, 2009a, 2009b) and potentially limits

the ability of these techniques to detect continued or late-stage growth of an orogen. As reviewed by Molnar (2010), orographic precipitation and

changes in water vapor isotope concentrations depend not only on topographic slope of the orogen being traversed, but also on the wind speed

of the air mass and the amount of moisture in the atmosphere, which are sensitive to the prevailing paleoclimate in terms of temperature and seasonality of precipitation (dominantly summer versus dominantly winter). Water vapor isotope concentrations also depend on the initial isotopic ratio of the vapor, which is source dependent. Finally, samples (volcanic glass, kaolinite, and leaf fossils in these studies) must exhibit closed-system behavior to record the isotopic signature of water at the time of deposition. Large uncertainties still exist in paleo-storm trajectories and wind speeds, vapor sources, paleoclimate reconstructions (temperature and seasonality), and the reliability of assuming closed-system behavior (Jones et al., 2004; Molnar, 2010; Wakabayashi, 2013).

Although debate continues regarding the age and magnitude of late Cenozoic surface uplift, consensus is forming around diverse geophysical and geochemical measurements that there are reasonable mechanisms to create a late Cenozoic source of buoyancy that would uplift and then support high modern elevations. The degree to which these mechanisms were range-wide or more intensely impacted either the southern or northern parts of the range, however, remains unclear. Geophysical observations indicate that the Sierra range is not underlain by an anomalously thick crustal root that would support high elevations, but rather has a low-wavespeed mantle at depth that has been interpreted to be hot and buoyant (Carder, 1973; Jones et al., 1994). The petrology and composition of xenoliths entrained in Mio-Pliocene volcanic deposits in the southern Sierra suggest delamination of a dense, cold eclogitic root to the batholith between 8 and 3 Ma (Ducea and Saleeby, 1998, 1996). Buoyancy associated with such a removal event in the southern Sierra is estimated to have triggered ~1200 m of rock and surface uplift at the crest (Ducea and Saleeby, 1996; Saleeby et al., 2013). Other seismic imaging and geodynamic modeling also put the delamination event only in the southern Sierra between 10 and 3 Ma (Zandt et al., 2004). A link between highly potassic magmatism and root removal further constrains the timing of root removal to a period of <500 k.y. centered on 3.5 Ma (Farmer et al., 2002; Manley et al., 2000). More recent results from p-wave tomography have been interpreted to indicate that removal of high density lithosphere and replacement with lower density asthenosphere has occurred in the eastern portion of the southern Sierra, as well as the northern Sierra up to a latitude of ~39°N and the American River basin (Jones et al., 2014). Other seismic imaging techniques suggest that delamination of the eclogitic root may be actively progressing from south to north and from east to

west (Frassetto et al., 2011; Gilbert et al., 2012). The eclogitic root in the northern Sierra is estimated to be thinner and more dispersed than in the southern Sierra (Cecil et al., 2012; Ducea and Saleeby, 1996) and thus removal would likely have triggered less uplift in the northern Sierra than in the south (Jones et al., 2014). Additionally, late Cenozoic unloading resulting from km-scale down-to-the-east normal slip on the Sierra Frontal Fault System bounding the eastern escarpment has the potential to produce hundreds of meters to ~1 km of uplift at the Sierra crest (Martel et al., 2014; Thompson and Parsons, 2009). Isostatic uplift in response to climatically induced erosional unloading has also been suggested as a mechanism for uplift (Small and Anderson, 1995). However, more recent analysis indicates that this mechanism is unlikely a dominant control on surface uplift given the low rates of bedrock erosion on upland surfaces and limited mass removal from narrow, deep canyons that show little evidence of extensive valley widening (Jones et al., 2004; Small et al., 1997; Stock et al., 2005). Other plausible mechanisms of uplift that would have more dramatically influenced the northern Sierra include thermal uplift related to the northward migration of the ancestral Cascades arc and Mendocino triple junction (Busby et al., 2008; Busby and Putirka, 2009) or passage of the Yellowstone plume swell to the north (Saleeby et al., 2013).

Major geologic events that occurred in the late Cenozoic that may or may not have accompanied surface uplift, but that radically impacted Sierra geomorphology in ways that may confound interpretation of tectonics from river geomorphology include western migration of the main Sierra drainage divide (Cassel et al., 2009a; Garside et al., 2005; Henry, 2009; Henry et al., 2012; Henry and Faulds, 2010; Yeend, 1974) and widespread volcanism that blanketed pre-existing topography in the northern half of the range (Bateman and Wahrhaftig, 1966; Busby et al., 2008; Christensen, 1966; Curtis, 1953; Durrell, 1966; Slemmons, 1966). In Late Cretaceous–early Cenozoic time, the Sierra is thought to have formed a western ramp to an orogenic plateau, commonly termed the Nevadaplano (Cassel et al., 2009a, 2012a, 2014; DeCelles, 2004). Fluvial gravel deposits (auriferous gravels) dated from 42.7 to 28.6 Ma are evidence of large paleoriver systems in the northern Sierra (Cassel et al., 2012b; Lindgren, 1911; Yeend, 1974). Correlation of Oligocene ash-flow tuffs, which were deposited on top of auriferous gravels and have source calderas in central Nevada demonstrates that paleorivers extended ~100 km farther east than modern rivers to drain the western portion of the Nevadaplano (Cassel et al., 2009a; Henry, 2008; Henry

et al., 2012; Henry and Faulds, 2010). Beheading of the major Eocene-Oligocene paleorivers is thought to postdate the youngest dated ash-flow tuff at 23 Ma that made it to the western slope of the Sierra (Henry and Faulds, 2010). River truncation likely resulted from a combination of Basin and Range extension, which began in the Miocene (Colgan et al., 2010, 2008; Colgan and Henry, 2009; Henry, 2008), or from volcanic constructional topography generated by the ancestral Cascades arc, which blanketed the western slope of the Sierra Nevada north of the mainstem of the Tuolumne River with andesite, andesitic block-and-ash-flows and lahar deposits from ca. 16 to 3 Ma (Bateman and Wahrhaftig, 1966; Busby et al., 2008; Christensen, 1966; Curtis, 1953; Durrell, 1966; Slemmons, 1966). Clear evidence of beheaded paleorivers that extended to the east of the modern drainage divide exists as far south as the San Joaquin River (Henry et al., 2012; Huber, 1981). Farther south, sediment provenance data collected from Paleogene basin deposits east of the modern crest suggests the presence of a southward draining paleoriver that turned westward near the southern end of the modern Sierra (Lechler and Niemi, 2011).

The ongoing debate, the differences along strike of the range, and the possibility of mid to late Cenozoic perturbations to fluvial geomorphology beyond surface uplift call for a range-wide investigation and a systematic approach to separate tectonic from non-tectonic origins of disequilibrium fluvial profiles.

GEOLOGIC SETTING, EXHUMATION RATES, AND MILLENIAL-SCALE EROSION RATES

The Sierra Nevada and the Great Valley currently move as an independent semi-rigid microplate between the Pacific and North American plates (Argus and Gordon, 1991; Dixon et al., 2000; Kreemer et al., 2014; Wernicke and Snow, 1998). This microplate is bounded on the east and south by the Walker Lane and eastern California shear zone (Dixon et al., 2000; Dokka and Travis, 1990a, 1990b; Unruh et al., 2003; Wesnousky, 2005), on the west by the San Andreas Fault System (Argus and Gordon, 1991) and the Coast Range fold belt (Argus and Gordon, 2001; Namson and Davis, 1990, 1988; Wentworth and Zoback, 1989), and on the north by the northern California shear zone (Wesnousky, 2005). Modern surface geology is predominantly a mix of Mesozoic granitic plutons, Paleozoic–Jurassic metamorphic terranes, and Cenozoic volcanics (Fig. 2). The Sierra Nevada batholith, largely emplaced during arc magmatism in the Mesozoic, forms the core of the Sierra Nevada (Bateman and Wahrhaftig, 1966). The depth of

exhumation of the Sierra Nevada batholith is relatively similar throughout much of the Sierra except in the far southern Sierra where exhumation depth increases rapidly (Ague, 1997; Nadin et al., 2016; Pickett and Saleeby, 1993). Belts of metamorphic rocks compose much of the western portion of the Sierra in both the northern and central parts of the range. Cumulatively termed the “western metamorphic belt,” this belt expands in width northward and consists of tectonically accreted terranes of Paleozoic to early Mesozoic age that are folded, faulted, and metamorphosed, including the major formations of the Shoo Fly complex and Calaveras complex (Bateman and Wahrhaftig, 1966). Rock types in these belts are a complex mix of schist, slate, phyllite, greenstone, serpentinite, chert, marble, and quartzite (Fig. 2; Bateman and Wahrhaftig, 1966).

Thermochronology data from both the northern and southern Sierra highlight that less than 2–3 km of exhumation have occurred in the Cenozoic and show slow, steady, and uniform exhumation rates throughout the early to middle Cenozoic (Cecil et al., 2006; Clark et al., 2005; House et al., 2001, 1998). Along the entire length of the range, apatite (U-Th)/He ages from the low-relief upland surface consistently fall between 50 and 80 Ma, which indicates that less than 2–3 km of exhumation have occurred on this surface in the Cenozoic (Cecil et al., 2006; Clark et al., 2005; House et al., 2001). Six different vertical transects that sample deeper crustal levels from the deeply incised canyons in the central and southern Sierra show that each apatite (U-Th)/He age-elevation profile is well fit by steady exhumation rates of 40–60 m m.y.⁻¹ (Clark et al., 2005). These slow and steady rates were present by the oldest samples at ca. 80 Ma and continue at least until the youngest sample, which on the west-side Sierra is 32 Ma from Kings Canyon, whereas on the east side along the Sierra Nevada Frontal Fault deeper crustal levels yield an age of 11 Ma. Thus, slow steady exhumation is thought to have continued at least until 32 Ma and potentially as young as 11 Ma (Clark et al., 2005). Similarly, apatite and zircon (U-Th)/He ages from the northern Sierra indicate slow exhumation rates of 20–40 m m.y.⁻¹ over the younger samples from 60 to 40 Ma, but much more rapid exhumation rates of 200–800 m m.y.⁻¹ from 90 to 60 Ma (Cecil et al., 2006). Modeling of isochrones developed from apatite (U-Th)/He ages in the Kings and San Joaquin river basins suggests that westward tilting may have uplifted the Sierra crest 2 km since 20 Ma (McPhillips and Brandon, 2012).

Concentrations of ¹⁰Be and ²⁶Al in exposed bedrock allow for calculation of exposure age and time-averaged erosion rate of the surface (Lal, 1991). Similarly, erosion rates that are

spatially averaged over a river basin upstream of the sampling point and temporally averaged over 10–100 k.y. timescales can be derived from measured concentrations of ¹⁰Be in quartz river sand (Granger et al., 1996). Erosion rates calculated from unglaciated low-relief interfluvial surfaces in the southern Sierra range from 3 to 21 m m.y.⁻¹ (Callahan et al., 2019; Stock et al., 2004). Erosion rates from catchments that drain the unglaciated low relief surface between the San Joaquin and Kings rivers range from 9 to 87 m m.y.⁻¹ with a mean of 39 ± 9 m m.y.⁻¹ (Callahan et al., 2019). Catchment-average erosion rates from small sub-basins in the southern South Fork Kern River basin range from 29 to 73 m m.y.⁻¹ and from 10 to 99 m m.y.⁻¹ in sub-basins in the upper Poso River basin (Portenga and Bierman, 2011; Riebe et al., 2000). In the northern Sierra, erosion rates in the headwaters of the Feather River basin range from 19 to 68 m m.y.⁻¹ (Portenga and Bierman, 2011; Riebe et al., 2000). In the foothills of the Feather River basin, erosion rates from upland sub-basins range from 13 to 91 m m.y.⁻¹, but in tributaries draining into the steep and incised reach of the Middle Fork Feather River, rates are as high as 254 m m.y.⁻¹, as much as fifteen times the rates from a low-relief surface nearby (Hurst et al., 2012; Riebe et al., 2000).

Caves perched at various elevations above the modern river level and dated by ²⁶Al/¹⁰Be ratios in buried cave sediments show that river incision history in the Kings and Kaweah rivers reflects a pulse of incision between 3 and 1.5 Ma, during which incision rates accelerated from ~70 m m.y.⁻¹ to ~300 m m.y.⁻¹ and subsequently slowed to ~20 m m.y.⁻¹ (Stock et al., 2005, 2004). Farther north in the Stanislaus River basin, ²⁶Al/¹⁰Be ratios in cave sediments yield an age of ca. 1.6 Ma, a pre-burial erosion rate of ~46 m m.y.⁻¹ and an average river incision rate of 60 m m.y.⁻¹ since ca. 1.6 Ma (Stock et al., 2005, 2004). High long-term average rates of river incision into basement rock below Cenozoic volcanic deposits have been documented for many deeply incised mainstem rivers north of and including the Tuolumne River, with rates ranging from 190 to 400 m m.y.⁻¹ (Wakabayashi, 2013). In the San Joaquin River, incision rates below Cenozoic volcanic deposits range from 91 to 240 m m.y.⁻¹ (Wakabayashi, 2013).

In total, millennial-scale rates of river incision on the low-relief upland surface are similar in both the northern and southern Sierra and range from 3 to 73 m m.y.⁻¹, which are similar to the long-term rates derived from thermochronology. In contrast, steep tributaries that drain into the deeply incised canyons yield millennial-scale rates almost an order of magnitude higher. This discrepancy between generally low rates of inci-

sion on upland surfaces and much higher rates from the deeply incised canyons highlights that large gradients in erosion rates exist between the high-relief canyons and the low-relief upland and quantifies to first-order that the Sierra landscape is in a disequilibrium or transient state. While the dichotomy between deep, steep canyons and low-relief uplands appears uniform along the length of the Sierra Nevada (Fig. 2B), the crest elevation and geology vary systematically along strike. Crest elevation ramps up gradually toward the south, reaching a peak at the Kings River (Fig. 1D), and in contrast to the surface geology of the southern Sierra, which is primarily granodiorite, the northern Sierra has large bands of Paleozoic–Mesozoic aged metamorphic rocks in addition to widespread late Cenozoic volcanic rocks (Fig. 2A). These systematic variations along strike indicate not only that uplift history could differ along strike, but also that the response to surface uplift may vary along strike.

OVERVIEW OF METHODS

To investigate the spatial and temporal pattern of regional-scale perturbations recorded in river networks on the western slope of the Sierra Nevada, we conducted topographic analysis of river geomorphology and surrounding topography using an ensemble of methods. We then interpreted the results of this topographic analysis using 1-D and 2-D landscape evolution modeling based on the stream power fluvial erosion rule. In this section we present an overview of methods used and theoretical background of river incision into bedrock, while the details of each method and the required assumptions are described in the sections associated with each method.

Our general workflow was as follows. First, we mapped potential disequilibrium in planform river basin geometry that might impact a river’s ability to record tectonic perturbations (Scheingross et al., 2020; Willett et al., 2014) and we used this map to focus our analysis on select mainstems and tributaries that should best record tectonic forcing. Second, we analyzed river longitudinal profiles and their χ -transformed counterparts for mainstems and tributaries to identify systematic deviations from equilibrium longitudinal river profiles. We then compared the disequilibrium profile forms observed in the Sierra to a variety of disequilibrium profile forms that result from different types of perturbations. We interpreted the results of this comparison as showing that tectonic tilting is a likely cause of disequilibrium forms in Sierra river profiles. Third, we examined other metrics of the modern river network to determine if they too were consistent with tectonic tilting.

In particular, we analyzed relationships between azimuth and channel slope and compared these relationships to those formed in a 2-D landscape evolution model during tectonic tilting, as well as metrics of stream capture and network rearrangement expected from tilting. We found that, similar to river profile forms, these other metrics of network morphology reflect a down-to-the-west tilting event. Fourth, to estimate the timing of this tilting event, we used the locations of migrating mainstem knickpoints and migrating tributary knickzones along with a calibrated stream power river incision model to estimate knickpoint travel times. Fifth, with timing of tilting constrained by knickpoint positions relative to points of origin, we used three independent methods to estimate the magnitude of uplift that likely resulted from tilting: (1) regressions of spatial gradients in incision into basement rock below Cenozoic deposits as a function of distance from the mountain front, or where Cenozoic deposits were sparse or absent, regressions of spatial gradients in mainstem canyon relief with distance from the mountain front; (2) regressions of spatial gradients in tributary knickzone drop height as a function of distance from the mountain front; and (3) geometric analysis of knickzones formed in anomalously erodible rock. Lastly, we investigated how both discrete and ongoing changes in drainage area may have impacted the degree to which Sierra rivers record tectonic tilting.

We used a combination of 1 arc-second (~ 30 m) and 1/3 arc-second (~ 10 m) digital elevation models (DEMs) of the Sierra Nevada. The 30 m DEMs were derived from the U.S. National Aeronautics and Space Administration's Shuttle Radar Topography Mission and the 10 m DEMs were derived from the U.S. National Elevation Data set. We used 30 m DEMs for most analyses and maps and 10 m DEMs for the river network analysis of azimuth-gradient relationships and all large-scale hillshade images. Topographic analysis was conducted with the MATLAB-based software package TopoToolbox 2 (Schwanghart and Scherler, 2014). We used TopoToolbox 2 to map the river network by first filling topographic depressions in the DEMs and then calculating flow direction and accumulation using a steepest descent flow algorithm. We restrict our analysis to bedrock rivers of the western slope of the Sierra Nevada and thus clipped all DEMs to the mountain front, which was identified using a slope threshold of 0.01 on a DEM that was smoothed with a 20 km² moving window mean. This slope threshold on the smoothed DEM proved effective at removing alluvium of the Great Valley from the analysis (Fig. 2A). We defined channel heads using a critical drainage area, A_c , of 0.5 km², which is a

commonly used value below which the network is typically fluvial (DiBiase et al., 2012; Stock and Dietrich, 2003).

For all river profile analysis, we analyzed the longest stream of each crest-draining basin, unless this stream ran oblique to mountain front strike and there was another comparably long branch that ran more perpendicular to strike, in which case that branch was used. We use a naming convention in which the name given to the mainstem near the mountain front is used to refer to the entirety of the analyzed river and the associated drainage basin. However, many rivers have a collection of names over their course from the chosen channel head and in some cases smaller tributaries that were not analyzed retain the name of the mainstem near the mountain front. We include a kmz file in the Supplemental Material¹ of channel head points to clarify exactly which rivers were analyzed.

Theoretical Background for Evolution of River Channel Elevation

Bedrock erosion can be described by the stream power model (Howard, 1994; Siedl and Dietrich, 1992) or shear stress model (Howard and Kerby, 1983) for detachment-limited river incision, with simple versions of both relationships resulting in the following model for the time rate of change in river elevation, z , with distance upstream, x :

$$\frac{\partial z(x,t)}{\partial t} = U(x,t) - K(x,t)A(x,t)^m \left| \frac{\partial z(x,t)}{\partial x} \right|^n \quad (1)$$

where U is rock uplift rate, K is a lumped parameter for erosional efficiency that incorporates rock properties, channel geometry, and climate, A is drainage area that serves as a proxy for discharge, and m and n are empirical exponents. Equation 1 takes the form of a kinematic wave equation, which implies that information about changes in baselevel, climate, or uplift rate, travels upstream through river networks in a wave-like manner (Anderson and Rosenbloom, 1994). Rivers evolve toward an equilibrium grade (Mackin, 1948) that for bedrock rivers is defined as a state in which the rate of rock erosion keeps pace with the rate of rock uplift relative to baselevel such that the time rate of change of river profile elevation is equal to zero (Howard, 1994; Howard and Kerby, 1983; Siedl and Dietrich, 1992). Assuming steady-state

¹Supplemental Material. Figures S1–S12; Derivations of equations for knickpoint locations; kmz file. Please visit <https://doi.org/10.1130/GSAB.1.7912156> to access the supplemental material, and contact editing@geosociety.org with any questions.

conditions, Equation 1 can be arranged to yield an equation for channel slope in terms of stream power parameters and in a form that captures the widely observed power law scaling between channel slope and drainage area (Flint, 1974; Hack, 1957; Lague, 2014; Morisawa, 1964):

$$\left| \frac{\partial z}{\partial x} \right| = k_s A(x)^{-m/n} \quad (2)$$

where

$$k_s = \left(\frac{U}{K} \right)^{1/n} \quad (3)$$

k_s is the channel steepness index, or the rate at which channel slope changes with drainage area. If U and K are assumed to be uniform, Equation 2 can be integrated with respect to x to yield an equation for steady-state river elevation:

$$z(x) = z_b + \frac{k_s}{A_0^m} \chi \quad (4)$$

where

$$\chi = \int_{x_b}^x \left(\frac{A_0}{A(x')} \right)^{m/n} dx \quad (5)$$

A_0 is a scaling drainage area used to give χ units of length (set to 1 m² throughout) and m/n is river concavity, θ , or the rate at which channel slope changes with distance downstream (Perron and Royden, 2013).

Identifying Equilibrium and Transients Using Transformed River Profiles

Equation 4 shows that, under steady-state conditions with uniform parameters, river elevation scales linearly with χ . An equilibrium river profile with uniform rock uplift rate, erodibility, and river concavity will thus be linear on a plot of river elevation as a function of χ , termed a χ plot, as long as the correct value for river concavity is chosen (Perron and Royden, 2013). Further, all segments of an equilibrium river network in which river concavity, rock erodibility, and uplift rate are uniform will collapse to a single straight line on a χ plot. The χ transformation of river profiles removes the effect of drainage area not only from river longitudinal profile shape but also from perturbation travel distances such that knickpoints propagating through a river network that originated from a common perturbation will collapse to the same χ value (with uniform U and K). The slope of the χ plot is the channel steepness index, k_s

(Equations 3 and 4). The channel steepness index has been shown to increase monotonically with uplift rates or millennial-scale erosion rates (DiBiase et al., 2010; Kirby and Whipple, 2001, 2012; Ouimet et al., 2009; Snyder et al., 2000; Wobus et al., 2006) and decrease with greater rock erodibility (Bernard et al., 2019; Duvall et al., 2004; Gailleton et al., 2021; Jansen et al., 2010; Yanites et al., 2017). These properties of χ transformed river profiles provide the foundation to identify to what degree river networks are in equilibrium and whether deviations from a linear, collapsing χ plot result from nonuniformity in U , K , or θ , or from propagating transients with a common origin.

Characteristics of Migrating Knickpoints in Transient River Profiles

Following terminology used in Haviv et al. (2010) and Whipple et al. (2013), we call a point at which channel segments of similar steepness are offset a “vertical-step knickpoint,” a point that separates portions of a river profile with dissimilar channel steepness a “slope-break knickpoint,” and a portion of the river profile that has locally high channel steepness a “knickzone.” We recognize two different types of slope-break knickpoints: (1) migrating knickpoints that reflect a past change in climate/rock erodibility, or a change in the rate of baselevel fall/rate of rock uplift rate relative to baselevel; and (2) stationary knickpoints found at lithologic contacts that reflect a change in the erodibility of the underlying rock.

The horizontal, x_{kp} , and vertical, z_{kp} , locations of mobile knickpoints can be predicted using the stream power model of river incision to constrain knickpoint velocities and travel times (Berlin and Anderson, 2007; Lague, 2014; Mitchell and Yanites, 2019b; Niemann et al., 2001; Royden and Perron, 2013). Under the stream power model of bedrock incision, the celerity, or wave speed, of propagating knickpoints is given by $C = KA^m S^{(n-1)}$, which for $n = 1$ takes on the power law function of drainage area found in many field studies of knickpoint velocity (Harkins et al., 2007; Hayakawa and Matsukura, 2003; Jansen et al., 2011; Lague, 2014; Loget and Van Den Driessche, 2009). The time it takes for knickpoints caused by some perturbation to travel from the point of origin, commonly baselevel, x_b , to any point on the river network is termed the fluvial response time, τ , and is given by the upstream integral of the inverse wave speed (Whipple and Tucker, 1999):

$$\tau(x) = \int_{x_b}^x \frac{1}{KA(x)^m S(x)^{n-1}} dx \quad (6)$$

With a few simplifying assumptions, we can find an analytical solution to Equation 6 to get a general understanding of how knickpoints move horizontally through river networks under different conditions (see Supplemental Material in the DR for more detailed solutions). If we assume that K is spatially uniform and assume a 1-D representation of a river in which drainage area can be described by Hack’s Law (Hack, 1957), $A = k_a(L - x)^h$, where L is river length, k_a is Hack’s coefficient, and h is the length exponent, and that both hm and n are unity we can evaluate the definite integral in Equation 6 from $x_b = 0$ to the location of a knickpoint, x_{kp} , to find the following equation for knickpoint location as a function of time:

$$x_{kp}(t) = L \left(1 - e^{-k_a m K t} \right) \quad (7)$$

Knickpoint location in χ space is then given by the definite integral from baselevel to x_{kp} (Equation 5), which simplifies to:

$$\chi_{kp}(t) = Kt \quad (8)$$

Equation 8 shows that in χ space, where the effect of drainage area on knickpoint velocity has been removed, the position of migrating knickpoints depends only the rate parameter K and time since knickpoint formation, such that knickpoints in various branches of a river network, but that share a common origin, will collapse to the same point in χ space. Substituting the channel response time, τ , in for time in Equation 8 yields

$$\tau = \frac{\chi}{K} \quad (9)$$

We estimated K for the Sierra batholith (described below) and used this relationship between τ and χ to estimate τ for mainstem channel heads, mainstem knickpoint locations, and the top of tributary knickzones.

While the horizontal velocity of transient signals marked by knickpoints depends on the wave speed, the vertical velocity of knickpoints depends on rock uplift rates (Mitchell and Yanites, 2019a; Niemann et al., 2001; Royden and Perron, 2013; Whipple and Tucker, 1999). In the case of a single perturbation, knickpoints mark the most upstream end of a new equilibrium river profile, so we can use the equation for steady-state river elevation (Equation 4) to write an equation for knickpoint elevation as a function of time and uplift rate. We first consider the case in which knickpoints are caused by a step change in spatially uniform uplift rate from U_1 to U_2 . In this case, knickpoint elevation depends only on the new uplift rate, U_2 :

$$z_{kp}(t) = U_2 t \quad (10)$$

A spatially uniform change in uplift rate should therefore produce knickpoints at the same elevation across a river network. If, however, the new uplift field is a linear gradient such that $U_2(x) = \alpha x + U_0$, where α is the uplift gradient, and U_0 is the uplift rate at the mountain front, then knickpoint elevation depends not only on the new uplift rate but also on K :

$$z_{kp}(t) = U_L t - \frac{U_L - U_0}{k_a m K} \left(1 - e^{-k_a m K t} \right) \quad (11)$$

where U_L is the rock uplift rate at the channel head (see Supplemental Material in the DR for more derivation). Equation 11 implies that knickpoint elevations will be lower in rivers in which the knickpoint has not propagated far from the mountain front owing to either small drainage area or a path that traversed less erodible rocks (smaller K). In contrast, knickpoints in large rivers (with headwaters at larger U_L) or with more erodible rocks (larger K) will be at greater elevations as they will have propagated further and therefore experienced higher uplift rates (Fig. S1; see footnote 1).

In the case where n is not unity, the solutions are more complicated as wave speed and travel time also depend on channel slope (Equation 6). When $n < 1$, wave speed is inversely correlated to channel slope, so knickpoints move faster in portions of the river network with gentler slopes. When $n > 1$, wave speed is positively correlated to channel slope, so knickpoints move faster in portions of the river network with steeper slopes. This can result in a knickpoint being stretched or consumed (Mitchell and Yanites, 2019b; Royden and Perron, 2013). Predicting knickpoint location and elevation becomes even more complex in cases where perturbations are not step changes and channel slope is not equilibrated to the previous uplift field. We therefore use the analytical expressions shown in equations 7–11 as an intuitive guide for what determines horizontal and vertical knickpoint locations, but explore how deviations away from $n = 1$ influence knickpoint propagation and response times following perturbations specific to the Sierra Nevada using published numerical simulations of river response (Beeson and McCoy, 2020).

χ Analysis of River Basin Geometries

We mapped χ for the river network dissecting the western slope of the Sierra to visualize disequilibrium in the planform geometry or distribution of drainage area that could potentially obscure geomorphic signatures of late

Cenozoic tectonic uplift in the longitudinal profiles of Sierra rivers. The linearity between χ and steady-state elevation shown in Equation 4 implies not only that χ profiles of rivers equilibrated to uniform fields of U and K will be linear but that χ can be used as a proxy for the theoretical steady-state river elevation in rivers. Differences in channel-head χ values in rivers that originate on a common divide can reflect disequilibrium in river basin geometry and can indicate that the geometry of the river basins need to adjust to bring channel-head χ values to equilibrium (Beeson et al., 2017; Chen et al., 2021; Hu et al., 2021; Willett et al., 2014). Maps in which the river network is colored by χ values (“ χ maps”) visualize the degree of river basin disequilibrium across a landscape and can be used to determine if drainage divides are likely to be stationary or in motion. Additionally, χ plots can reveal drainage area exchange between basins, with the expectation that basins gaining drainage area will have profiles that plot above the regional trend, whereas basins experiencing area loss will plot below. If area exchange occurs via discrete stream capture, the captured reach will plot above the regional trend as expected from area gain, but will retain the pre-capture channel steepness (Beeson et al., 2017; Scheingross et al., 2020; Willett et al., 2014).

Normalized Channel Steepness

Normalized channel steepness, k_{sn} , is a commonly used metric for channel steepness that is calculated using a reference concavity, θ_{ref} , such that steepness values can be compared across basins (Wobus et al., 2006). We used $\theta_{ref} = 0.45$ to calculate χ for all basins (based on slope-area fits described below) and used the slope of χ plots to measure k_{sn} . Thus, k_s as calculated here is equivalent to k_{sn} and hereafter “channel steepness” will refer to k_{sn} . We estimate uncertainty in k_{sn} by calculating the 95% confidence interval on the slope of each least-squares regression line made on χ plots.

Assumption of Uniform U , K , and θ in χ Analysis

To remove rock uplift relative to baselevel, U , and rock erodibility, K from the integral quantity χ , we assumed uniform U and K across the Sierra for this calculation. We also assumed uniform river concavity, θ . Violation of these assumptions has two implications: (1) steady-state elevation will not scale perfectly with χ as in Equation 4, and (2) equilibrated channels will not plot as straight lines on a χ plot. Deviations from linearity on a χ plot may therefore reflect nonuniformity in either U , K , or θ . Although we

know rock type is nonuniform, particularly in the northern Sierra, assuming uniform K reveals whether changes in channel steepness occur at lithologic boundaries. To help separate perturbations in channel steepness resulting from a transient erosional response as opposed to lithologic heterogeneity, we compare χ plots from the Sierra to the signatures that heterogeneous lithology impart on χ plots in a 1-D model of river evolution (Beeson and McCoy, 2020). Similarly, if U is nonuniform, channel profiles equilibrated to this nonuniform uplift field will have nonuniform channel steepness observable on χ plots (Beeson and McCoy, 2020). Thus, if the Sierra Nevada is simply equilibrated to an uplift gradient, this should be recognizable in χ plots made by assuming uniform uplift as a curved χ -plot. Equilibrium river concavity falls in a narrow range between 0.4 and 0.7 with no statistically significant impact from uniform uplift rate nor rock erodibility (Lague, 2014 and references therein). Deviations outside this range are therefore likely to reflect a transient state in the river network. We found a regional value for equilibrium river concavity (described below) and assumed that the river network is adjusting toward this concavity, although the current concavity of the transient portions of the river network is lower. We find no evidence that equilibrium river concavity varies systematically away from the mountain front (Fig. S3; see footnote 1), thus we interpret systematic deviations from linear χ plots as the result of transience in the river network rather than resulting from the use of a regional average equilibrium θ .

Although χ in the northern Sierra will not perfectly reflect steady-state river elevation owing to the poor assumptions of uniform rock erodibility and uniform rock uplift, identifying disequilibrium in river basin geometry via comparison of cross-divide differences in channel-head χ only requires that the path integral of lithology and uplift rate is similar on both sides of the divide in question, which is commonly the case on the west side of the Sierra given the north-south strike of the geology and the east-west orientation of the rivers.

Estimating Parameter Values

The Erodibility Coefficient, K

K can be estimated using Equation 3 if the uplift rate, U , normalized channel steepness, k_{sn} , and slope exponent, n , can be constrained, and the river profile is near equilibrium. To estimate a representative K value for Mesozoic plutonic rocks (the Sierra batholith), we used published catchment-average erosion rates from near-equilibrium granitic basins within the unglaciated, low-relief upland surface that drains into

the lower reaches of the San Joaquin and Kings rivers (Callahan et al., 2019). From this compilation of published erosion rate data, we selected erosion rates from basins that had approximately linear χ plots above the location of the erosion rate measurement (R^2 values ≥ 0.9 for linear regression of χ elevation data) and thus measured erosion rates should be in approximate equilibrium with rock uplift rates. We measure k_{sn} values from linear regression of χ plots of the river network upstream of the sampling location and assumed $n = 1$. This method limited our analysis to 30 basins that display limited transient features (Fig. S2; see footnote 1). Calculated K values from these basins range from 1.1×10^{-7} to $4.1 \times 10^{-6} \text{ m}^{0.1}\text{yr}^{-1}$, with a mean K of $9.0 \times 10^{-7} \pm 1.6 \times 10^{-7} \text{ m}^{0.1}\text{yr}^{-1}$ (\pm standard error of the mean), which we used to calculate τ in the Sierra using Equation 9. Standard error was used in all error propagation calculations, but 95% confidence intervals on K were used to calculate confidence intervals on all measurements of τ .

River Concavity Index, θ

The standard procedures of using Flint’s Law to estimate the concavity index from slope-area data (Flint, 1974; Hack, 1973; Wobus et al., 2006) or picking the concavity index that results in straight χ plots (Perron and Royden, 2013) cannot be applied using data from any single complete drainage basin owing to the disequilibrium state of Sierra rivers. We also chose not to use a novel method designed for transient river networks because of its inherent assumption that tributaries and mainstems should be collinear (Mudd et al., 2018). Thus, we used slope-area data from lower sections of the major crest-draining basins that had relatively straight χ plots and hence were interpreted to be near equilibrium. Slope and area data from these reaches were then fit in log-log space with a linear function, the slope of which is the concavity index (Flint, 1974). Concavity indices from these slope-area data range from 0.41 to 0.48 (Fig. S3; see footnote 1), thus we chose to use $\theta = 0.45$ for all analyses, which is within the observed range of 0.4–0.7 for equilibrium channels (Lague, 2014; Stock and Montgomery, 1999; Tucker and Whipple, 2002; Whipple and Tucker, 1999). Although concavity can strongly influence the shape of χ plots, the first-order forms of χ plots for Sierra rivers are similar across many values of concavity (Fig. S4; see footnote 1).

Stream Power Slope Exponent, n

The slope exponent, n , can theoretically be calculated along with K from the relationship between channel steepness and erosion rate for steady-state channels (Equation 3). However, we

did not have a large enough data set of erosion rates from equilibrated channels to do this and therefore rely on the literature for this parameter. Although relationships of channel steepness with erosion rate are best fit with a value of n greater than unity (DiBiase and Whipple, 2011; Harel et al., 2016; Lague, 2014; Ouimet et al., 2009), data on knickpoint propagation support a value of n close to unity (Lague, 2014 and references therein) and mechanistic approaches yield estimates of n that range between 2/3 and 5/3, depending on the erosional mechanism (Whipple et al., 2000; Larimer et al., 2019). We therefore assume $n = 1$ as our objective in this study is to interpret tectonic histories from knickpoints/knickzones and associated basement rock incision. Assuming $n = 1$ also allows us to easily solve for τ and therefore to estimate the timing of perturbations in the Sierra. However, calibration of stream power model parameters in the Idaho Batholith suggests that n may be closer to 2/3 for rivers in granitic terrain (Larimer et al., 2019). The Sierra is largely composed of Mesozoic plutonic rocks (the Sierra Batholith) so it is possible that $n = 2/3$ is more appropriate. We use published numerical simulations of river response (Beeson and McCoy, 2020) to explain how deviations away from $n = 1$ would influence response times calculated for the Sierra using $n = 1$.

GEOMORPHIC SIGNATURES IN SIMULATED BEDROCK RIVER PROFILES OF THE TRANSIENT FLUVIAL RESPONSE TO PERTURBATIONS

Beeson and McCoy (2020) used a model river network composed of linked one-dimensional detachment-limited stream-power river profile models (Whipple and Tucker, 1999) to simulate the transient response of bedrock river networks to a variety of perturbations that move a river away from equilibrium. We summarize their results here to allow comparison between the morphology of rivers draining the western slope of the Sierra Nevada made herein to the characteristic signatures of the transient response to different perturbations they define. We note that the 1-D river profile evolution model of Beeson and McCoy (2020) was not explicitly calibrated to the Sierra Nevada and is thus not intended to specifically simulate behavior of Sierra Nevada rivers. Comparison of Sierra Nevada river profiles with simulated profiles is intended to identify first-order profile forms in order to identify possible large-scale perturbations. We anticipate that many secondary river profile forms of Sierra rivers will not be captured by the dynamics of simple detachment-limited stream power.

The model set up consisted of a 200-km-long mainstem river with three 40-km-long tributaries that entered the mainstem at 20, 80, and 140 km upstream of the outlet (Fig. 3A). The tributaries were made to run perpendicular to the mainstem such that the uplift rate for each tributary was equal to the rate experienced by the mainstem at the tributary confluence. All simulations started with equilibrated river profiles as the initial condition (Fig. 3B) and at $t = 0$ were subject to a single perturbation that moved the river away from equilibrium. A uniform background uplift rate of 50 m m.y.^{-1} was imposed in all simulations, except for the simulation of continuous rigid-block tilting in which the background uplift rate was set to zero. To simulate the elevation of potential paleoriver deposits and the elevation of a relict upland surface left behind as the river network begins to respond to the perturbations, the initial river profile was advected at the rock uplift rate throughout the simulation such that surface uplift of this profile equals rock uplift. Beeson and McCoy (2020) used this profile that experiences only rock uplift and zero erosion to track incision depth below paleotopography markers.

We summarize and compare five simulations from Beeson and McCoy (2020) that are idealizations of perturbations that either have geologic evidence for having occurred in the Sierra or that result in river profile shapes that share characteristics of those found in the Sierra: (1) an instantaneous uniform pulse of rock uplift of 1 km (note that there is no geologic evidence for uniform uplift, this simulation is simply used to demonstrate simple propagation of transient signals through a river network and for comparison purposes); (2) a step decrease in equilibrium profile steepness achieved by a step increase in bedrock erodibility (an increase in K as might be associated with a changing climate or increase in “tools” to erode the river bed owing to changing sediment flux from upstream glaciation); (3) major truncation or beheading of the mainstem river; (4) an instantaneous rigid-block tilt about a horizontal axis perpendicular to the mainstem river and located at the river outlet that increases the headwater elevation by 1 km with respect to the outlet (tilt of $\sim 0.3^\circ$); and (5) continuous rigid-block tilting that increases headwater elevation by 1 km over 3 m.y. Further, we explore four variations on rapid tilting in which rigid-block tilting toward the channel outlet induces a total of 1 km of rock uplift at the channel head over 1, 3, 5, and 10 m.y. For these simulations, the initial condition is a profile equilibrated to a linear uplift field that is zero at the mountain front and 100 m m.y.^{-1} at the crest. The uplift rate then returns to this uplift gradient following the period of more rapid tilting. The uplift gradient is held constant for the entire simulation

in the 10 m.y. case. Beeson and McCoy (2020) provide a more detailed description of the transient fluvial response to each perturbation and animations of each simulation are available as an associated online resource (see Beeson, “Geomorphic signatures of tilt: Animations of transient bedrock river response to perturbations,” 2019, <https://doi.org/10.6084/m9.figshare.8111498.v1>.

In all simulations, a knickpoint forms at the mainstem outlet and propagates upstream, tracking the timing of the perturbation and leaving a section of river with the new, equilibrium k_{sn} in its wake (Fig. 3). With a uniform K value of $1 \times 10^{-6} \text{ m}^{0.1} \text{yr}^{-1}$, χ values of the knickpoint can be interpreted as knickpoint travel times, τ , in millions of years (Equation 8) as shown by the knickpoint χ value equal to three at 3 m.y. after a perturbation.

Following both a uniform pulse of uplift (Fig. 3C) and a step decrease in equilibrium profile steepness resulting from an increase in bedrock erodibility (Fig. 3D), river profile steepness is unaffected by the perturbation until the knickpoint propagates upstream. Consequently, the river network upstream of the knickpoint retains the pre-perturbation uniform equilibrium k_{sn} and erosion rate. A vertical-step knickpoint is formed by the uniform pulse of uplift whereas a slope-break knickpoint is formed by the step decrease in equilibrium steepness. Tributaries collapse with the mainstem throughout both simulations. Following a uniform pulse of uplift, incision below paleotopographic markers is uniform both above and below the knickpoint but greatest downstream of the knickpoint, whereas following a step decrease in equilibrium steepness, incision increases up to the mainstem knickpoint and is greatest and uniform upstream of the knickpoint.

In contrast to these two simulations, both mainstem beheading (Fig. 3E) and rigid-block tilting (Figs. 3F and 3G) immediately perturb channel steepness along the entire mainstem away from an equilibrium state causing a slope-break knickpoint to form at the outlet and propagate upstream (hereafter referred to as the “mainstem knickpoint”). The mainstem knickpoint separates a downstream reach that is in equilibrium with the ongoing uplift rate (uniform k_{sn} in the cases with uniform background uplift and nonuniform k_{sn} in the case of continuous rigid-block tilt) from an upstream disequilibrium reach with nonuniform k_{sn} . Additionally, these perturbations to channel steepness along the entire mainstem initiate an immediate, but transient, response along the entire mainstem.

For the case of mainstem beheading (Fig. 3E), channel steepness along the entire mainstem profile is decreased such that the erosion rate is

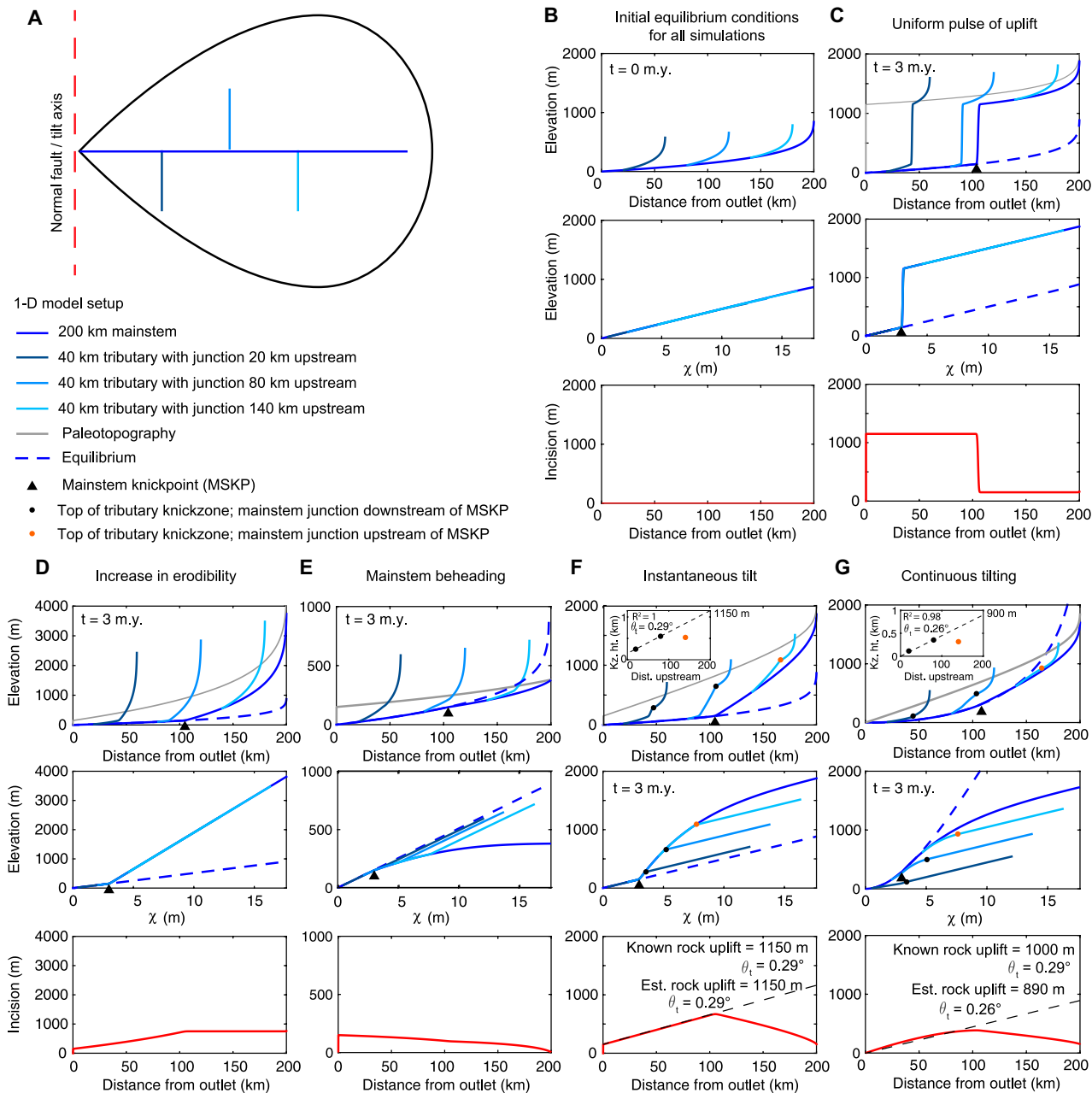


Figure 3. Results from linked 1-D simulations of an equilibrated river network subject to various perturbations at $t = 0$ that move river profiles away from equilibrium; adapted from Beeson and McCoy (2020). (A) Linked 1-D river profile model setup with 200-km-long mainstem and 40-km-long tributaries oriented perpendicular to mainstem. (B) Initial conditions for all simulations in Figure 3 in which the idealized river network is equilibrated to uniform rock uplift rate of 50 m m.y.^{-1} and rock erodibility of $1 \times 10^{-6} \text{ m}^{0.1} \text{ yr}^{-1}$. (C–G) Results at $t = 3$ m.y. for simulation of instantaneous uniform uplift of 1 km (C), a step-increase in erodibility or equivalently a step decrease in rock uplift rate (D), instantaneous truncation of a 300-km-long river to a 200-km-long river (E), instantaneous tilting with tilt axis at the river mouth, perpendicular to the mainstem, and 1 km maximum uplift at the channel head (F), and continuous tilting with tilt axis at the river mouth, perpendicular to the mainstem, that results in 1 km of rock uplift at the channel head after 3 m.y. (G). The upper row of plots shows longitudinal profiles with shades of blue corresponding to mainstem and tributaries shown in A. The gray line marks the pre-perturbation elevation of the river at $t = 0$ m.y. and advects with the rock uplift rate through time to track the potential elevation of paleoriver deposits, i.e., “paleotopography.” The middle row shows χ plots for the mainstem and tributaries, and the lower row shows incision below the paleotopography markers since $t = 0$ m.y. In all plots the dashed blue line denotes the final equilibrium state post-perturbation. Upper insets in F and G show calculation of tilt magnitude from tributary knickzone drop height using knickzones downstream of mainstem knickpoint (black markers). Regressions in lower plots of F and G show calculation of tilt magnitude from incision below paleotopography downstream of mainstem knickpoint. Est.—estimated.

less than the rock uplift rate, allowing the mainstem to begin steepening. The profile near the truncation point experiences a greater fractional change in drainage area than the river outlet. This causes the profile to have negative curvature on a χ plot and the new headwaters to be farthest below equilibrium with the lowest k_{sn} . The incision depth below paleotopography markers is maximum at the outlet and decreases toward the headwaters largely mirroring the decreasing values of k_{sn} . In response to the ongoing relative baselevel rise at the mainstem-tributary junctions, low-gradient reaches begin to form at the outlet of each tributary, but otherwise tributary steepness is not impacted by the perturbation and thus they plot above the mainstem and do not collapse onto it.

For the case of instantaneous rigid-block tilting (Fig. 3F), the mainstem experiences a uniform increase in profile gradient (equal to the tilt angle) that results in the greatest elevation change at the channel head. However, owing to the nonlinear downstream increase in drainage area, k_{sn} is increased by a greater degree near the outlet, resulting in negative curvature of the mainstem χ plot. With increased k_{sn} , erosion is greater than the background rock uplift rate, allowing the mainstem to begin incising. Tributary knickzones form at each mainstem-tributary junction as a result of the ongoing baselevel fall in the mainstem. These knickzones are unique in that they have nonuniform steepness that mirrors that of the mainstem and they record both the magnitude and timing of tilt. The timing of tilt can be found by subtracting the τ value of the top of the knickzone from that of the mainstem-tributary junction. Once the mainstem knickpoint has passed, the drop height from the top of the knickzone to the mainstem-tributary junction records the total rock uplift that occurred from the rigid-block tilt and from the background uplift rate since tilting (Fig. 3F inset in top plot). Incision below paleotopography markers increases linearly upstream to the location of the mainstem knickpoint, reflecting complete incision of the rock uplifted during the pulse of tilting, and then decreases upstream from the knickpoint to the channel head where passage of the mainstem knickpoint has yet to incise through the majority of rock uplifted during the pulse of tilting. The magnitude of rock uplift at the crest can be found by projecting the trends downstream of the mainstem knickpoint in either tributary knickzone drop height or mainstem incision up to the channel head (inset plots in Fig. 3F). Tributary steepness upstream of the knickzone is unaffected by tilting owing to tributary orientation parallel to the tilt axis and thus they plot below the mainstem and do not collapse onto it.

The signatures generated by a step change from uniform background uplift to continuous rigid-block tilting are similar in appearance as those generated by a instantaneous pulse of rigid-block tilting but with some important distinctions (compare Figs. 3F and 3G). In the instantaneous tilting simulation, the mainstem below the knickpoint is linear in the χ plot and projection of that steepness to the headwaters shows that the pulse of uplift raised the landscape above equilibrium such that the post-pulse landscape is in a falling state. In contrast, in the simulation of a step increase in continuous tilt rate, the mainstem near the outlet has positive curvature in the χ plot owing to the ongoing nonuniform uplift field and projection of the new equilibrium steepness to the headwaters reveals the landscape is below equilibrium and hence is in a rising state. With continuous tilting, the downstream section of the mainstem with equilibrium k_{sn} is separated from the upstream section with disequilibrium k_{sn} by a subtle negative-curvature knickpoint rather than a distinct positive-curvature knickpoint (Fig. 3G). Tributary knickzones are similar in character to those formed in response to instantaneous tilting, though they do not collapse with the mainstem and instead plot below the mainstem with increasing knickzone steepness in tributaries with junctions farther from the mountain front. The most important distinction between a punctuated tilt and a step change to continuous tilting is that, with a punctuated tilt, the mainstem knickpoint and top of tributary knickzones track the *cessation* of the punctuated tilting event, whereas with a step change to continuous tilting these track *onset* of tilting. The differences between the signatures of punctuated tilting and step change to continuous tilting are subtle and may be more difficult to discern in real landscapes with complications such as non-uniform K and variable stream azimuth.

The four tilting simulations in which 1 km of rock uplift at the channel head occurs over 1, 3, 5, and 10 m.y. but initial and final uplift gradients are equal illustrates how the duration over which tilting occurs impacts the fluvial response (Fig. 4). As tilt duration increases, the signatures of the tilting event become less pronounced because the equilibrium steepness for the increased tilt rate becomes closer to that of the initial condition. The mainstem knickpoint tracks the timing of the cessation of rapid tilting but, as tilt duration increases, the exact location of this knickpoint becomes more difficult to distinguish amid a broader zone of positive curvature. The transition to uniform steepness at the top of tributary knickzones tracks the timing of the onset of rapid tilting and the departure away from mainstem channel steepness tracks the cessation of rapid tilting, though tributary

knickzones get less well defined with increasing tilt duration and consequently both these points become increasingly more difficult to visually identify. Mainstem incision only slightly underestimates accumulated rock uplift in the first three simulations in which there is a transient response. Tributary knickzone drop height from the top of knickzones to the mainstem-tributary junction perfectly records the magnitude of rock uplift but as mentioned, the top of tributary knickzones becomes increasingly difficult to identify. In the fourth simulation in which 1 km of rock uplift occurs over 10 m.y. and uplift gradient remains unchanged, mainstem and tributary profiles retain equilibrium steepness throughout. The rate of mainstem incision is constant and equal to the rock uplift rate throughout this simulation, thus mainstem incision perfectly records the magnitude of rock uplift but no record of the magnitude of rock uplift is found in tributary profile form.

Beeson and McCoy (2020) also simulated the transient bedrock river response to instantaneous rigid-block tilt with the simplest cases of vertically bedded heterogeneous lithology: (1) a vertical bed of more erodible rock at 70–120 km upstream and (2) a vertical bed of less erodible rock at 30–50 km upstream. They showed that, following rapid tilting, knickpoints can form anywhere in the river network where more erodible rock occurs upstream of less erodible rock (Figs. 5A and 5B). Following their terminology, we refer to these knickpoints as “rock-type slope-break knickpoints.” In the case with a bed of more erodible rock, the passage of the rock-type slope-break knickpoint, well ahead of the knickpoint that started at baselevel, lowers channel steepness within the more erodible bed to form a quasi-equilibrium reach that is separated from the upstream river segment by a large knickzone (Fig. 5A). This transient response appears as a “bite” out of the river profile and the geometry of this bite reflects the magnitude of tilt such that the degree of tilt can be estimated by subtracting the angle of the quasi-equilibrium reach from the angle off the horizontal of the bite as a whole (Beeson and McCoy, 2020; Fig. 5C). Note that this method of estimating tilt magnitude relies on the assumption that the slope of the quasi-equilibrium reach through the bed of more erodible rock is similar to the initial river slope, with the slope of the quasi-equilibrium reach set by the erodibility of the rock as well as the rate of baselevel fall at the downstream end of the bed. In the case with a bed of less erodible rock, a knickzone forms at the downstream end of the bed when the mainstem knickpoint gets stalled in the less erodible rock and an additional rock-type slope-break knickpoint forms at the upper end of the bed (Fig. 5B). The river upstream of

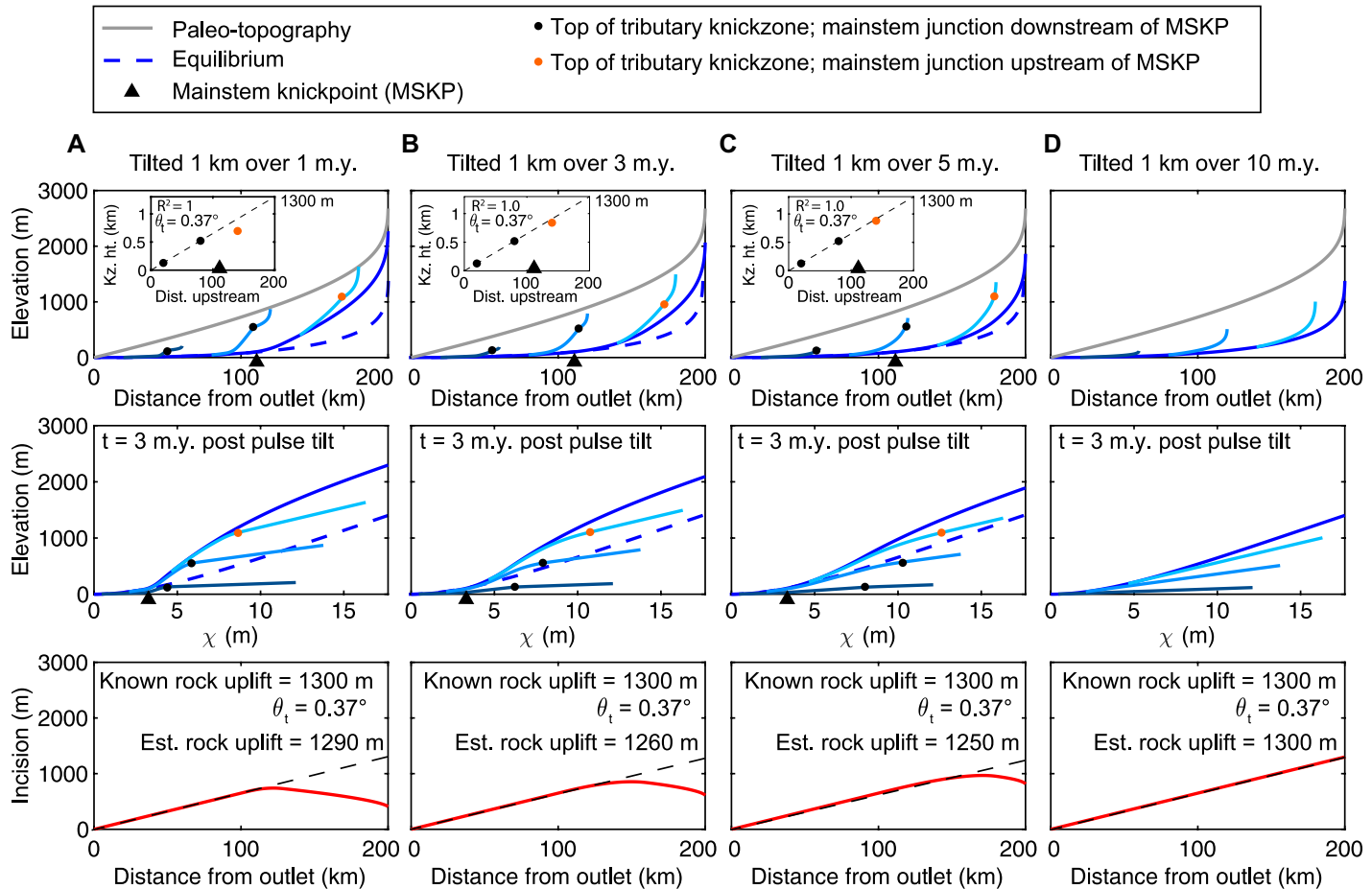


Figure 4. Results from linked 1-D simulations of an equilibrated river network subject to rigid-block forward tilting of equal accumulated tilt magnitude but of increasing duration; adapted from Beeson and McCoy (2020). All simulations began with initial conditions equilibrated to a tilting rate of 100 m m.y.^{-1} at the channel head and were returned to this tilting rate after the period of higher magnitude tilting ended. Columns show the results 3 m.y. following the cessation of more rapid tilting that uplifted the channel head by 1 km over 1, 3, 5, and 10 m.y. Upper insets show calculation of tilt magnitude from tributary knickzone drop height using knickzones downstream of the mainstem knickpoint (black markers). Regressions in lower plots show calculation of tilt magnitude from incision below paleotopography downstream of the mainstem knickpoint. Est.—estimated.

the bed erodes to a near-equilibrium slope while the mainstem slope-break knickpoint propagates very slowly through the hard rock. Although the river approaches a near-equilibrium slope it remains much higher than equilibrium elevation and thus the depth of incision is less than the magnitude of rock uplift.

MAPPING THE DEGREE OF PLANFORM RIVER BASIN GEOMETRIC DISEQUILIBRIUM IN RIVER NETWORKS DISSECTING THE WESTERN SLOPE OF THE SIERRA NEVADA

The map of χ across the Sierra Nevada reveals substantial geometric disequilibrium in river basin geometry north of the Merced River, as indicated by the disparity in channel-head χ val-

ues across many divides (Fig. 6). Smaller basins that do not reach to the crest have consistently high channel-head χ values relative to their neighboring crest-draining basins and in many cases appear much narrower than their neighbors and terminate in anomalous “spear tip” shapes. South of the Merced River the degree of geometric disequilibrium is noticeably lower. The high degree of geometric disequilibrium in the northern Sierra river networks corresponds to areas with documented beheading of the former river network (Cassel et al., 2009a; Garside et al., 2005; Henry, 2009; Henry et al., 2012; Henry and Faulds, 2010; Yeend, 1974) as well as to areas with deposition of Mio-Pliocene volcanics that altered or obliterated the course of the former river network (Bateman and Wahrhaftig, 1966; Busby et al., 2008; Christensen, 1966; Curtis, 1953; Durrell, 1966; Slemmons, 1966).

These patterns of geometric disequilibrium suggest that many divides separating river basins draining the western slope of the northern Sierra are unstable and are likely moving or are going to move in a direction that would decrease the overall degree of geometric disequilibrium (Chen et al., 2021; Hu et al., 2021; Willett et al., 2014). To evaluate current divide motion in the Sierra Nevada, we calculated local relief over a moving window with radius 250 m, which has been shown to be a strong predictor of active divide migration (Forte and Whipple, 2018). Basins in the southern Sierra that appear to be close to geometric equilibrium commonly have relatively symmetric divides and/or concordant knickpoints (Fig. 7A). Drainage divides in the northern Sierra have strong asymmetry and prominent changes in local relief between mainstem rivers and sub-basins in a direction that would promote motion

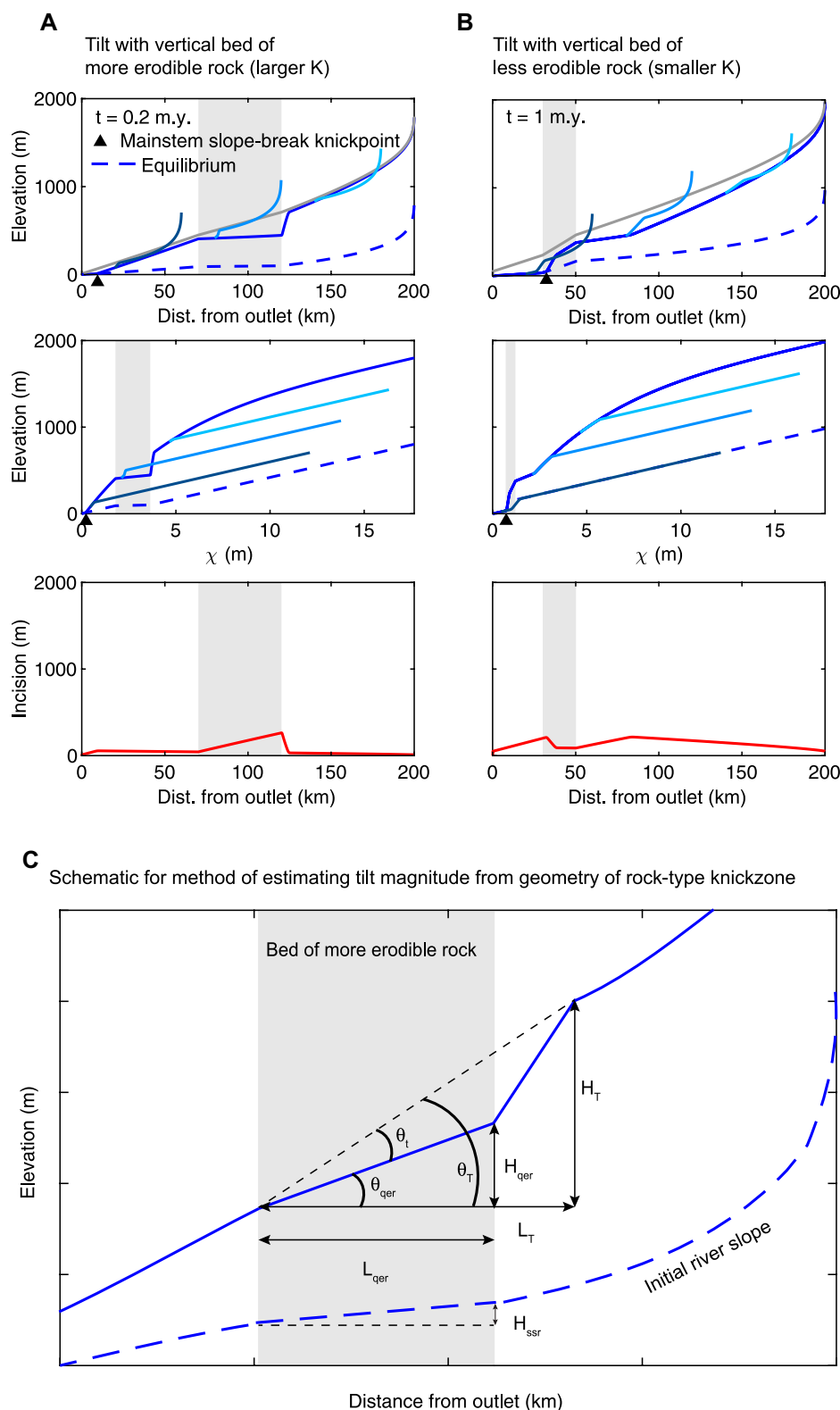


Figure 5. Results from 1-D simulations of instantaneous tilt with simple cases of vertically bedded heterogeneous lithology; adapted from Beeson and McCoy (2020). (A) Results at $t = 0.2$ m.y. for simulation of instantaneous rigid-block tilt that raised the channel head 1 km with a band of more erodible rock at 70–120 km upstream. (B) Results at $t = 1$ m.y. for simulation of instantaneous rigid-block tilt that raised the channel head 1 km with a band of less erodible rock at 30–50 km upstream. (C) Schematic showing how the tilt angle (θ_t) can be estimated by subtracting the angle of the quasi-equilibrium channel through the band of more erodible rock (θ_{qer}) from the angle off the horizontal of the bite as a whole (θ_T) provided the quasi-equilibrium slope is similar to the initial river slope through the band. Dist.—distance.

both the magnitude of relief and the location of maximum relief relative to divides differs between adjacent basins (Figs. 7B and 7C). In multiple locations, this appears to have driven large headwater captures in which basins predicted by χ to be gaining drainage area captured the headwaters from basins predicted to be losing drainage area. These proposed captures are supported by anomalous topology and χ plots with the signature of area exchange and a knick-zone upstream of a capture point in the capturing stream (e.g., Fig. 8; Fig. S4). Large wind gaps occur in some cases (e.g., Fig. 8), but in other cases the topography appears to have adjusted to the post-capture distribution of drainage area. Captures most frequently occur where topology is favorable for an intersection and divide migration is not channel-head on channel-head.

We mapped potential stream captures throughout the Sierra using topology, topography, and χ maps (Fig. 9). All the potential stream captures mapped in Figure 9 occur in directions that reduce geometric disequilibrium. A handful of stream captures in the southern Sierra are not in the direction predicted by geometric disequilibrium and for that reason were not included in this map and as discussed in a later section can be interpreted as resulting from rapid tilting. In the majority of cases, we could identify channel heads which may have lost drainage area. However, we were unable to identify possible topologic reconstructions in all cases, possibly because further geometric change had obscured the pre-capture topology. We thus present the map in Figure 9 of potential captures to demonstrate the expected size distribution of recent captures as well as to demonstrate that rivers draining the western slope of the Sierra Nevada

toward geometric equilibrium (e.g., basins with locally high χ values have asymmetric divides that would move the divide inwards to shrink the basin) (Fig. 7B). Furthermore, many of these

asymmetric divides appear to be coincident with multiple small stream captures (Fig. 7C).

Although the major transients in the northern Sierra have yet to reach the main divides,

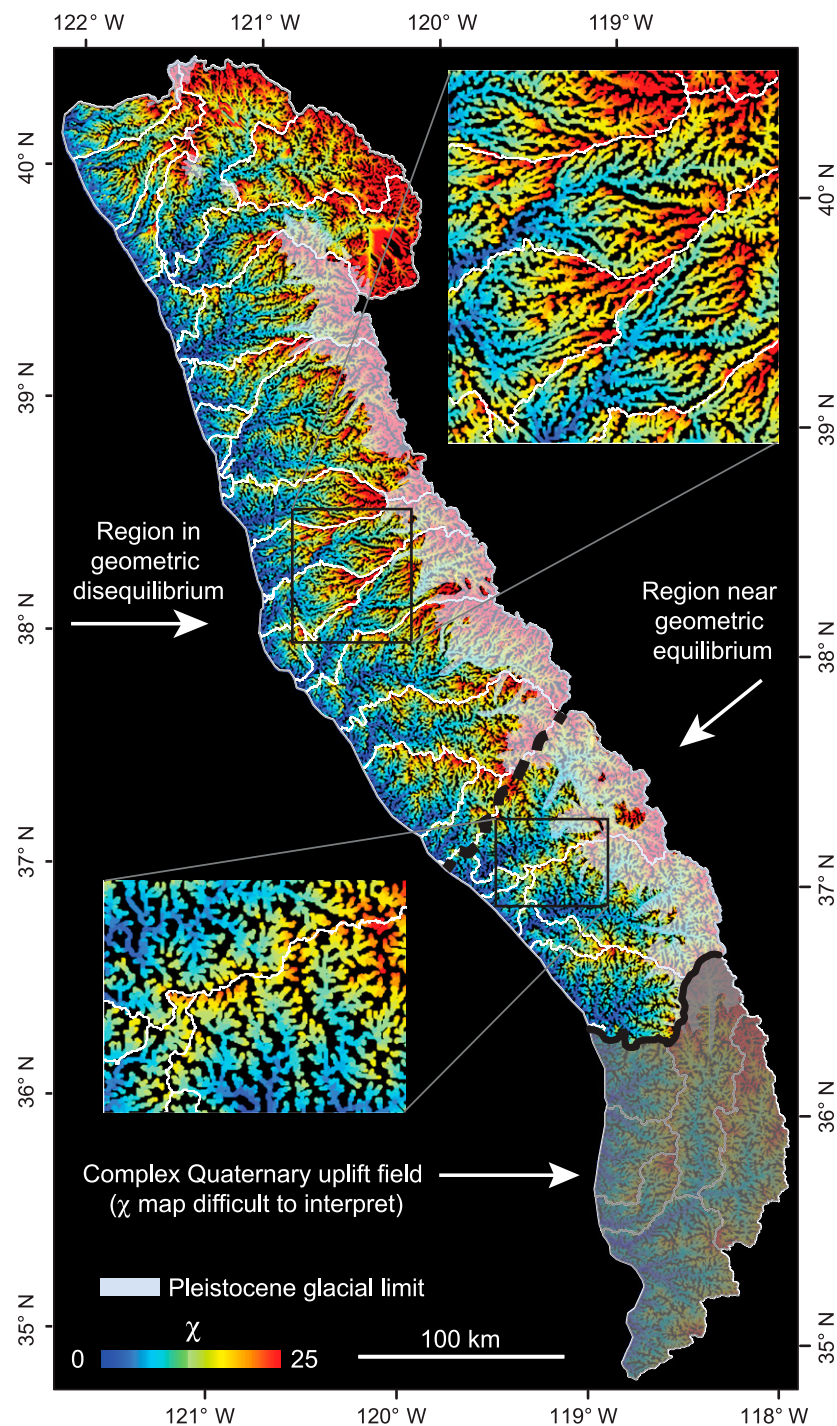


Figure 6. Map of χ for rivers dissecting the western slope of the Sierra Nevada, California, USA. Thick dashed black line separates the region with geometric disequilibrium in the northern Sierra from the region with a higher degree of geometric equilibrium in the southern Sierra. White lines delineate river basins at the USGS hydrologic unit code 8 scale. Extent of Pleistocene glaciation shown with light purple polygon. Upper right inset shows a close-up of the geometric disequilibrium characteristic of the northern Sierra, with large differences in channel-head χ across divides. Lower left inset shows a close-up of the geometric equilibrium characteristic of the southern Sierra, with similar channel-head χ across divides. River basins in the far southern Sierra are grayed out because χ is difficult to interpret in these basins owing to complicated Quaternary uplift on the Pond-Poso, Kern Gorge, and Garlock faults.

are actively reorganizing but not to suggest that the topology of any river basin could necessarily be reconstructed for a given time.

Both discrete and continuous changes in drainage area can impact channel profiles (Scheingross et al., 2020; Willett et al., 2014) and may thus modulate or obscure tectonic signatures. In the subsequent analysis, we focus on rivers that drain the Sierra crest and tributaries of those rivers that are the least likely to be highly impacted by ongoing drainage area exchange. Further, we reconstruct pre-capture topology for the largest stream captures in these basins to quantify the degree to which discrete changes in drainage area might have modified tectonic signatures. It is difficult to reconstruct continuous drainage area loss and to quantify exactly how it may have impacted tectonic signatures. We therefore do not include the non-crest draining rivers (Bear, Cosumnes, or Calaveras rivers) in our systematic analysis of tectonic signatures as we interpret χ values within and around these basins to indicate persistent drainage area loss in these basins. We do, however, discuss the tectonic signatures in these basins in order to address the question of how a transient response to a tectonic perturbation may be modulated by persistent drainage area loss.

CHARACTERISTICS OF DISEQUILIBRIUM CHANNEL PROFILE FORMS IN SIERRA RIVERS

Mainstem and Tributary Longitudinal Profiles and χ Plots

We identified equilibrated sections proximal to the mountain front in all mainstem rivers in the Sierra north of the Poso River (Fig. 10). In each river, the upstream end of the equilibrated section marks the location of a positive-curvature slope-break knickpoint, hereafter referred to as “mainstem tectonic knickpoints.” The locations of these knickpoints were identified as the point in each mainstem profile at which a generally abrupt and often sustained upstream rise in k_{sn} occurs that brings k_{sn} above the relatively low values measured near the mountain front (Fig. S6; see footnote 1). Note that the point at which k_{sn} begins to rise is not necessarily the point at which the largest increase in k_{sn} occurs or where the highest value of k_{sn} occurs. In the Merced and Mokelumne rivers, for example, the mainstem tectonic knickpoint marks the upstream point where k_{sn} begins to rise, but k_{sn} rises rapidly resulting in a prominent knickzone upstream of the mainstem tectonic knickpoint. Note that the mainstem tectonic knickpoints in these rivers are best seen in χ plots (Fig. 10), though we plot them on longitudinal river

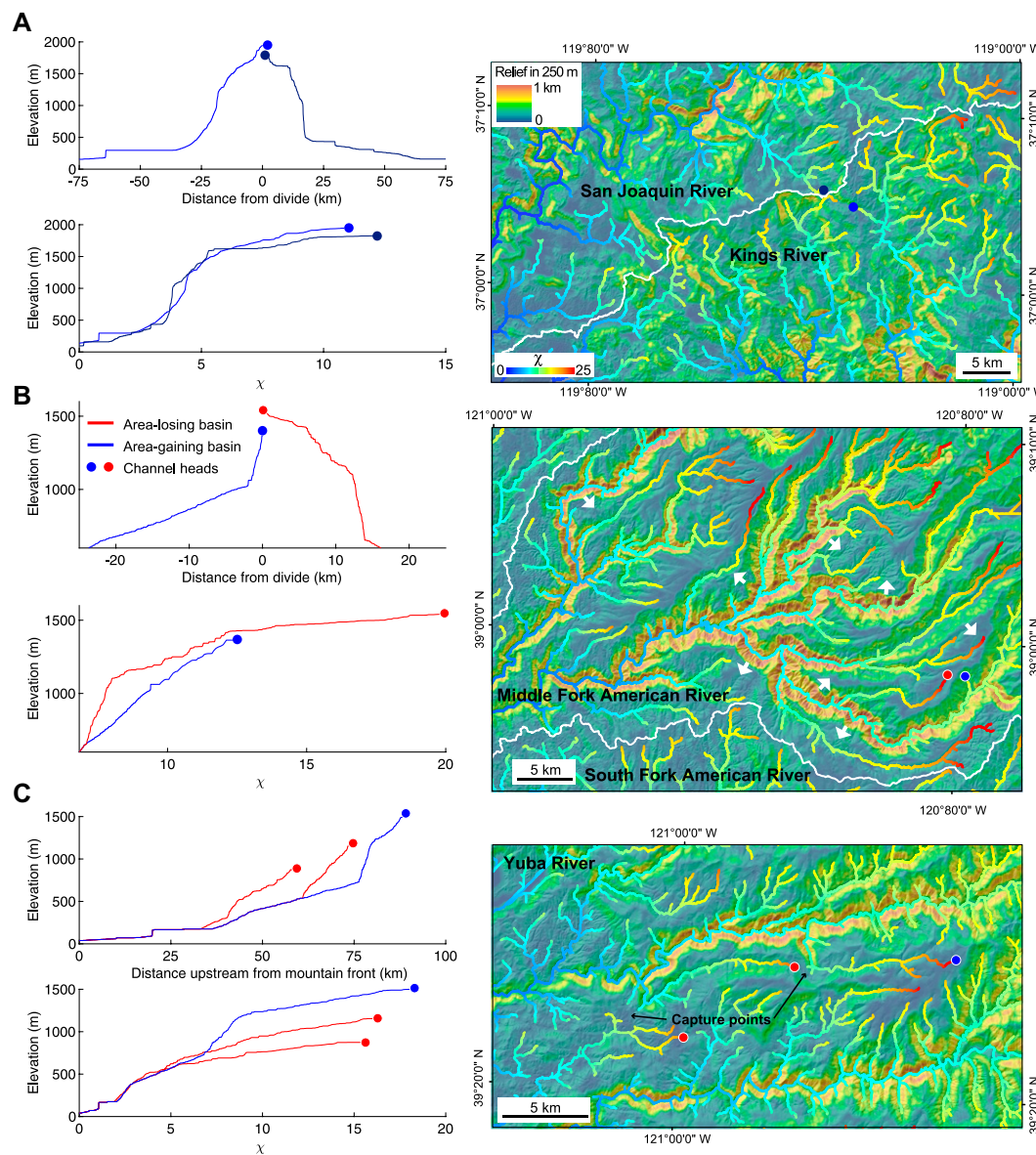


Figure 7. A representative symmetric divide in the southern Sierra compared to representative asymmetric divides in the northern Sierra, California, USA. Longitudinal river profiles and χ plots (left) and χ map overlaid on local relief calculated in a 250 m radius moving window (right). (A) Profiles and map for two streams originating on opposite sides of a symmetric divide separating the San Joaquin and Kings rivers, southern Sierra. (B) Profiles and map for two streams originating on opposite sides of an asymmetric divide separating sub-basins to the American River basin, northern Sierra. (C) Profiles and map for three tributary streams within the Yuba River basin showing stream captures that likely occurred sequentially as the wave of incision propagated up the mainstem.

profiles as well (Figs. 10 and 11). Surface geology mapped at 1:500,000 (Ludington et al., 2005) is shown underneath profiles with vertical contacts to schematically show the generally steep dips of contacts found in the Sierra (Fig. 11).

We calculated the mean k_{sn} for the equilibrated section proximal to the mountain front on each river using linear regressions. Based on the high goodness of fit of linear models to data in these sections, we projected the equilibrium profiles with uniform k_{sn} to the headwaters of each river. Comparison of these theoretical equilibrium profiles with modern profiles show that all major river basins appear to be in a declining state in that modern river elevations plot above the equilibrium line. In projecting these, we are assuming uniform rock erod-

ability and rock uplift, but we recognize that correct equilibrium profiles would have step changes in steepness that correspond to lithologic boundaries. In addition, we later present evidence that suggests a nonuniform modern uplift field. The equilibrium profiles shown in Figure 10 therefore represent a rough estimate of the equilibrium fluvial relief associated with modern boundary conditions.

Almost every river has a major reservoir built near the mountain front. These reservoirs were not removed from the longitudinal profiles or χ plots and show up within the equilibrated reaches as a vertical step followed by a flat reach. They were, however, removed from the linear regressions of χ and elevation data that were used to calculate average k_{sn} . Additionally, ~ 9 km of stream length that

ran through a region mapped as Quaternary alluvium in the 1:500,000 geology map (Ludington et al., 2005) near the river outlet was removed from the regression in all forks of the Yuba River. Although the Kaweah and Poso rivers run through mapped Quaternary alluvium for much of their equilibrated sections, in these rivers the mapped alluvium are narrow swaths in otherwise steep-walled bedrock valleys and field observations reveal exposures of bedrock in the active river channel not mapped at the 1:500,000 scale (Fig. S7; see footnote 1). Thus, we assume the deposition of Quaternary alluvium has not appreciably modified channel gradients associated with canyon cutting on million-year timescales and we include these reaches in our analysis.

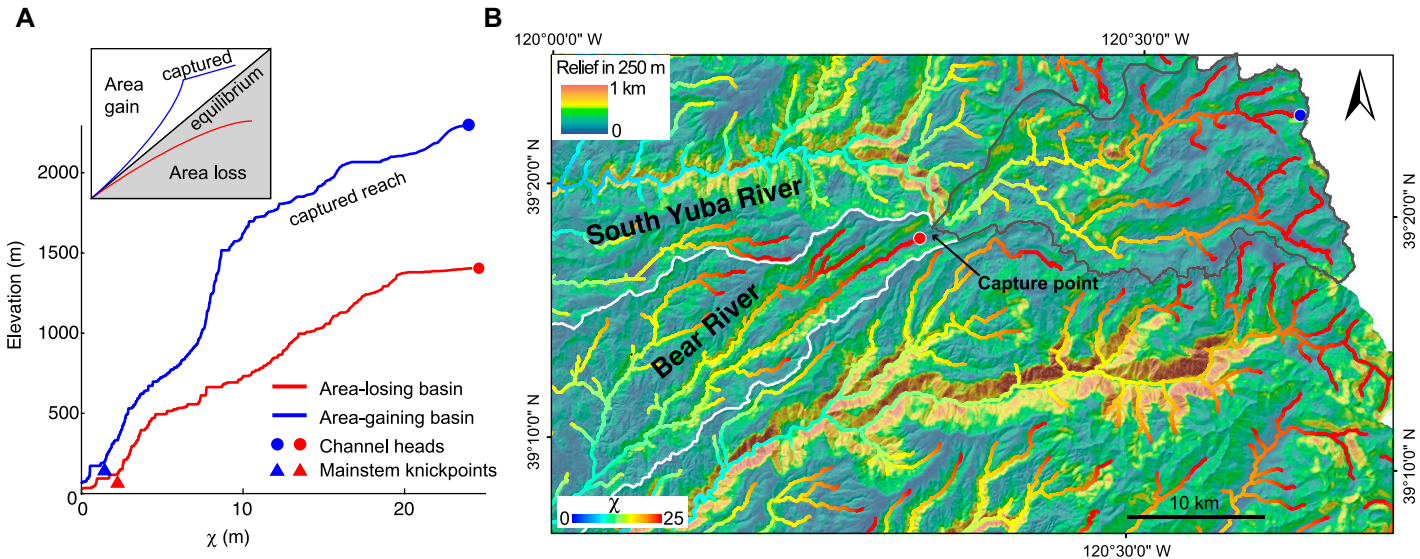


Figure 8. Map of proposed capture of the Bear River by the South Fork Yuba River in the northern Sierra Nevada, California, USA. (A) χ plot for the South Fork Yuba River (blue) and Bear River (red). Inset shows schematic of characteristic signatures of area exchange in χ plots. (B) χ map overlaid on map of local relief calculated in a 250 m radius moving window for the Bear and South Fork Yuba rivers. Area proposed to be captured by the South Fork Yuba is outlined in gray.

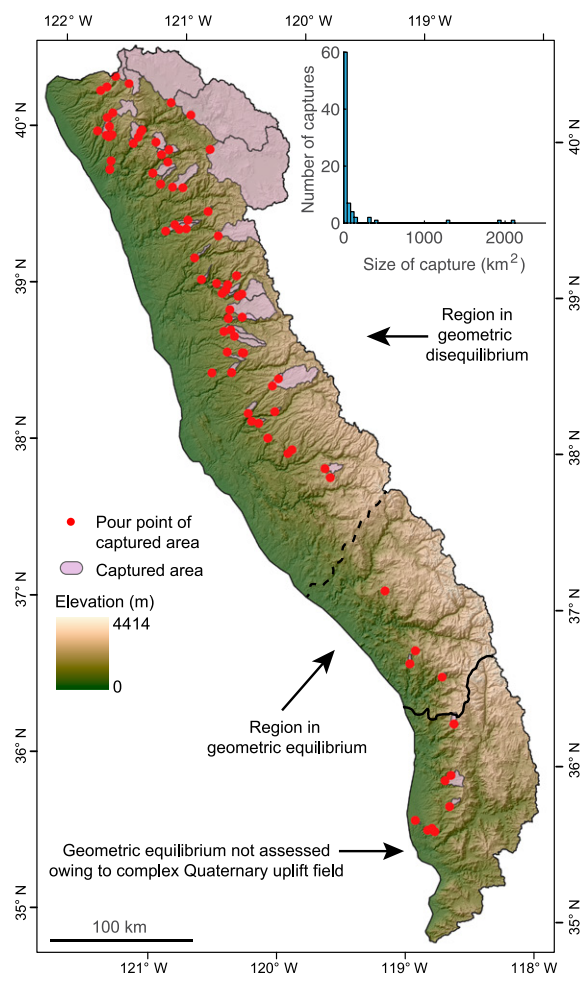


Figure 9. Map of potential stream captures in the Sierra Nevada, California, USA. Each captured area enclosed by a purple polygon represents a region with anomalous topology, a knickzone in the capturing basin upstream of the capture point, and local disequilibrium in river basin geometry. The dashed black line separates the region with geometric disequilibrium in the northern Sierra from the region near geometric equilibrium in the southern Sierra. Inset shows histogram of capture sizes.

Upstream of the mainstem tectonic knickpoints, χ plots of mainstem river longitudinal profiles from the Feather River south to Deer Creek have negative curvature, plot above the projected equilibrium χ profile (dashed blue line) and generally define the highest elevation portion of the cloud of χ -elevation data that represents the network of tributaries (Fig. 10). These mainstem longitudinal and χ profile forms suggest that the Sierra is in a transient state of adjustment to a change in boundary conditions. The location of the mainstem relative to tributaries in the cloud of χ -elevation data highlights the greater degree of disequilibrium in the mainstem as compared to the tributaries.

We examined tributary profiles for all major basins between the North Fork Yuba and the Kaweah rivers. We selected only sizeable tributaries that flowed through unglaciated terrain as mapped by Gillespie and Clark (2011) such that fluvial processes were assumed to be dominant. The Middle Fork Yuba was not included independently as its confluence with the North Fork occurs at 345 m and thus it shares the three lowest tributaries with the North Fork. Despite displaying a wide variety of forms, almost all tributaries analyzed have one prominent knickzone that is characterized by very high, but nonuniform, channel steepness, generally directly upstream from the tributary junction with the mainstem and downstream of headwaters with much lower channel steepness (Fig. 12). Many of these tributary knickzones collapse with the mainstem on χ plots. Some tributaries have a second or even a

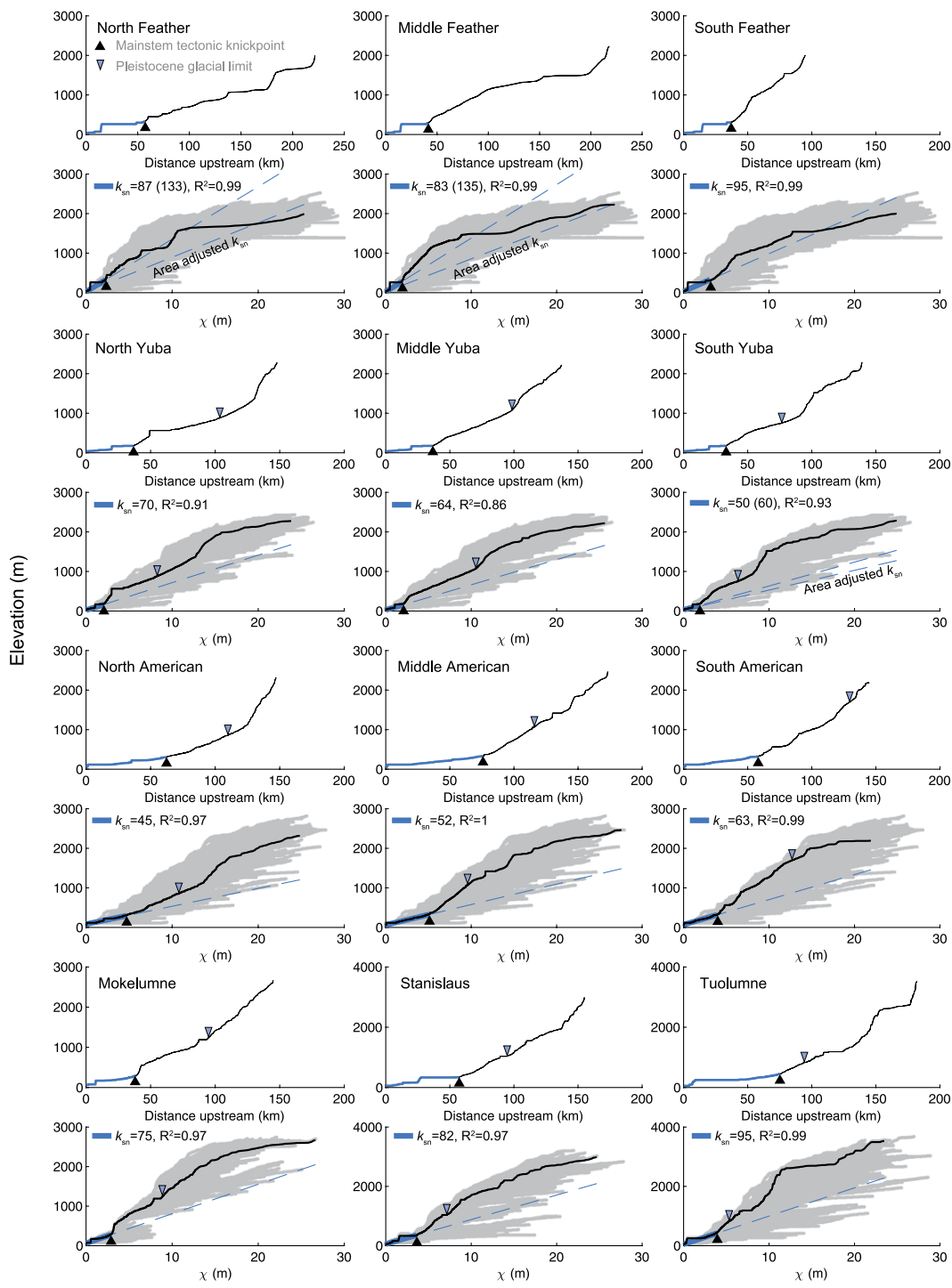


Figure 10. Longitudinal profiles and χ plots of all major rivers that drain the western slope of the Sierra Nevada, California, USA, with headwaters at the range crest. The upper plot for each basin shows the longitudinal profile of the mainstem. The lower plot is the χ plot for each basin. The gray envelope is formed by all points on the river network, whereas the black line connects points only on the mainstem. On both the upper and lower plots, portions of the mainstem with near-uniform steepness that were considered to be near an equilibrium grade are highlighted in blue and terminate at the mainstem tectonic knickpoint marked with a black triangle. Fluvial steepness, k_{sn} , determined from linear fits to the blue portion of the χ plot is reported for each basin and the dashed blue line illustrates an equilibrium profile with this steepness projected to the crest. Pleistocene glacial limit from Gillespie and Clark (2011) is shown with an inverted light purple triangle. Note that most rivers have reservoirs near the outlet that result in the flat reaches upstream of a vertical step, both of which were excluded from the regression analyses.

third smaller knickzone, particularly in the southern Sierra, though the presence, location, and drop height of these secondary profile forms are less consistent both within each river basin and among basins, and thus it is hard to distinguish a strong pattern in these secondary forms.

For each tributary, we identified the top of the most prominent knickzone as the first negative-curvature inflection point in channel steepness

on the χ plot and measured the difference in elevation between the top of each knickzone to the corresponding mainstem-tributary junction. Here we call this “knickzone drop height,” although for knickzones that have propagated upstream of the tributary junction, the measurement includes small portions of the tributary below the knickzone that are in equilibrium. We used the mainstem-tributary junction in all

cases because the bottom of the knickzone is not always easy to identify. We plotted knickzone drop height against the Euclidean distance from the mountain front to the corresponding mainstem-tributary junction (Fig. 12 insets). We chose to use Euclidean distance to the mountain front rather than river distance upstream because distance from the mountain front better reflects distance from the hypothesized tilt axis.

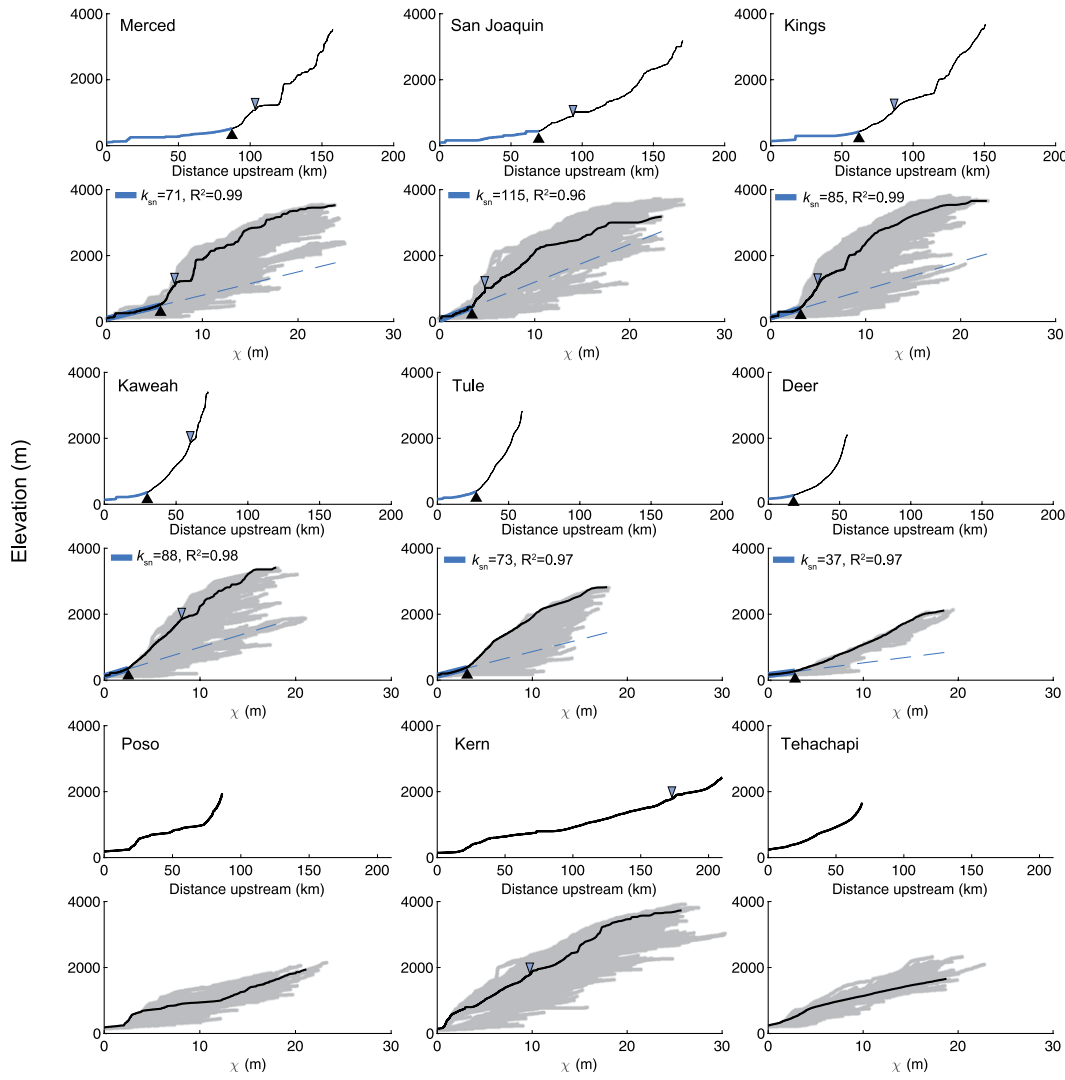


Figure 10. (Continued)

In the majority of basins, tributary knickzone drop height increases with distance from the mountain front up to the mainstem tectonic knickpoint (Fig. 12 insets), though no sizeable tributaries exist downstream of the mainstem tectonic knickpoint in the Mokelumne River. Tributary knickzone drop height continues to increase in many rivers upstream of the mainstem tectonic knickpoint, particularly in the northern Sierra, likely owing to incision in more erodible rocks upstream of the mainstem tectonic knickpoint that can lower the elevation of the mainstem relative to the tributaries. Trends in tributary knickzone drop height are further explored in subsequent sections.

Spatial Patterns in Normalized Channel Steepness and Rock Erodibility

To investigate the spatial and temporal patterns in rock uplift in the Sierra Nevada, we measured (1) mean k_{sn} of the equilibrium reach

downstream of the mainstem tectonic knickpoint in each river (as mentioned above), (2) mean k_{sn} of near-equilibrium sub-basins draining the unglaciated low-relief upland surface in the southern Sierra, and (3) mean basin k_{sn} for all basins (Fig. 13A). The k_{sn} values of equilibrium reaches between the mountain front and the mainstem tectonic knickpoint that occurs in most Sierra rivers should reflect recent to modern uplift rates and bedrock erodibility. In the North and Middle forks of the Feather River and in the South Fork Yuba River, topologic and geomorphic evidence of large stream captures suggests significant increases in drainage area to which the rivers have not yet adjusted (Figs. 8 and 9; Fig. S5; see footnote 1). Stream capture results in a transient increase in k_{sn} downstream of the capture point (Fig. 8A inset). Because we use k_{sn} of lower equilibrium reaches to understand spatial patterns in modern rock uplift, we additionally calculated k_{sn} for the equilibrium reaches in these rivers with

the drainage area of the proposed recent stream captures removed.

The low-relief upland surface in the southern Sierra is thought to primarily reflect Eocene boundary conditions (Clark et al., 2005), thus k_{sn} values for near-equilibrium sub-basins within this surface likely reflect Eocene rock uplift rates. To eliminate the influence of late Cenozoic processes, we chose upland sub-basins that (1) are below the Pleistocene glacial limit as mapped by Gillespie and Clark (2011); (2) are relatively parallel to strike such that, if younger tectonic tilting were present, their channel steepness would be unaffected; and (3) have nearly straight χ plots with $R^2 \geq 0.9$ on linear regressions to eliminate basins with transient river profile forms. We calculated the mean k_{sn} value for all sub-basins on the low-relief upland surface that fell within each major river basin as well as the mean k_{sn} of all sub-basins (Fig. 13A).

As a comparison to k_{sn} measurements that should correlate with modern and ancient rock

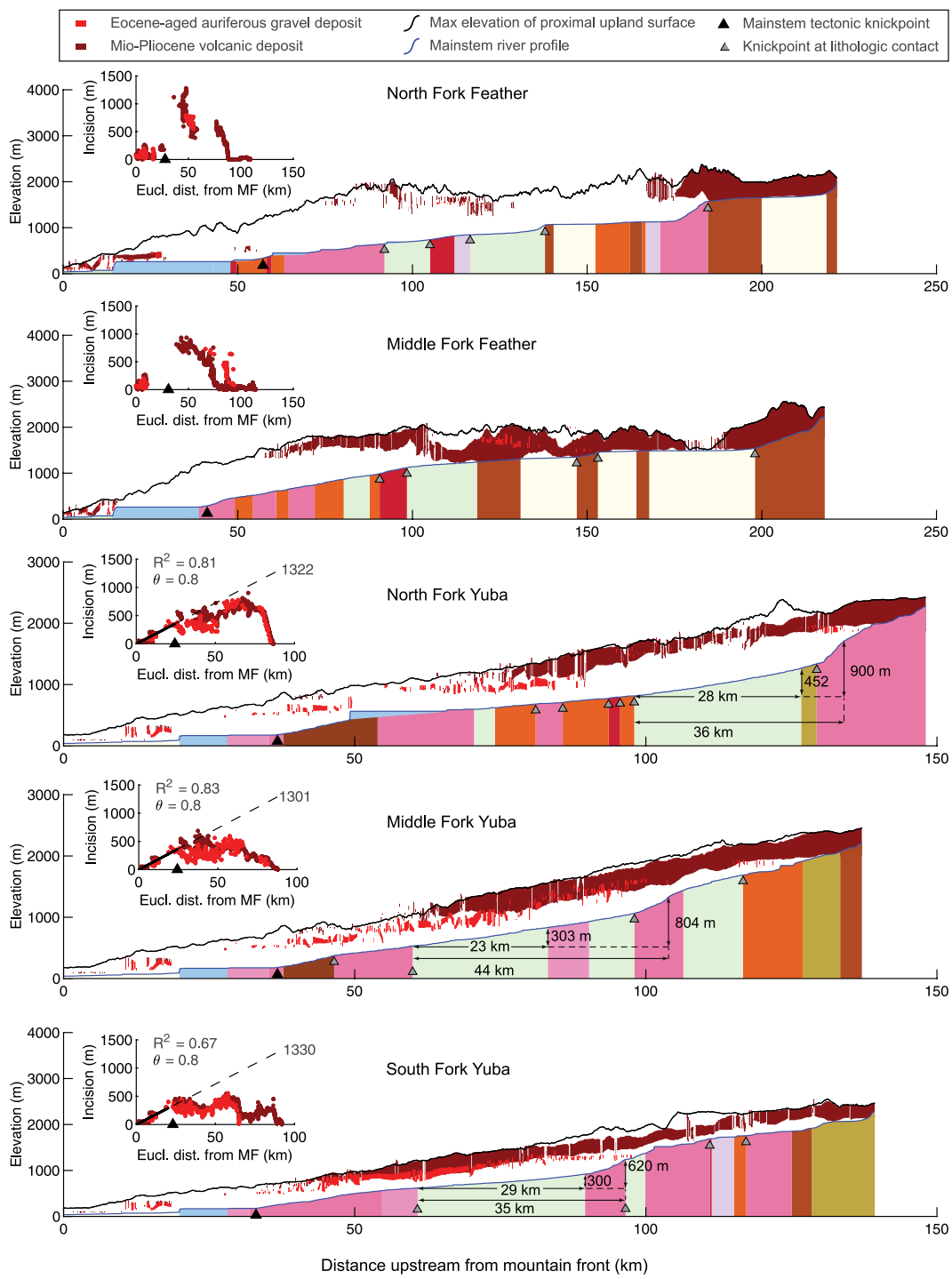


Figure 11. Longitudinal river profiles with surface geology and depth of river incision into basement rocks in the Sierra Nevada, California, USA. River longitudinal profiles are shown in blue with simplified surface geology (Ludington et al., 2005) shown underneath each profile with vertical contacts to schematically depict the generally steep dips of contacts found in the Sierra (see Fig. 2 for rock type legend). The maximum elevation of the upland surface found within a 15-km-wide swath centered on the river and smoothed with a 5 km moving window shown in black, with the minimum and maximum elevations of interfluve-capping Mio-Pliocene volcanic deposits (brown) and Eocene-aged auriferous gravels (red) in the swath encompassed by polygons. In the large reservoirs near the mountain front, water is projected to depth, whereas small reservoirs that occur within a single rock type are shown in light blue above surrounding geology. Black triangles mark the locations of the mainstem tectonic knickpoints. Small gray triangles mark a subset of knickpoints that occur at lithologic boundaries. The sections of river that we interpret to be deeply incised as a result of highly erodible rocks are annotated with arrows, with the shorter horizontal arrow demarcating the bed of more erodible rock, the longer horizontal arrow demarcating the full length of the incised section, and the longer vertical arrow demarcating the full drop height of the anomalously

incised section. Inset plots show incision into basement rock calculated as the difference between the modern river profile and the minimum elevation of proximal Cenozoic volcanic deposits (brown) or Eocene auriferous gravels (red) (Ludington et al., 2005; Saucedo and Wagner, 1992; Wagner et al., 1981). Where Cenozoic cover is absent or sparse, canyon relief is plotted as the difference in upland surface elevation proximal to the deeply incised canyons and modern river elevation. Incision depth or canyon relief is plotted against Euclidean distance (Eucl. dist.) from the mountain front (MF) calculated for the corresponding river nodes. Thick black lines on inset reflect linear fits to all incision data (Cenozoic volcanics and auriferous gravels) below mainstem tectonic knickpoints and dashed black lines show these fits projected to the modern range crest for each river. Number is crest uplift in meters estimated from regression. Insets that use canyon relief as an incision depth proxy use blue lines, but the same line styles. Profiles are labeled with basin name and are displayed by basin location from north to south.

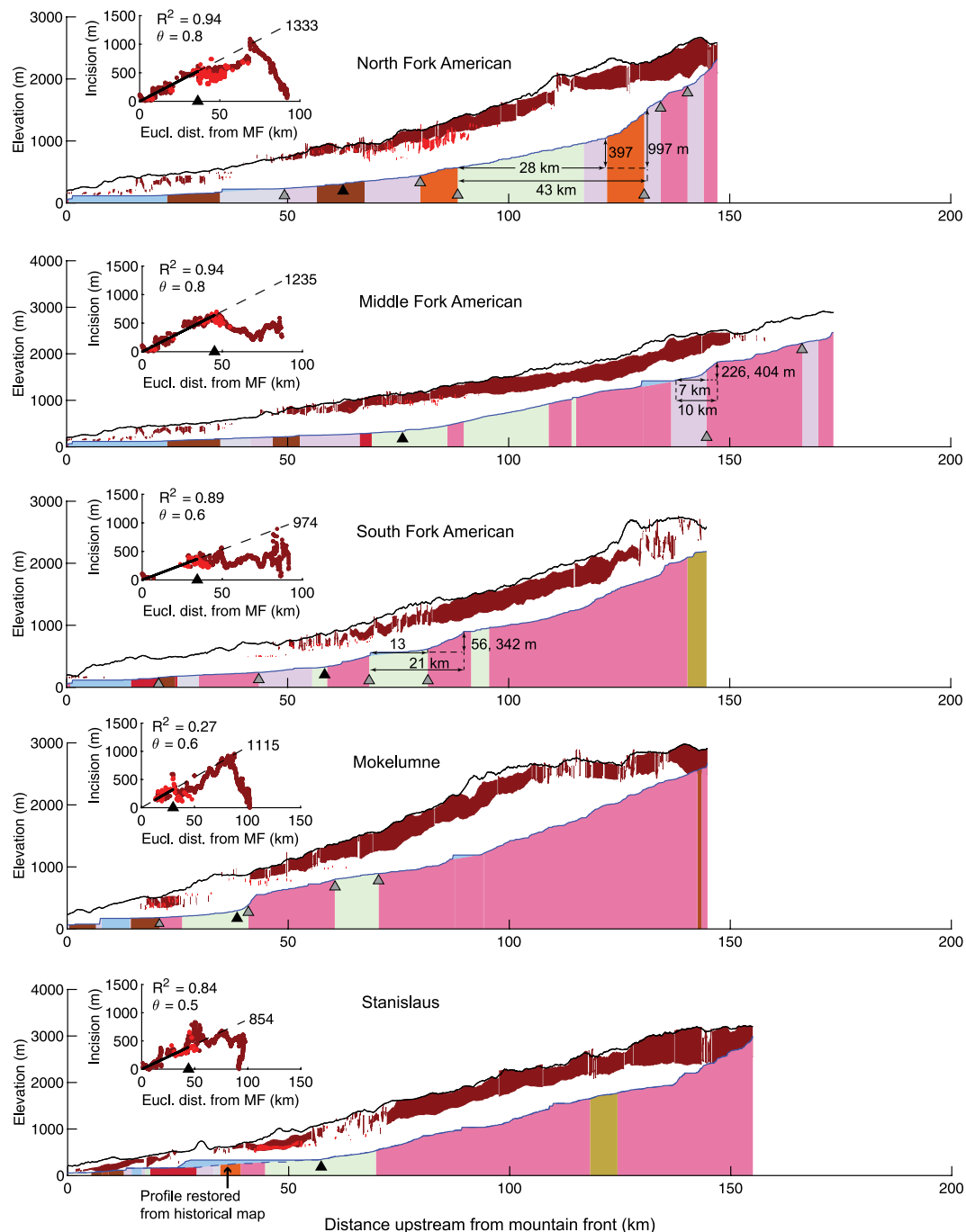


Figure 11. (Continued)

uplift rates, we also calculated a mean k_{sn} value for each major river basin by dividing mainstem fluvial relief (calculated as mainstem channel head elevation minus elevation of the river mouth) by the maximum channel head χ value. Given the disequilibrium state of Sierra rivers, mean basin k_{sn} values do not reflect steady uplift rates over a particular timescale but rather they are an integrated measure of the degree to which the steepness of the entire river basin is different than portions of the net-

work equilibrated to modern or past rock uplift rate. Mean basin k_{sn} values are closely related to modern crest elevation and thus surface uplift accumulated over an unknown period in the past. Mean basin k_{sn} exhibits a peak in the southern Sierra, with a maximum of $\sim 200 \text{ m}^{0.9}$ in the Kaweah River and $<100 \text{ m}^{0.9}$ at both ends of the range (Fig. 13A). Mean k_{sn} for upland surface sub-basins is $69 \text{ m}^{0.9}$, although substantial variability exists within each basin. Values of k_{sn} for the equilibrium reach down-

stream of the mainstem tectonic knickpoint are generally lower than mean basin k_{sn} and similar to or slightly higher than the mean of upland sub-basins. There is significant variability in k_{sn} values of equilibrium reaches downstream of the mainstem tectonic knickpoint, even among adjacent basins.

To investigate the role rock erodibility plays in shaping the spatial pattern in channel steepness, we measured k_{sn} in 3 km segments that occur within formations (not crossing lithologic

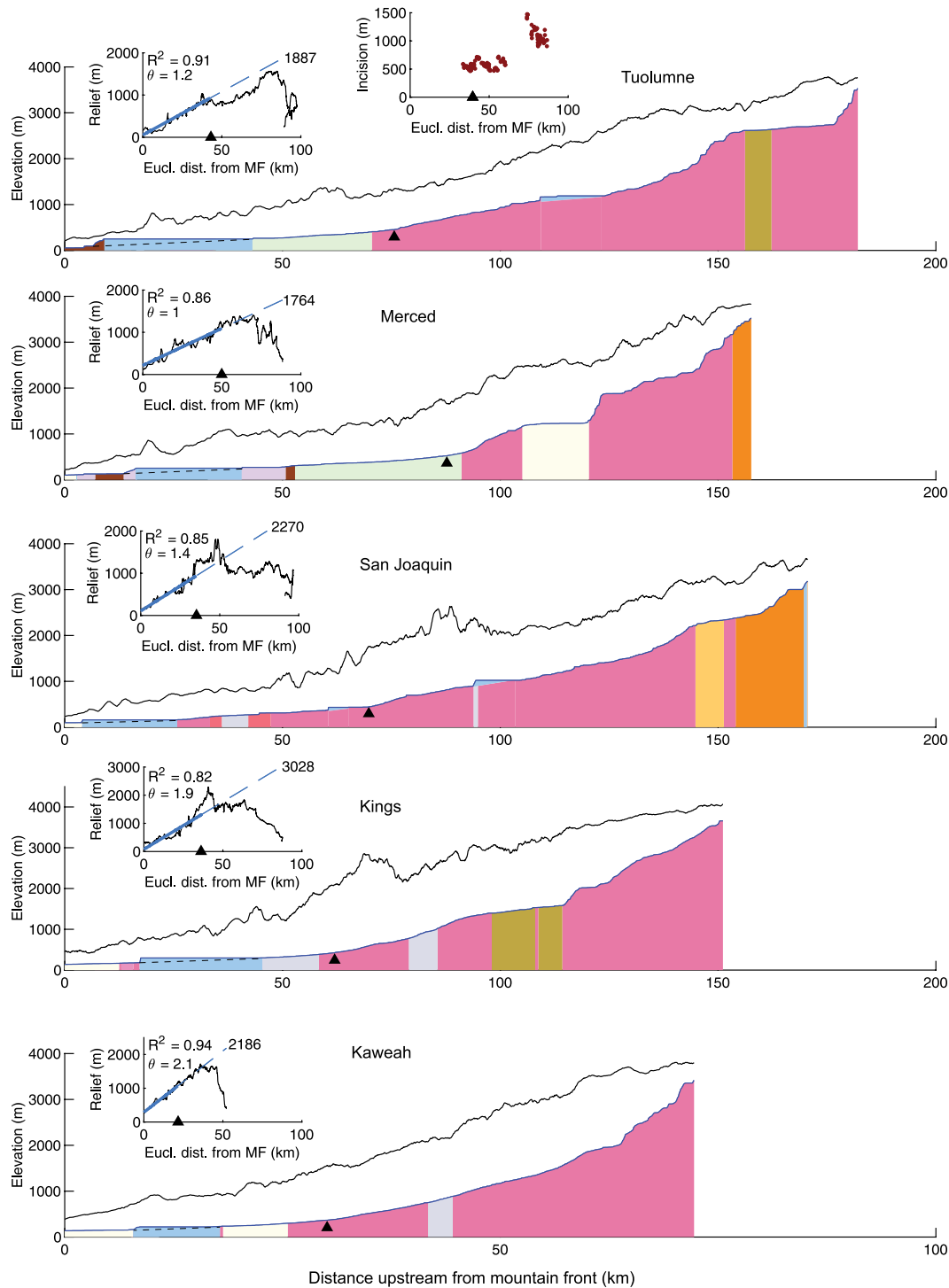


Figure 11. (Continued)

contacts) as defined by a simplified 1:500,000 geologic map (Ludington et al., 2005) in all crest-draining mainstem rivers from the Feather River south through the Kaweah River. We further grouped these segments into those downstream of the mainstem tectonic knickpoint in each basin and those upstream of the knickpoint (Fig. 14). Downstream of the mainstem tectonic knickpoint, the difference in k_{sn}

values between rock types is significant in only half the comparisons—when comparing Mesozoic plutonic rocks with variably metamorphosed Jurassic marine rocks and with Mesozoic volcanic and metavolcanic rocks, as well as when comparing Mesozoic volcanic and metavolcanic rocks with Paleozoic metasedimentary rocks ($p < 0.05$, Wilcoxon Rank Sum Test; Fig. 14A). Upstream of the

mainstem tectonic knickpoint, the difference in k_{sn} values between rock types is significant in five of the six comparisons ($p < 0.05$, Wilcoxon Rank Sum Test)—all but the comparison between Mesozoic plutonic rocks and Mesozoic volcanic and metavolcanic rocks. Lastly, and most notably, comparing k_{sn} values for segments within the same rock type, we find that k_{sn} values are significantly higher in 3 km

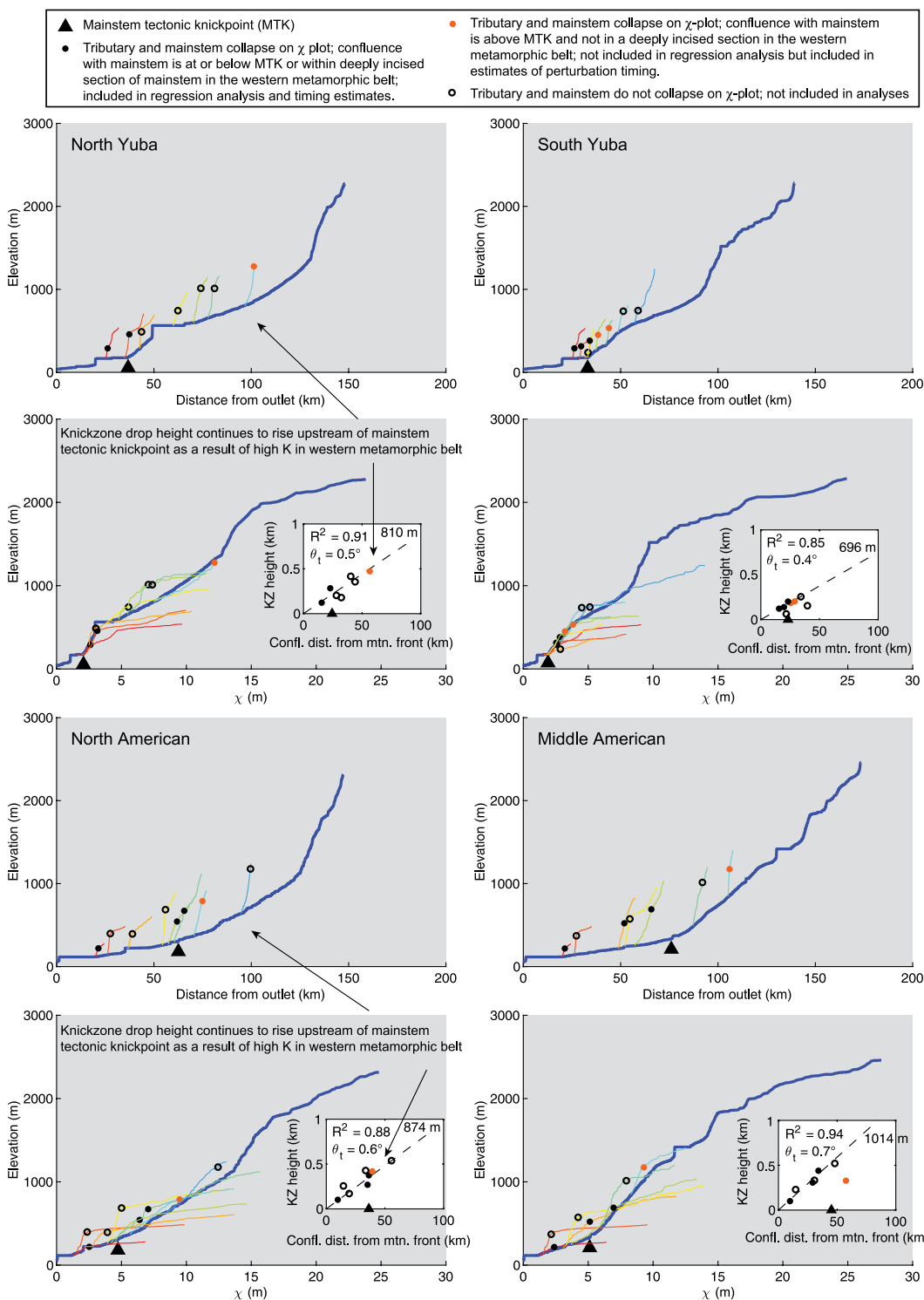


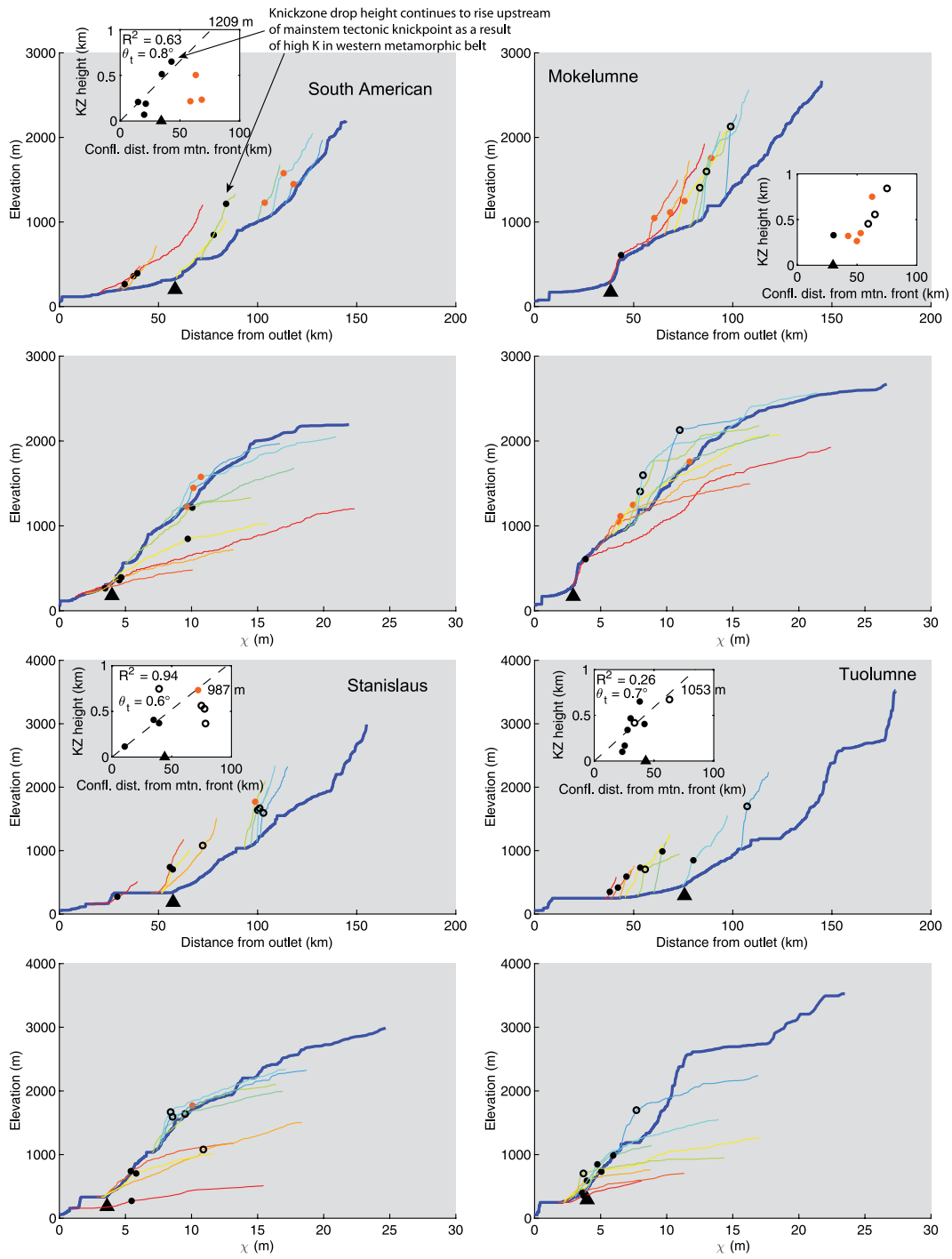
Figure 12. Longitudinal profiles and χ plots for mainstems and major tributaries draining the western slope of the Sierra Nevada, California, USA. Mainstems are shown as thick blue lines; tributaries change from warm to cool colors as the distance upstream from the mountain front to the mainstem-tributary junction increases. Insets show knickzone drop height plotted against Euclidean distance from the mountain front to the corresponding mainstem-tributary junction. Linear regressions shown with dashed line are projected to the location of the modern Sierra crest and only use measurements from tributaries that collapse toward the mainstem on the χ plot and have tributary-mainstem confluences located downstream of mainstem tectonic knickpoints or are within the western metamorphic belt (solid black circles). Best fit tilt angle (θ_t), R^2 , and surface uplift at the crest in meters inferred from regression are reported. Black triangles mark locations of mainstem tectonic knickpoints. KZ—knickzone; K—erodibility coefficient in stream power model; Confl. dist. from mnt. front—Confluence distance from mountain front.

segments upstream of the mainstem tectonic knickpoint compared with downstream of the knickpoint within Mesozoic plutonic rocks and Mesozoic volcanic and metavolcanic rocks ($p < 0.05$, Wilcoxon rank sum test; Fig. 14).

We used the K value for Mesozoic plutonic rocks (see Methods) to estimate K values for

other geological formations dominant on the western slope of the Sierra. Segments downstream of the mainstem tectonic knickpoint are assumed to be in approximate equilibrium with modern uplift rates and thus differences in k_{sn} should reflect differences in rock erodibility, K , rather than uplift, U (Equation 3). Assuming

segments flowing through Mesozoic plutonic rocks downstream of mainstem knickpoints have the same K value as the upland basins in Mesozoic plutonic rocks, we estimated a mean modern uplift rate of 98.0 ± 21.7 m m.y.⁻¹ (\pm standard error [\pm SE]) by using the equation $U = K * k_{sn}$ and substituting the

**Figure 12. (Continued)**

mean k_{sn} for stream segments downstream of the knickpoint flowing through Mesozoic plutonic rocks. We estimated the standard error on this estimate of uplift rate by adding the fractional standard error in quadrature and multiplying this by the estimate of U . Using this uplift rate and the mean k_{sn} value for each rock type, we calculated K values for three additional formations: Mesozoic volcanic and metavolcanics rocks ($K = 1.65 \times 10^{-6} \pm 4.3 \times 10^{-7}$

$m^{0.1}\text{yr}^{-1}$), Paleozoic metasedimentary rocks ($K = 1.11 \times 10^{-6} \pm 2.6 \times 10^{-7} m^{0.1}\text{yr}^{-1}$), and Jurassic marine rocks that have been variably metamorphosed ($K = 1.52 \times 10^{-6} \pm 4.1 \times 10^{-7} m^{0.1}\text{yr}^{-1}$) (Fig. 14). Uncertainty again reflects the propagated standard error of the means (SEM) using the SEM for the mean K for Mesozoic plutonic rocks and the SEM for the mean segment k_{sn} of each rock type. The results indicate that, between dominant lithologies, K likely var-

ies by less than a factor of 2. These dominant rock types occur at a range of distances from the mountain front such that if the modern uplift field is nonuniform, the change in U likely does not impact the mean k_{sn} .

The influence of rock erodibility on channel steepness can explain why the Yuba, San Joaquin, and Kaweah rivers, which all flow through Mesozoic plutonic rocks in their lower reaches, have comparatively higher k_{sn} values,

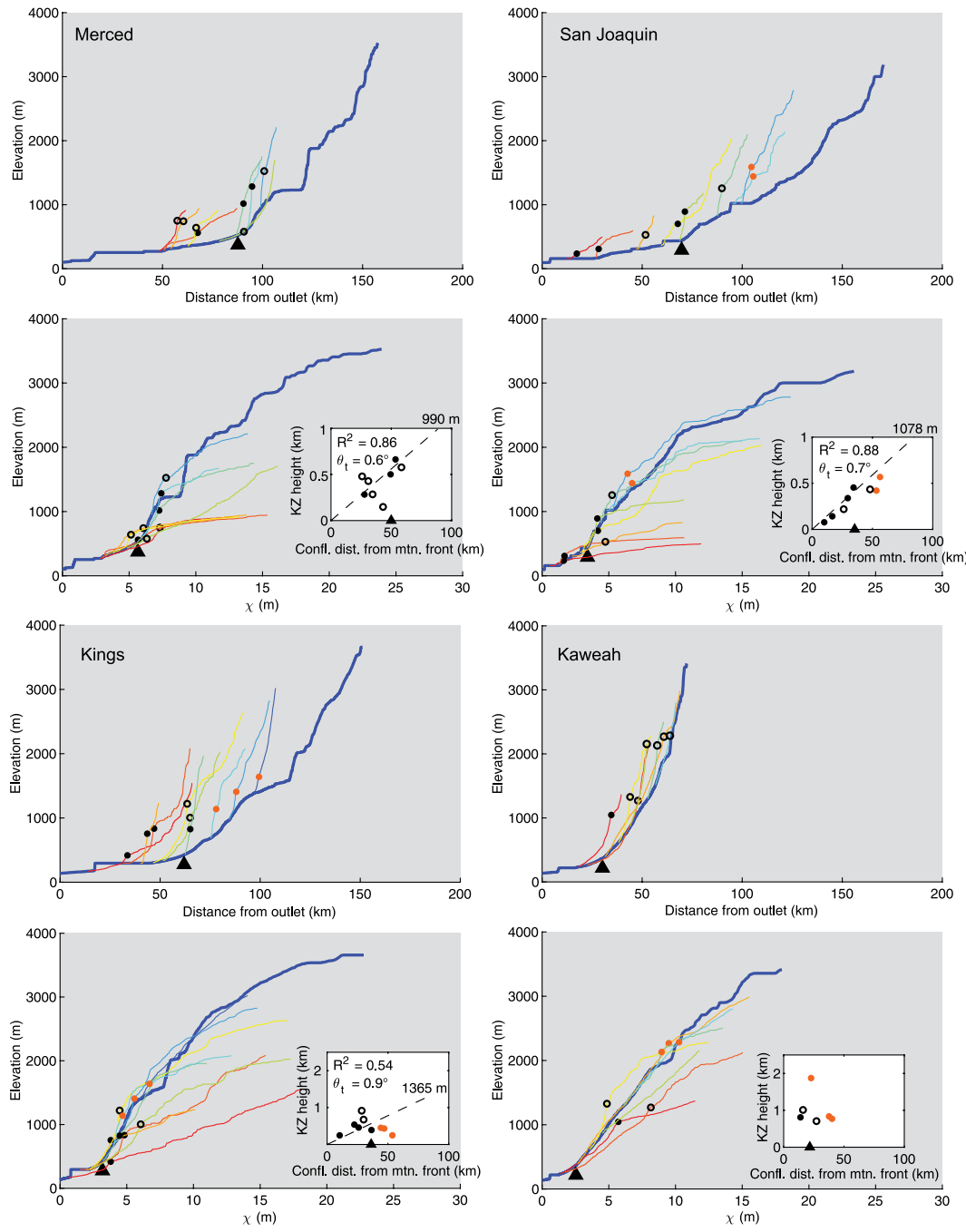


Figure 12. (Continued)

whereas the Mokelumne, American, Merced, and Kings rivers, which pass primarily through Paleozoic metasedimentary rocks and variably metamorphosed Jurassic marine rocks, have comparatively lower k_{sn} values in their equilibrium reaches (Figs. 13 and 11). Therefore, although the increase in k_{sn} values of the equilibrium reach downstream of the mainstem tectonic knickpoint in the central-southern Sierra may reflect an increase in modern uplift rates in that portion of the range, a strong pattern is difficult to distinguish amid the factor two

variability in erodibility and the influence of rock type.

Mean basin k_{sn} is less likely to reflect rock type as it incorporates significantly more channel length with heterogeneous lithology in all basins. Mean basin k_{sn} values south of the North Fork American River are greater than the k_{sn} of the corresponding equilibrated section and the overall mean k_{sn} of upland sub-basins (Fig. 13A). The discrepancy between the high values for mean basin k_{sn} and the lower k_{sn} values for equilibrium reaches

downstream of the mainstem tectonic knickpoint and upland sub-basins suggests that elevations along much of the modern Sierra Nevada crest are higher than elevations needed to have a river network in equilibrium with the modern uplift rate. In the central and southern Sierra where the difference between the equilibrium steepness and the modern mean basin steepness is greatest, crest elevations reside greater than a kilometer above what we interpret as the modern equilibrium line (Fig. 10). One explanation for this mismatch

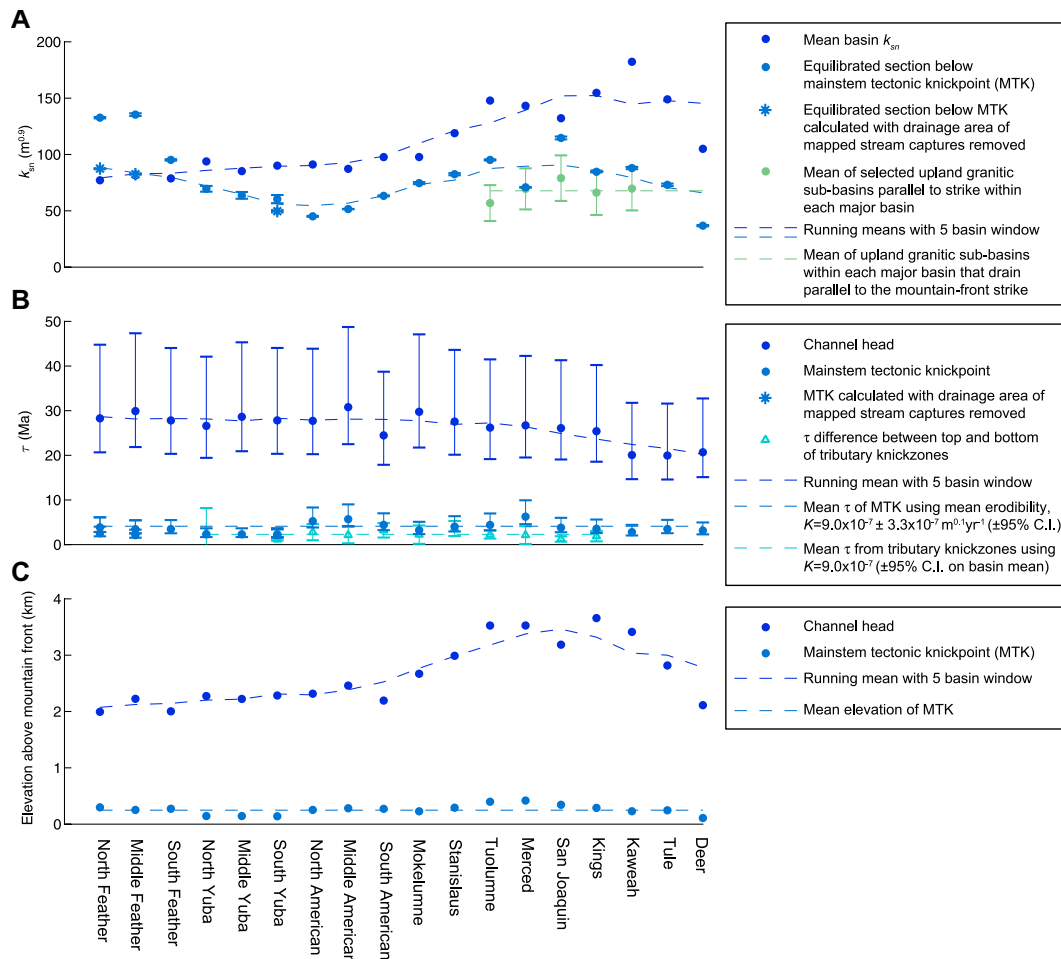


Figure 13. Summary of river steepness and channel response times for drainage basins and river segments in the Sierra Nevada, California, USA, displayed by basin name moving from north to south. (A) Normalized channel steepness, k_{sn} , for different sections of all major river basins draining the western slope of the Sierra. Error bars on the mainstem equilibrated reach measurements reflect the 95% confidence interval (C.I.) on the slope of the regression through χ -elevation data. Error bars on upland basins reflect the 95% C.I. for the mean k_{sn} of sub-basins within that basin. (B) Channel response time, τ , for channel heads and mainstem tectonic knickpoints, as well as time since cessation of pulse of tilt measured from tributary knickzones. Error bars reflect the 95% C.I. on the Sierra Batholith K (see Overview of Methods section and Fig. 14). (C) Elevations for mainstem channel heads and mainstem tectonic knickpoints.

could be a period of high rock uplift rate that is not matched by similarly high erosion such that significant surface uplift occurred.

Evidence that Mainstem Tectonic Knickpoints and Tributary Knickzones are Migrating

Changes in channel steepness along a river can reflect (1) spatial heterogeneity in rock erodibility, (2) migrating knickpoints/knickzones that are transmitting signals of changes in boundary conditions upstream, or (3) a combination of upstream migrating knickzones and heterogeneous lithology. Upstream migrating signals can be filtered through heterogeneous lithology to create spatial and temporal variability in channel steepness that does not always correspond to the erodibility of the underlying rock (Forte et al., 2016; Yanites et al., 2017). However, by taking lithology into account, it is possible to interpret tectonic signatures from landscapes (e.g., Gailleton et al., 2021). Changes in channel steepness that reflect spatial heterogeneity in rock erodibility should occur at lithologic boundaries and

thus as a group should show no consistency in terms of distance upstream or drainage area outside of the spatial pattern that may be imparted by the distribution of geologic formations. In contrast, migrating knickpoints/knickzones originate at baselevel and travel upstream at a rate that is a function of drainage area and rock erodibility (Equation 6). Migrating knickpoints that formed in response to the same perturbation should therefore show scaling between distance upstream and drainage area (e.g., Loget and Van Den Driessche, 2009).

To test whether the mainstem tectonic knickpoints and the tributary knickzones in the Sierra are indeed migrating, we measured distance upstream and mean drainage area between the knickpoint location and the outlet. For tributary knickzones, we measured distance upstream from the mainstem-tributary junction and mean drainage area between the top of the knickzone and the mainstem-tributary junction. For comparison, we identified a sample of mainstem knickpoints that occur at or near lithologic boundaries and measured distance upstream and mean drainage area for these as well (gray

triangle markers on Fig. 11). Mainstem tectonic knickpoints and tributary knickzones collectively show a strong relationship ($R^2 = 0.8$) between distance upstream and mean drainage area as found in many field studies constraining velocity of migrating knickpoints (Harkins et al., 2007; Hayakawa and Matsukura, 2003; Jansen et al., 2011; Lague, 2014; Loget and Van Den Driessche, 2009) (Fig. 15A). In contrast, no scaling is observed between mean drainage area and distance upstream for mainstem lithologic knickpoints. As described in the Overview of Methods section, the geometric parameter χ removes the effect of drainage area on river profiles, collapsing migrating knickpoints of the same origin to the same location in χ space. In the Sierra, both the mainstem tectonic knickpoints and tributary knickzones occur at similar locations in χ space upstream of their respective points of origin, whereas knickpoints at lithologic contacts have a much wider distribution that spans the entire river network from proximal to the mountain front to the headwaters (Fig. 15B).

A second line of evidence that the mainstem tectonic knickpoints are migrating lies in the

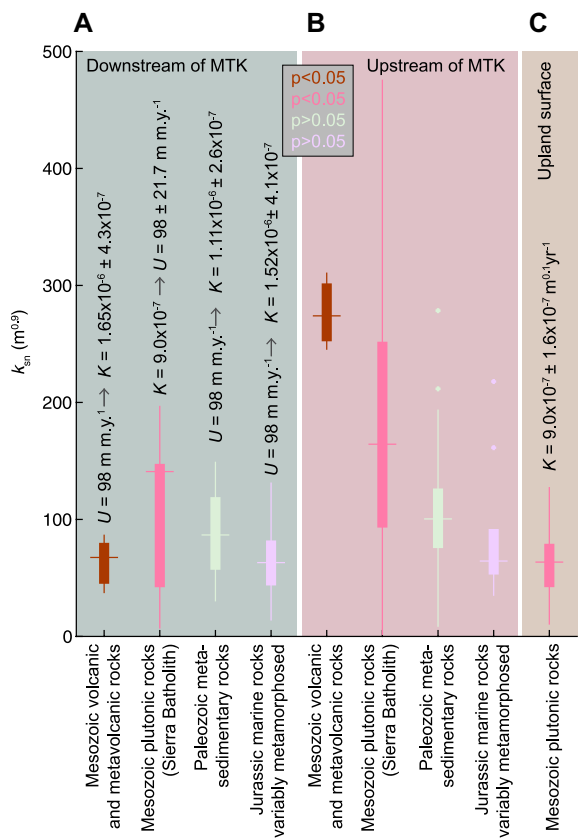


Figure 14. Spatial patterns in normalized channel steepness, k_{sn} , across the Sierra Nevada, California, USA. Boxplots show distributions of k_{sn} values measured from 3-km-long river segments that are grouped by location as well as the underlying lithology mapped on the 1:500,000 geologic map (Ludington et al., 2005). Colors of boxplots correspond to rock type (see legend in Fig. 2) and background panels correspond to segment locations. (A) Distribution of k_{sn} for 3-km-long segments extracted from mainstem rivers downstream of the mainstem tectonic knickpoint (Figs. 10 and 11). (B) Distribution of k_{sn} for 3-km-long segments extracted from mainstem rivers upstream of the mainstem tectonic knickpoint. (C) Distribution of k_{sn} values of small river basins underlain by granite within the unglaciated portion of the upland surface between the San Joaquin and Kings rivers that

we used to calibrate the stream power erodibility coefficient, K (a subset of those published in Callahan et al., 2019). Values for the erodibility coefficient, K , are shown above each rock type and were calculated as follows. Assuming segments flowing through Mesozoic plutonic rocks downstream of mainstem tectonic knickpoints have the same K value as the upland basins in Mesozoic plutonic rocks, we estimated a spatially averaged modern uplift rate of 98.0 ± 21.7 m m.y.⁻¹ (\pm SE). Using this uplift rate, we calculated K values for the other three formations shown here using segments downstream of the mainstem tectonic knickpoint that we assumed are in approximate equilibrium with the modern uplift field. Inset between A and B shows p-values for Wilcoxon Rank Sum tests comparing segments upstream and downstream of the mainstem tectonic knickpoint for each rock type, with p-values for each test colored by rock type. MTK—mainstem tectonic knickpoint; U—rock uplift rate.

spatial patterns in channel steepness relative to the location of the mainstem tectonic knickpoint. If the positive-curvature slope-break knickpoints that we identify as migrating tectonic knickpoints were instead stationary knickpoints generated by lithologic differences, we should not see systematic differences in channel steepness within the same rock type relative to the location of the mainstem tectonic knickpoint (Fig. 14). Additionally, the greater differences between the four dominant rock types upstream of the mainstem tectonic knickpoint (compared with smaller differences downstream) is consistent with the interpretation that upstream segments are in a transient state of adjustment to a perturbation, whereas downstream segments have reached a new equilibrium.

INTERPRETATION OF PERTURBATION TYPE RECORDED BY THE DISEQUILIBRIUM STATE OF SIERRA RIVERS

Disequilibrium Channel-Profile Forms along the Sierra Nevada are Consistent with a Short-Lived Rapid Pulse of Rigid-Block Tilting

In the Middle Fork American River south to the Deer River, the mainstem tectonic knickpoint separates a downstream reach of relatively low and near-uniform steepness from an upstream reach with much higher nonuniform steepness with negative curvature on χ plots (Fig. 10). Mainstems plot above most tributaries in χ

plots. Tributary knickzones in these rivers have nonuniform steepness, collapse at least in part with the mainstem on χ plots, and exhibit a trend of increasing drop height moving upstream to the mainstem tectonic knickpoint, at which point drop height begins to decrease (Fig. 12). Late Cenozoic drainage area loss (Henry et al., 2012; Huber, 1981; Wakabayashi, 2013) may have brought the mainstems below some of the tributaries in the χ plot (Willett et al., 2014) and glaciation could also have lowered mainstem elevations relative to tributaries (Gillespie and Clark, 2011) such that without these processes the mainstems might better define the upper envelope of the χ plots. In total, these signatures in the mainstem and tributaries are most consistent with those observed in the 1-D simulations of a short-lived rapid pulse of rigid-block tilting (Figs. 3F and 4A). However, the distinctions between signatures of a pulse of tilting versus onset of continuous rapid tilting are subtle (compare Figs. 3F and 3G) and the lower reaches of Sierra rivers, in which many of the important differences occur, are highly impacted by reservoirs and heterogeneous lithology. Although our preferred interpretation is that of a short-lived rapid pulse of tilting owing to the generally low and near uniform steepness of mainstems below the mainstem tectonic knickpoint that project well below the elevation of the upstream river network, the collapse of tributary knickzones with mainstems on the χ plot, and the distinct nature of both the mainstem knickpoints and the top of tributary knickzones, we recognize that a step change to rapid continuous tilting is difficult to rule out completely using only river profile forms. In both of these cases, however, mainstem incision and tributary knickzones record the magnitude of surface uplift, with the main difference being that, in the case of a punctuated tilt, knickpoints record the timing of cessation of tilting, whereas in the case of onset of continuous tilting, knickpoints record the onset of tilting. We revisit this uncertainty in the Discussion.

Evidence of Tilt in Transient Channel Profiles with Heterogeneous Lithology

In the North Fork American River and all forks of the Yuba River, channel profile forms have a different character than the majority of rivers to the south that are primarily underlain by the Sierra Batholith. Although positive-curvature mainstem slope-break knickpoints are evident and upstream reaches exhibit negative curvature in χ plots, large mid-profile knickzones, commonly well upstream of mainstem tectonic knickpoints, are striking disequilibrium forms in these northern Sierra rivers. These knickzones occur just upstream of more deeply incised

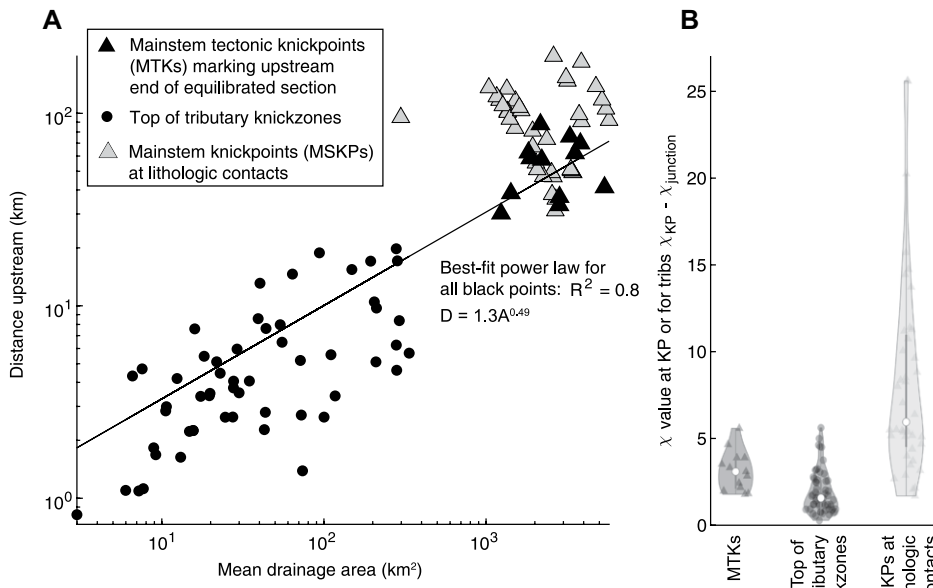


Figure 15. Comparison of knickpoint positions in river networks draining the western slope of the Sierra Nevada, California, USA, for knickpoints inferred to be in motion versus knickpoints fixed at lithologic boundaries. (A) Knickpoint distance upstream of mountain front for mainstem knickpoints or upstream of mainstem-tributary junction for tributary knickzones plotted as a function of mean drainage area along that distance. (B) Violin plots of χ values at mainstem knickpoints and change in χ between top of tributary knickzones and mainstem-tributary junctions. These distributions show that knickpoints inferred to be in motion in response to a single tectonic perturbation are tightly distributed in comparison to the broad distribution of χ values for knickpoints at lithologic boundaries that can be found at almost any point in the network. tributary D—distance upstream; A—drainage area.

reaches that correspond to at least a portion of the western metamorphic belt (light green and purple) if not the whole belt (Fig. 11), that we estimate to be up to two times more erodible than the Sierra Batholith (Fig. 14). In all forks of the Yuba, the mainstem tectonic knickpoint is located within granodiorite, a rock type shown to be less erodible than other common rock types upstream (Fig. 14). Anomalously steep reaches occur just upstream of the mainstem tectonic knickpoint in all forks of the Yuba River, with little to no incision below Mio-Pliocene volcanics or auriferous gravels at the top of the steep reach. Together these incision patterns are consistent with those observed in the simulations of rapid rigid-block tilting with bands of anomalously erodible rock (Figs. 5A and 5B).

The incision pattern in all forks of the Yuba River and the more vertical knickzone near the outlet in the Mokelumne River are consistent with the simulation of rapid tilt with a vertical bed of less erodible rock near the outlet in which slope-break knickpoints form simultaneously at the river outlet and at the top of the bed of less erodible rock, with the downstream mainstem

tectonic knickpoint propagating slowly through the bed of less erodible rock (compare Figs. 11 and 5B). Midprofile rock-type knickpoints in other rivers, such as the Middle Fork American and the South Fork American, are consistent with the simulation of rapid tilt with a vertical bed of more erodible rock mid-profile in which rock-type slope-break knickpoints form simultaneously at the outlet and at the downstream end of the bed of more erodible rock (compare Figs. 11 and 5A). The large knickzone at or upstream of the western metamorphic belt in many northern Sierra rivers is consistent with our interpretation that incision occurred as the result of a knickpoint that formed at the downstream end of the western metamorphic belt and eroded headward. The sections of river that we interpret to be deeply incised as a result of this process are annotated with arrows in Figure 11, with the shorter horizontal arrow demarcating the bed of more erodible rock, the longer horizontal arrow demarcating the full length of the incised section, and the longer vertical arrow demarcating the full drop height of the anomalously incised section. The similarity in mean k_{sn}

values across the mainstem tectonic knickpoint in rock types of the western metamorphic belt compared with the significant differences in the other two rock types relative to the mainstem tectonic knickpoint further supports the interpretation that channels within the western metamorphic belt have already incised, owing to their high erodibility, toward a near-equilibrium channel steepness in response to tilting.

In total, the transient response to tilting appears to be heavily modulated by heterogeneous lithology in the North Fork American and Yuba rivers and helps to explain the nonuniform patterns of incision observed in these rivers. Beeson and McCoy (2020) showed that when the transient fluvial response to a punctuated tilting event is modulated by heterogeneous lithology the depth of incision into basement rock below the base of Cenozoic deposits can vary substantially both along a single river profile and among adjacent basins upstream of the mainstem tectonic knickpoints without the need to invoke complex uplift patterns or complex paleotopography. This mechanism may also account for deviations in the collapse of tributary knickzones with mainstems in χ plots and the lower elevation of mainstems relative to tributaries in northern Sierra rivers as compared to southern Sierra rivers. We calculated χ assuming uniform K , thus χ is not expected to scale linearly with elevation for equilibrium channels that travel through heterogeneous lithology. Mainstems or tributaries that travel through highly erodible rock will have lower elevations than expected from a linear scaling with χ and thus plot below channels that do not pass through similarly erodible rock. Mainstems or tributaries that pass through more resistant rock will have higher elevations than expected from χ and thus plot above channels that do not pass through similarly resistant rock (Beeson and McCoy, 2020). Although the Yuba and North Fork American rivers exhibit the effects of heterogeneous lithology most dramatically, other smaller deviations in the characteristic signatures of tilt may be a result of thin bands of rock with variable erodibility.

Evidence of Tilt in Azimuth-Gradient Relationships in the Modern River Network on Broad Upland Surfaces

Beyond channel profiles, river networks can record tilt in the relationships between azimuth and channel gradient or steepness owing to how channels flowing in the tilt direction are steepened, whereas channels flowing against the tilt direction become less steep as they are back-tilted, and the steepness of channels flowing perpendicular to the tilt direction are unaffected. Beeson and McCoy (2020) showed that

in a two-dimensional (2-D) landscape evolution model with parameters similar to those calculated for the Sierra, a rapid tilting event leaves a systematic pattern in the relationship between gradient and azimuth, but this dissipates after 4 m.y. Simulated river networks also recorded tilt through stream captures in the tilt direction that occur coincident with a punctuated tilting event and anytime during the transient response as over-steepened reaches incised and knickpoints propagated upstream (Beeson and McCoy, 2020).

We explored these expected signatures of tilt in the Sierra Nevada by locating upland surfaces where the river network cut through near uniform geology and had an optimal orientation for recording a westward tilt in the relationship between azimuth and gradient—large tributaries oriented along the tilt axis with sub-basins running both toward and away from the mountain front. We located three regions on upland surfaces which met these conditions—one between the South Fork and Middle Fork American rivers, one between the Merced and Tuolumne rivers, and one between the San Joaquin and Kings rivers—and calculated azimuth, k_{sn} , and gradient for 3 km long segments (Fig. 16). We determined that 3 km was the ideal length scale in that it was long enough to smooth over noise in the DEM but small enough to capture variation in azimuth, k_{sn} , and gradient. The results reveal that gradient values are anomalously high for a range of azimuths on each upland surface (Figs. 16E–16G lower row), similar to results from a 2-D model of instantaneous tilt (Beeson and McCoy, 2020). We also mapped stream captures in which streams flowing in the predicted tilt direction captured streams running oblique to the tilt direction (“tilt-and-spill” captures), evident by anomalous topology including barbed tributaries and streams that cut across ridges (Fig. 17). These stream captures and the azimuth-dependency in modern channel gradient that we document provide further evidence that the river network in the Sierra is in a transient state of adjustment to a rapid tilting event. “Tilt-and-spill” stream captures are not prevalent in the northern Sierra, though it is unclear whether this is because of a lower tilt magnitude or because north of the Tuolumne River most segments of the river network are oriented primarily in the tilt direction (compare Figs. 16E and 16G).

River Profile Forms Near the Northern and Southern Boundaries of the Sierra Do Not Show Clear Signatures of Tilting

At the northern and southern ends of the Sierra, river profiles have disequilibrium forms

that are not consistent with the transient fluvial response to rapid rigid-block tilting. In the Feather River, although we identified a positive-curvature slope-break knickpoint, numerous large changes in channel steepness occur that potentially reflect a more complex uplift field than a simple rigid-block westward tilt (Fig. 10). Large vertical-step knickzones in the Poso and Kern river profiles are consistent with the 1-D simulation of a rapid pulse of more uniform uplift (compare Figs. 10 and 3C) and the negative-curvature slope-break knickpoint in the Tehachapi River is consistent with a recent step increase in uplift rates (compare Fig. 10 with the inverse form of Fig. 3D—i.e., flipped about a horizontal axis). Lastly, in the Kaweah River, tributary knickzones have more variable forms and exhibit no trend in drop height moving away from the mountain front. For the remainder of our analysis, we therefore focus on crest-draining river basins from the Yuba River south through the Kings River, which have disequilibrium forms that are most consistent with the forms expected following a short-lived rapid pulse of rigid-block tilting.

ESTIMATING TIMING AND DURATION OF PULSE OF WESTWARD TILT

Timing and Duration of Tilt from Disequilibrium River Profile Forms and Location of Mainstem Tectonic Positive-Curvature Slope-Break Knickpoints

The latest date for ash-flow tuffs that originated in eastern Nevada and were deposited in valleys of the northern Sierra is 23 Ma. Thus, it is thought that the large paleorivers originating on the Nevadaplano were truncated sometime after 23 Ma (Henry and Faulds, 2010 and references therein). However, we see little evidence of a major truncation event recorded in the longitudinal profile form of any Sierra rivers even though we expect a truncation signature to persist in the channel form for at least 20–30 m.y. (compare Figs. 10 and 3E). The strong truncation signature in modeled profiles relies on the assumption that the pre-truncated profile was in equilibrium, but rivers draining the western slope of the Sierra may not have been in equilibrium (Cassel and Graham, 2011). However, given the large paleodrainage areas and associated rapid response times implied by the eastern Nevada origins of the Oligocene ash-flow tuffs, it seems likely that rivers would have been close enough to equilibrium such that a large truncation event should have generated significant topographic signatures in channel profiles. One explanation for the lack of a truncation signature is

that westward tilting after 23 Ma has uplifted mainstem valleys downstream of the truncation point sufficiently high to have obscured the truncation signal (compare Figs. 3E and 3F to see how tilting toward the outlet largely compensates for the anomalously low upper network elevations after truncation).

More precise estimates of timing of tilting can be made from travel times of knickpoints found along the profiles that we assume to be initiated at baselevel by a tilting perturbation. Unfortunately, the subtle negative curvature slope-break knickpoint that tracks the onset of a rapid pulse of tilt is difficult to identify amid the negative curvature induced by tilting on a χ plot (Figs. 3G and 4). However, the positive-curvature slope-break knickpoint in the mainstem that tracks the timing since cessation of a pulse of rapid tilt is easy to identify in simulated profiles (χ can be read as τ because $K = 1 \times 10^{-6} \text{ m}^{0.1} \text{ yr}^{-1}$; Equation 9; Figs. 3F and 4). To calculate τ values for the locations of the mainstem tectonic knickpoints in the Sierra profiles, we divided their χ values by K . We used the mean K value for the Sierra Batholith ($9.0 \times 10^{-7} \text{ m}^{0.1} \text{ yr}^{-1}$; Fig. 14) for all profiles although many rivers pass through other rock types as this K value is the only one calculated directly from erosion rates and k_{sn} that were measured in the same basin. We calculated the 95% confidence interval on these τ values using the 95% confidence interval on the Sierra Batholith K and we show these as error bars on τ (Fig. 13B).

We found that the τ values, or travel times, of mainstem tectonic knickpoints fall between ca. 2 and 6 Ma for rivers between and including the Yuba and Kings rivers with a mean of 4.1 ± 0.6 Ma ($\pm 95\%$ confidence interval; Fig. 13B). The variability in τ between basins mirrors the variability in k_{sn} and thus, similar to the variability in k_{sn} , can largely be explained by differences in rock type near the outlet (see subsection, Spatial Patterns in Normalized Channel Steepness and Rock Erodibility). K values for other dominant rock types vary by almost a factor of two from Mesozoic plutonic rocks (Fig. 14), thus the variability in mainstem tectonic knickpoint τ values falls within the expected range given the differences in rock types that the mainstems traverse. We show τ values for channel heads to demonstrate that τ values of mainstem tectonic knickpoints are a small fraction of the time it takes for a perturbation to move all the way through the network to the headwaters, which highlights that much of the river network has not fully adjusted to the tilting perturbation.

Although the negative curvature slope-break knickpoints that mark the onset of rapid tilting are difficult to identify, we can estimate the duration of the pulse from the relative change in steepness

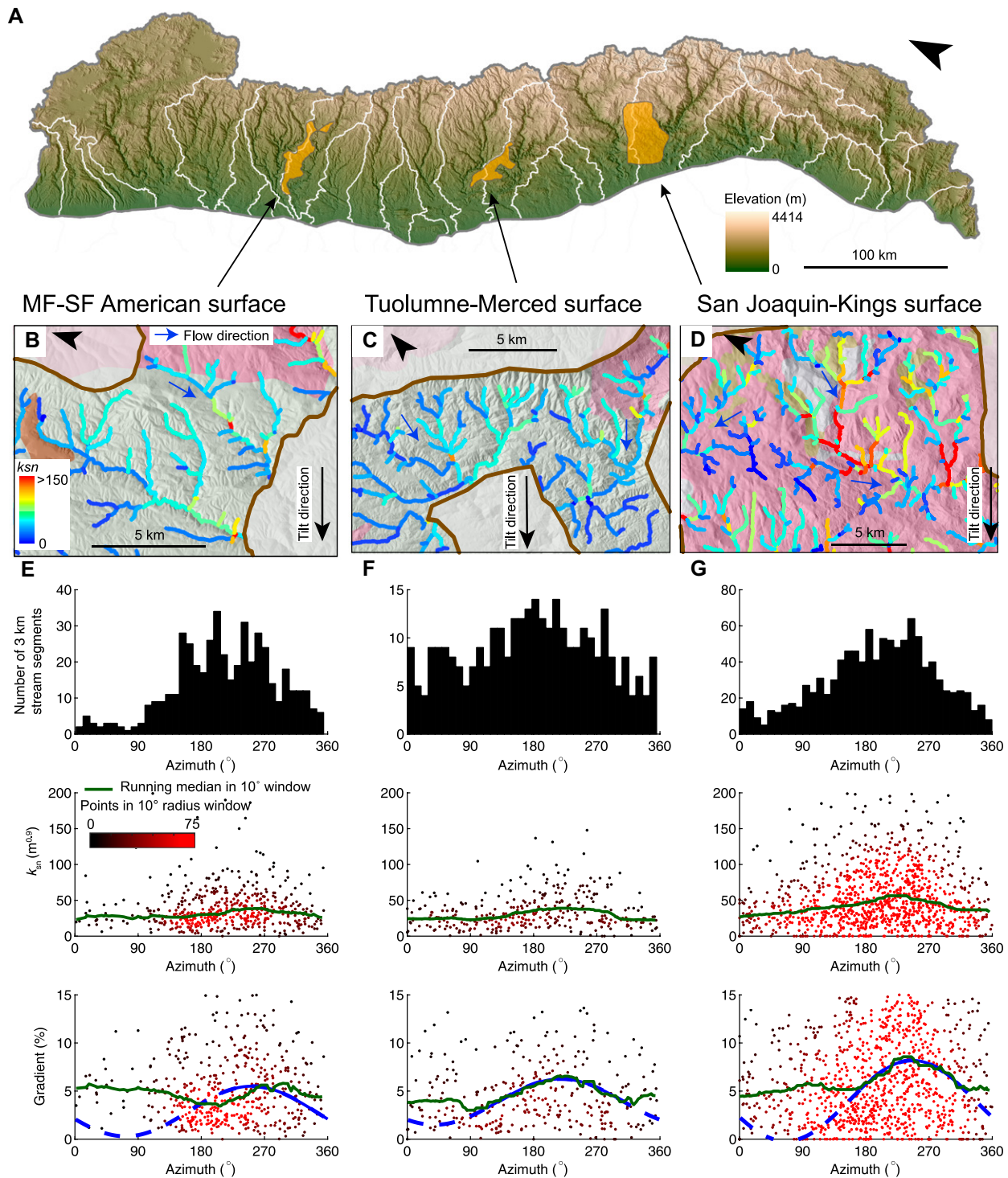


Figure 16. Evidence of tilt in relationships between azimuth and gradient and fluvial steepness, k_{sn} , of the modern river network on broad upland surfaces in the western Sierra Nevada, California, USA. (A) Upland surfaces mapped onto a 30 m digital elevation model (DEM) of the Sierra. (B–D) Hillshade images derived from 10 m DEM colored by geology (colors same as Fig. 2) for portions of each upland surface overlaid with the stream network colored by k_{sn} measured over 3 km stream segments. Note higher k_{sn} in segments flowing in the tilt direction and lower k_{sn} in segments flowing against the tilt direction. (E–G) Histograms of the azimuth distribution of 3 km stream segments (top row), azimuth- k_{sn} plots (middle row), and azimuth-gradient plots (bottom row) for each surface. Blue line in bottom row shows a cosine fit to the data to highlight the expected azimuth-gradient relationship for a static channel network after tilting a rigid block. Green line shows 10° moving-window median. MF-SF—Middle Fork-South Fork.

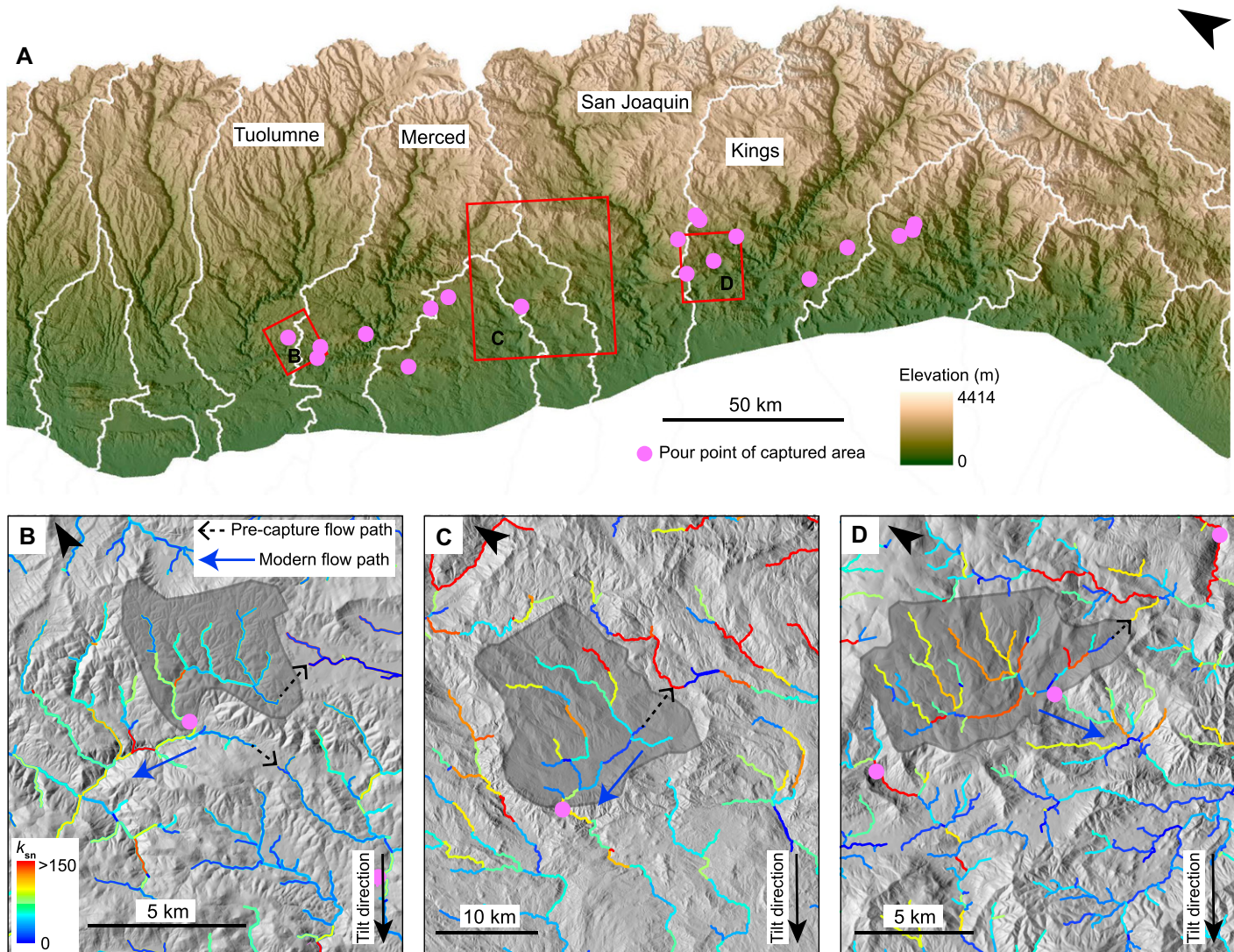


Figure 17. Maps of potential stream captures in the Sierra Nevada, California, USA, in which rapid westward tilt appears to have rerouted the river network through low points in ridges, here called tilt-and-spill captures. (A) Digital elevation model (DEM) of central and southern Sierra with the outlets of potential tilt-and-spill captures shown with pink dots. (B–D) Hillshade images derived from 10 m DEM of three examples of tilt-and-spill captures overlaid with the stream network colored by normalized channel steepness (k_{sn}) measured over 3 km stream segments. Captured areas shaded in dark gray. All hillshade images are oriented with the estimated tilt direction toward the bottom of the page.

between the equilibrium reach and the upstream transient reach, for which short-duration rapid pulses lead to large changes in steepness across the mainstem tectonic positive-curvature slope-break knickpoint (Fig. 4). For longer duration pulses, tributaries will have longer segments with channel steepness reflecting the elevated uplift rate of the pulse and thus plot below the mainstem in a fanning pattern, whereas for short duration pulses, tributaries have short segments with channel steepness reflecting the elevated uplift rate of the pulse and thus their knickzones tightly collapse with the mainstem. Tributary knickzone drop height also does not decrease dramatically

upstream of the mainstem slope-break knickpoint for longer duration pulses. Owing to these characteristics, we interpret the channel profile forms in the Sierra to be most consistent with a pulse duration that was short lived and likely less than 5 m.y., which when added to the estimates of tilt cessation at ca. 2–6 Ma, puts the onset of tilting at <7–11 Ma.

Timing of Rapid Tilt Cessation from Tributary Knickzones

As described above in the section, Geomorphic Signatures in Simulated Bedrock River

Profiles of the Transient Fluvial Response to Perturbations, tributary knickzones begin to form instantaneously in response to rapid tilting owing to mainstem incision or an increase in relative baselevel fall at the mainstem-tributary junction. The time since cessation of rapid tilting can then be calculated by subtracting the τ value at the tributary confluence from the τ value at the point where tributary knickzone steepness diverges from the mainstem. Tributary knickzones form independently of the mainstem knickpoint and thus provide an independent measurement of the timing of the cessation of rapid tilting in the Sierra. The

selection of tributaries and identification of tributary knickzones is described in the above subsection, Mainstem and Tributary Longitudinal Profiles and χ Plots. We grouped tributaries into three groups: (1) those that enter the mainstem downstream of the mainstem tectonic knickpoint and collapse with the mainstem on χ plots from the upstream end of tributary knickzones to the mainstem-tributary junction; (2) those that enter the mainstem upstream of the mainstem tectonic knickpoint and collapse with the mainstem on χ plots; and (3) those that do not collapse with the mainstem on χ plots from the upstream end of tributary knickzones to the mainstem-tributary junction. We used tributaries in groups 1 and 2 (those that collapse with the mainstem over their knickzones) to estimate the timing of cessation of rapid tilting (filled markers on Fig. 12). Tributaries in group 3 may be influenced by nonuniformity in K or n that impacts the propagation of knickzones from the mainstem-tributary junction upstream or a change in erosion mechanism that is not well represented by our simple stream power formulation. For the selected tributaries, we measured the difference in τ between the top of the knickzone and the corresponding mainstem-tributary junction and calculated the mean for each basin. We show the 95% confidence interval on the mean for each basin as error bars as this was higher than the uncertainty associated with the Sierra Batholith K . These estimates of the timing of tilt cessation in the Sierra range from 1.1 to 5.5 Ma with a mean of 2.6 ± 0.7 Ma ($\pm 95\%$ confidence interval on the mean; Fig. 13B).

ESTIMATING MAGNITUDE AND SPATIAL PATTERN OF WESTWARD TILT AND ASSOCIATED SURFACE UPLIFT

Throughout the Sierra, deeply incised valleys are separated by broad low-relief interfluvia. The preservation of Mio-Pliocene volcanic deposits on interfluvia in the northern Sierra (Bateman and Wahrhaftig, 1966; Busby et al., 2008; Christensen, 1966; Curtis, 1953; Durrell, 1966; Slemmons, 1966) and exposure dating with cosmogenic nuclides on bedrock surfaces on low-relief upland surfaces in the southern Sierra (Stock et al., 2005) demonstrate that long-term erosion rates on these interfluvia are very slow (mean of 10 ± 1 m m.y. $^{-1}$). With such low erosion rates, we assume that surface uplift and rock uplift are approximately equal on low-relief interfluvia and upland surfaces and thus all of our measures of rock uplift should closely approximate surface uplift experienced by these surfaces that are largely disconnected from the

more rapidly eroding river valleys (e.g., England and Molnar, 1990).

Magnitude of Accumulated Tilt and Rock Uplift from Longitudinal Pattern of Incision into Basement Rocks

We estimated the magnitude of tilt from spatial patterns of incision into basement rocks using two methods. For rivers in the northern Sierra, we measured incision into basement rocks below the base of Mio-Pliocene volcanic deposits and Eocene auriferous gravels (e.g., Wakabayashi, 2013; Wakabayashi and Sawyer, 2001). It is thought that the Mio-Pliocene volcanics covered almost the entire northern Sierra landscape and thus the basal contact inherited the paleorelief of the buried landscape (Wakabayashi, 2013). Although the Eocene auriferous gravels are a superior marker from which to measure incision as they define former river valleys, they are sparse, particularly near the mountain front, and thus it is difficult to establish longitudinal trends in incision using them alone. As Wakabayashi (2013) and Cassel and Graham (2011) have described, the gravel deposits are usually thin (order 10s of meters with the thickest deposits described by Cassel and Graham (2011) ~140 m) and they are commonly directly subjacent to the volcanics (Fig. 11). In some regions of the Sierra, Oligocene-aged ash-flow tuffs occur stratigraphically between basement rock and Mio-Pliocene volcanics or between Eocene gravels and Mio-Pliocene volcanics. In the high Sierra these deposits range from 50 to 400 m thick, but in the western foothills these deposits thin to no more than 20 m (Cassel et al., 2009a). Furthermore, these deposits are constrained to Oligocene paleovalleys, which the modern river network crosses in many locations (Henry et al., 2012 and references therein). The bottom of the Cenozoic volcanic deposits is therefore the best available widespread approximation of a pre-incision surface that can be used for the entire western slope of the northern Sierra. However, variations in incision depth below this marker at the basin scale likely reflect that modern rivers are incising obliquely across both paleovalleys and paleointerfluvia, with incision values expected to be lower where river segments incise into a paleovalley and greater where segments incise into a paleointerfluve (Fig. S8; see footnote 1). We interpret local deviations in incision depths measured using the auriferous gravels (order 100 m) from those measured using the base of Mio-Pliocene volcanics as the effects of paleorelief (i.e., base of Mio-Pliocene volcanics on a paleointerfluve would be above the gravels in a nearby paleovalley), intervening Oligocene ash-flow tuffs, or as resulting from faulting after

gravel deposition but before volcanic rocks were deposited, which Lindgren (1911) showed could be ~10–100 m.

South of the Tuolumne River where Miocene volcanic deposits are not widespread, we could only measure canyon relief below the upland surface elevation. Beeson and McCoy (2020), showed that, in the case where perturbation magnitude was significantly larger than paleorelief, this method was able to recover the magnitude of rock uplift, though with a slight underestimate owing to erosion of the upland surface. Thus, if paleorelief is of the same order as perturbation magnitude, this method is likely an overestimate as incision measurements include paleorelief. Paleorelief in the southern Sierra is likely on the order of 1 km (Wakabayashi, 2013), with isolated locations having paleorelief up to 2 km (Stock et al., 2005, 2004). To minimize the effect of localized areas with anomalously high paleorelief, we smoothed the mean upland surface elevation and regressed through incision data (rather than using the minimum envelope). This method does not however account for the broad canyon paleorelief that existed prior to the most recent pulse of uplift, which is likely on the order of 1 km. To present conservative estimates for uplift magnitude, we subtracted the estimated paleorelief (Wakabayashi, 2013) from these measurements, though we recognize that there is uncertainty in the paleorelief estimates. Both of these methods rely on the additional assumptions that the transient river profile is equilibrating to the same steepness and fluvial relief as the initial river profile, and that the Sierra is behaving as a rigid block. These assumptions are difficult to constrain, and we address how deviations away from these assumptions might impact our estimates in the Discussion.

In the northern Sierra, we ran 15 km wide swath profiles down the center of all mainstem rivers that had Mio-Pliocene volcanic deposits on the interfluvia. At each point along the river (~30 m spacing), we measured the elevations of Mio-Pliocene volcanic deposits and auriferous gravel deposits that fell within each swath segment (insets in Fig. 11). For each river node we also measured the Euclidean distance to the mountain front. We chose to use Euclidean distance to the mountain front rather than distance upstream because distance from the mountain front should better reflect a linear uplift field due to tilting on an axis parallel to the mountain front. Note that the elevation range of patches denoting volcanic and auriferous gravel deposits do not necessarily reflect thickness of any single deposit, but rather an amalgamation of elevations within a 15 km wide swath perpendicular to each river node. At any given river node, the swath may cross deposits up to 7.5 km at either

greater or lesser Euclidean distances from the mountain front owing to our method of snapping the center of the swaths to sinuous river channels. Although this method introduces variability in incision measurements, each river node is then associated with elevations of the nearest deposit. This is preferable to the alternative method of associating each river node with deposits that are at the same Euclidean distance from the mountain front but may not be the nearest deposit.

For the American and Yuba rivers, we used 1:250,000 scale geologic maps to identify locations of the Mio-Pliocene volcanics (Saucedo and Wagner, 1992; Wagner et al., 1981) but for the Feather, Mokelumne, Stanislaus, and Tuolumne rivers we used a 1:500,000 scale map (Ludington et al., 2005) because a higher resolution digitized map was not available. We chose to use a 15-km-wide swath because this width always captured the broad upland surface on either side of the mainstem river canyon but never extended into adjacent canyons. To calculate incision into basement rock, we subtracted the river elevation from both the corresponding minimum elevation within the volcanic deposits and the corresponding minimum elevation within the auriferous gravels (Fig. 11 insets). Reservoirs that ran through a single rock type were filled in with that rock type below a reconstructed river profile that was made by connecting the upper limit of mapped water with the lowest elevation of mapped water. In all of these cases, the elevation of the top of the reservoir was used for calculating incision rather than the elevations of the reconstructed rivers. In the lower Stanislaus River, a reservoir occurs between the outlet and the mainstem knickpoint where significant late Cenozoic deposits exist. In this case accurately estimating incision is critical, so we reconstructed the river profile using historical maps (USGS, 1916). Accurate reconstructions were not necessary in other rivers owing to relative differences in reservoir and knickpoint locations and prevalence of late Cenozoic deposits. The reservoir on the Stanislaus is younger than other reservoirs in the region and thus the colors under the profile reflect the original mapped rock types.

In the southern Sierra, we measured upland surface elevation in a 15 km-wide swath that ran along the mainstem river and smoothed it with a 5 km moving window. To measure canyon relief, we subtracted the river elevation at each node from the smoothed maximum. To compare these measurements with those made where Mio-Pliocene volcanic deposits do occur, we also measured incision below upland surface elevation north of the Tuolumne River (Fig. S9; see footnote 1).

The results of both methods of measuring incision into basement rocks reveal a triangular

pattern of incision, with little to no incision at the mountain front, maximum incision mid-profile and little to no incision at the crest. This pattern is consistent with incision patterns exhibited in the 1-D simulations of rapid nonuniform uplift by tilting, in which incision increases approximately linearly upstream, reaches a maximum at the mainstem knickpoint, and decreases upstream (compare Fig. 11 insets with Fig. 3F lower row). Deviations in the overall triangular pattern in incision largely correspond to heterogeneous lithology or variations in ridgecrest topography. For example, maximum incision in the northern Sierra corresponds to the deeply incised sections in the western metamorphic belt and maximum incision in the Kings River corresponds to anomalous peaks in ridgecrest topography.

In the 1-D simulations of a pulse of rapid rigid-block tilting, the magnitude of incision downstream of the mainstem knickpoint reflects the magnitude of rock uplift and the rate at which incision increases with distance upstream is equal to the tilt magnitude (Figs. 3 and 4). We stress that incision depth only records the magnitude of rock uplift in the reach that has eroded through the rock uplifted during the pulse and equilibrated to modern boundary conditions, which is only the reach that spans downstream of the mainstem knickpoint to the mountain front. Upstream of the knickpoint, much of the rock uplift has raised the river profile to its above-equilibrium elevation and steepness and has not yet been incised. To estimate the magnitude of tilt in the Sierra, we assumed rigid-block tilting and regressed incision into basement rock against Euclidean distance from the mountain front for points downstream of the mainstem tectonic knickpoint in each river. To then estimate surface uplift at the Sierra crest, we projected each regression to the maximum Euclidean distance from the mountain front in each mainstem (Fig. 11 insets; Fig. S9; see footnote 1). We used incision data calculated from both Mio-Pliocene volcanic deposits and auriferous gravels in the regression where both were available. We chose to regress through these data rather than use a minimum envelope curve to account for the variability in incision measurements introduced by our method of snapping swaths to sinuous river profiles and the fact that only 1:250,000 and 1:500,000 digitized geological maps were available and thus deposit elevations may not be precise.

The resulting estimates of tilt magnitude made using incision into basement rock for rivers including and between the Yuba River to the Stanislaus River range from 0.5 to 0.8° with a mean of 0.7°, or ~860–1330 m of surface uplift at the crest with a mean of 1180 m (Fig. 18).

Estimates of tilt magnitude made using mainstem relief below ridgecrests for rivers from the Yuba south through the Stanislaus are similar, though slightly higher, ranging between 0.6 and 1.0° with a mean of 0.8° (Fig. 18). Prior to subtracting paleorelief, estimates made using this method for rivers south of the Stanislaus are higher, ranging from 1.0 to 2.1° with a mean of 1.5°, or 1760–3030 m of surface uplift at the crest with a mean of 2230 m (Fig. 18). However, once paleorelief is subtracted, estimates from the southern Sierra are in line with those from the northern Sierra, ranging from 0.8 to 0.9° or 1160–1430 m of surface uplift at the crest. We show the 95% confidence interval on the slope of the regression line as error bars on tilt magnitude in degrees and we show the 95% confidence interval on the full regression line (slope and intercept) as error bars on surface uplift at the crest in meters. We did not incorporate any uncertainty from paleorelief in the error bars, though we recognize that this is a considerable source of uncertainty.

Magnitude of Accumulated Tilt and Rock Uplift from Spatial Gradient of Tributary Knickzone Drop Height

In the 1-D simulation of *instantaneous* non-uniform uplift due to tilting, tributaries downstream of the mainstem slope-break knickpoint record the magnitude of accumulated rock uplift in the difference in elevation between the top of tributary knickzones and the tributary junction. In the 1-D simulations of rapid tilting over *longer periods*, instead of sharp transitions in channel steepness, the tops of tributary knickzones have negative curvature and the magnitude of accumulated rock uplift is recorded in the elevation difference between the upstream point where tributary steepness becomes uniform and the mainstem-tributary junction (Beeson and McCoy, 2020). Given that these points are difficult to identify in a 1-D model and that tributary profiles in the Sierra often do not have upstream portions with uniform steepness, we chose to use the most downstream deviation in tributary knickzone steepness. Estimates made from tributary knickzone drop height are thus more likely to be underestimates of accumulated tilt and rock uplift than overestimates. However, given that river profiles are consistent with a rapid pulse, this method likely does not greatly underestimate tilt magnitude. As described above in the subsection, Mainstem and Tributary Longitudinal Profiles and χ Plots, we measured knickzone drop height for unglaciated tributaries to major Sierra rivers and plotted them against the Euclidean distance from the mountain front as measured from

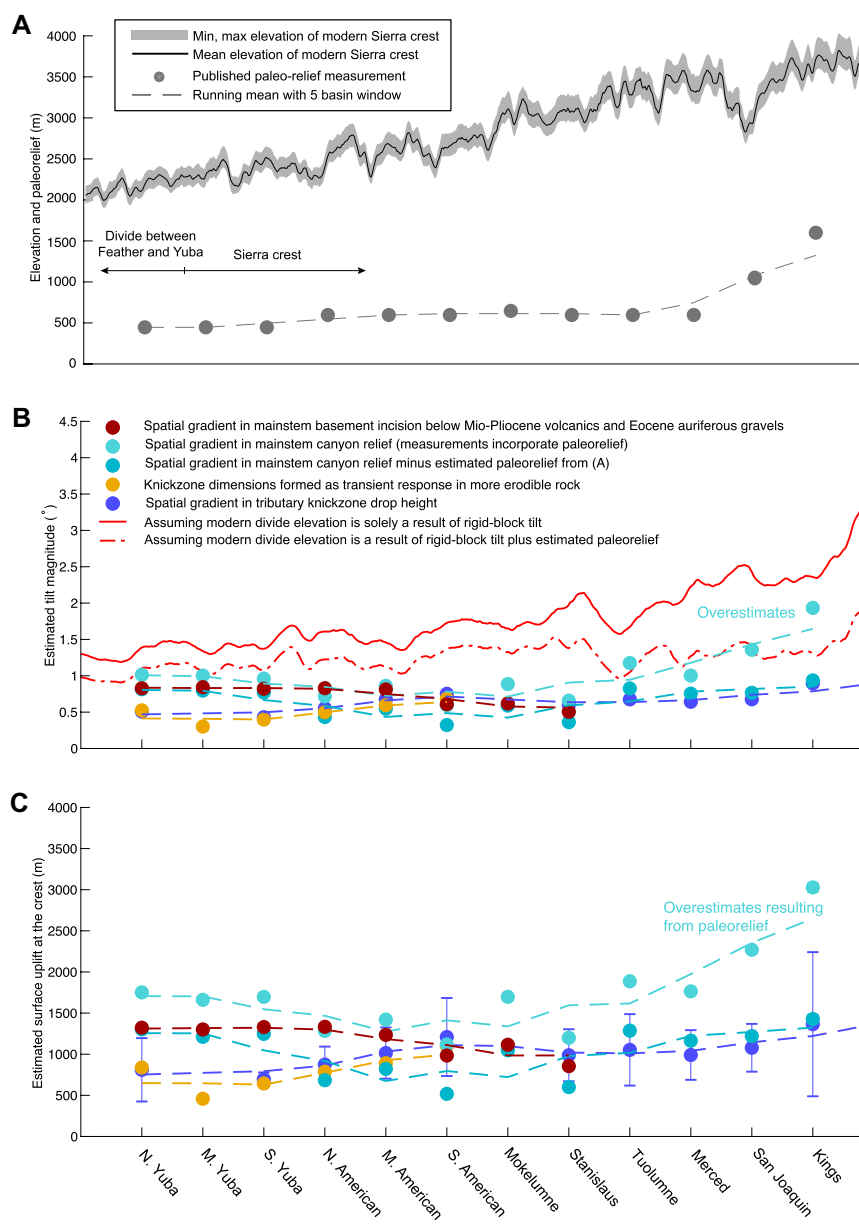


Figure 18. Summary of modern elevation, paleorelief, and estimates of tilt magnitude displayed by basin name moving from north to south along strike of the Sierra Nevada, California, USA. (A) Modern divide elevation and paleorelief estimated near the crest (Wakabayashi, 2013 and references therein; Wakabayashi and Sawyer, 2001). (B) Summary of all estimates of tilt magnitude in degrees made in this study (colored circles) in comparison to maximum tilt magnitudes estimated by assuming crest elevations result purely from a single rigid-block tilting event (solid red line) or allowing for pre-tilt crest elevation equal to published values of paleorelief (dashed red line). (C) Summary of all estimates made in this study of tilt magnitude in meters of crest uplift assuming rigid-block tilting and zero erosion on the upland surface. Error bars in C reflect the 95% confidence interval calculated for the best-fit linear regression line.

the corresponding mainstem-tributary junction (Fig. 12 insets).

This method relies on the assumptions that the transient river profile is equilibrating to the same steepness and fluvial relief as the initial

river profile, that initial tributary profiles were in equilibrium (no pre-existing knickzones), and that the Sierra is behaving as a rigid block. Deviations away from these assumptions are addressed in the Discussion. To estimate the

magnitude of tilt in each basin, we regressed distance from the mountain front against knickzone drop height, using only data from tributary knickzones in group 1 (those that collapsed with the mainstem on χ plots and were downstream of mainstem tectonic knickpoints; black markers in Fig. 12). Given the evidence for tilt and our interpretation that tilting hinged about the mountain front, along with the limited amount of data within each basin, we fixed the y-intercept to the origin. The slope of the least-squares regression line for each basin is the estimated magnitude of tilt and the uncertainty on each slope is thus the uncertainty in that estimate. To estimate the magnitude of surface uplift at the crest for each basin, we projected the best fit spatial gradient of knickzone drop height to the crest using the maximum Euclidean distance to the mountain front for each mainstem (Fig. 12 insets). The uncertainty in each estimate of surface uplift at the crest is thus the uncertainty in the maximum predicted value of knickzone drop height. We show the 95% confidence interval on the slope of the regression line as error bars on tilt magnitude in degrees and the 95% confidence interval on the regression line as error bars on tilt magnitude in meters (Fig. 18).

The resulting estimates of tilt magnitude made using this method range from 0.4 to 0.9° tilt, or ~ 700 –1350 m of uplift at the crest, for rivers south through the San Joaquin with no systematic trend along strike (Fig. 18). Tributaries with knickzones that do not collapse with the mainstem in χ plots are likely influenced by heterogeneous lithology and/or have erosional processes that deviate from those represented well by the detachment-limited stream power model used here.

Magnitude of Accumulated Tilt from Rock-Type Slope-Break Knickpoints in the Northern Sierra

The geometry of the deeply incised sections in the western metamorphic belt in the northern Sierra may reflect the tilt angle as described above in the section, Geomorphic Signatures in Simulated Bedrock River Profiles of the Transient Fluvial Response to Perturbations (Fig. 5C). This method relies on the assumption that the slope of the quasi-equilibrium reach formed during the transient response to tilt is similar to the slope of the initial river through the western metamorphic belt. The slope of the quasi-equilibrium reach will depend on the rate of baselevel fall at the downstream end. Some of the variability in these estimates may therefore be a result of differing rates of baselevel fall owing to different rock types at the downstream end of the quasi-equilibrium reach.

To estimate the magnitude of surface uplift in the Sierra based on this method, we identified mainstem rivers in the Sierra with knickzones upstream of the western metamorphic belt and took all relevant measurements—the length of river through the western metamorphic belt (L_{qer}), the elevation change over the western metamorphic belt (H_{qer}), the total length of the deeply incised section (L_T), and the total elevation change over the affected section (H_T) (Fig. 11). Using these measurements, we estimated tilt magnitude by subtracting the angle off the horizontal of the river through the quasi-equilibrium reach in the western metamorphic belt (θ_{qer}) from the angle off the horizontal over the deeply incised section (θ_T).

Our estimates of tilt magnitude using this method range from 0.3 to 0.7° with a mean of 0.5° (Fig. 18). By projecting these estimates of tilt magnitude to the maximum Euclidean distance from the mountain front measured in each basin we estimated 460–1100 m of surface uplift in the Sierra with a mean of 790 m (Fig. 18). Figure 11 presents a simplification of Sierra geology, but the western metamorphic belt is a mélange of rock types and may include thin bands of less erodible rock flanked by more erodible rock types that make up the majority of the belt. We explored this effect using the numerical model and found that thin bands of different erodibility do not change the first-order response and thus this approach can still be applied when the local response is dominated by the more erodible bed.

Magnitude of Modern Uplift Rate

In this section we use the elevations of the mainstem tectonic knickpoints and the longitudinal profile steepness below these knickpoints to estimate the average uplift rate experienced after the cessation of rapid tilting until the present. Elevations of the mainstem tectonic knickpoints increase with distance from the mountain front in a linear fashion, but knickpoints in southern Sierra rivers, from the Tuolumne south through the Kings River, are systematically higher at a given distance from the mountain front than those found in northern Sierra rivers from the Yuba south through the Stanislaus (Fig. 19A). Equation 10 shows that if uplift rates are uniform in space this pattern can result from perturbations that originated at channel outlets at different times. However, in the presence of an uplift gradient for which rates are low at the mountain front and high near the crest, such a pattern can represent a single perturbation that originated simultaneously in all basins. In this scenario, knickpoints propagate upstream at different rates in each basin owing to cross-basin differences in drainage area and rock erodibility. Knickpoints

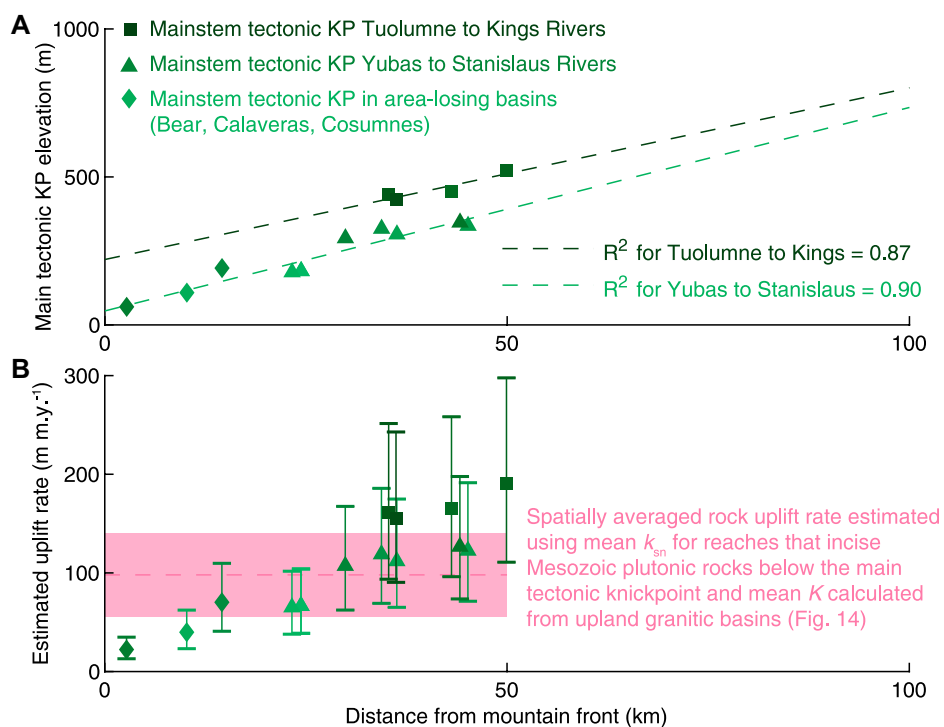


Figure 19. Mainstem tectonic knickpoint elevations and estimated uplift rates for the Sierra Nevada, California, USA. (A) Measurements of mainstem tectonic knickpoint elevations. (B) Estimated uplift rates following cessation of more rapid tilting calculated by dividing knickpoint elevation by the mean timing of onset of lower magnitude tilting at 4.1 Ma and multiplying by a factor of 1.5 to account for non-uniform knickpoint velocity. Error bars show the uncertainty in this conversion factor (from 1 to 2) as well as the 95% confidence interval on our estimate of τ . Light pink polygon shows the 95% confidence interval on the estimated spatially averaged rock uplift rate, $U = 98.0 \pm 42.5 \text{ m m.y.}^{-1}$ ($\pm \text{SE}$). KP—knickpoint; k_{sn} —normalized channel steepness; K —erodibility coefficient in stream power model.

in large basins and/or that move through comparatively more erodible rock propagate faster and travel farther over a given time increment and thus experience the higher uplift rates that exist farther from the mountain front (Equation 11). In contrast, knickpoints in small basins and/or that move through comparatively less erodible rock propagate slower and thus spend most of their time near the mountain front where uplift rates are low. It seems unlikely that the spatial pattern in knickpoint elevations reflects differences in timing of knickpoint initiation along strike given the lack of an observed systematic trend in timing along strike (Fig. 13B). Therefore, we interpret the pattern as evidence for a nonuniform modern uplift field in which rates increase away from the mountain front.

To demonstrate how an uplift gradient can generate knickpoint elevations that increase with distance from the mountain front in a simple, idealized system, we ran 20 simulations with our linked 1-D river profile evolution model in which a river profile equilibrated to a low background rigid-block tilting rate was subjected to

an instantaneous pulse of tilting, after which the uplift rate returned to a low background rate of tilting. In each simulation, the river traversed a vertical bed of varying thickness near the mountain front that either had anomalously high erodibility or anomalously low erodibility (e.g., Figs. 5A and 5B). The simulations were all stopped at $t = 3$ m.y. following the pulse of rapid tilting. After compiling knickpoint elevations across all simulations, we find that the variation in knickpoint celerity owing to the beds of anomalous erodibility results in mainstem knickpoint elevations that increase away from the mountain front and occur at apparent τ values ranging from 0.3 to 5.7 Ma as compared to the known timing of tilting at 3 Ma (Figs. S10A and S10B [see footnote 1]; we can read χ as τ because $K = 1 \times 10^{-6} \text{ m}^{0.1} \text{yr}^{-1}$ in our simulations]).

Knickpoint elevations reflect the integrated uplift rate experienced by the knickpoint as it transits the river profile (see Overview of Methods section). Knickpoint celerity is nonuniform owing to along path changes in drainage area and erodibility, which makes conversion from

knickpoint elevations to an uplift rate difficult. In Sierra rivers there are additional complications, such as heterogeneous lithology, variation in mainstem azimuth between basins, and mainstem sinuosity, that make this conversion even more difficult. If celerity is uniform and the uplift gradient is linear, the integrated uplift rate experienced by the knickpoint is half the uplift rate at the knickpoint location. Knickpoint elevation can thus be converted to an uplift rate at the knickpoint by dividing knickpoint elevation by time since rapid tilt cessation (3 m.y.) and multiplying by two. This gives us maximum estimates. If, in contrast, we assume knickpoints migrated instantaneously to their current location, the integrated uplift rate is just equal to knickpoint elevation divided by time. We can therefore use conversion factors of one and two to bracket estimates of uplift rates from knickpoint elevations, and a conversion factor of 1.5 to show the middle of this envelope. In the simulations, the resulting uplift estimates fall close to the known background uplift field (Figs. S10B and S10C). However, knickpoints that traveled through less erodible rock and are closer to the mountain front plot below the known uplift field, and knickpoints that traveled through more erodible rock plot above the known uplift field.

Based on the results of these simulations, we interpret the observed linear increase in knickpoint elevations with distance from the mountain front seen in the Sierra as consistent with a linear uplift gradient that was sampled to different extents in each basin owing to cross-basin differences in drainage area and lithology (compare Fig. 19 and Fig. S10). As in the simulations, we converted mainstem tectonic knickpoint elevations in the Sierra to uplift rates by dividing by the mean mainstem tectonic knickpoint τ , 4.1 Ma, and using conversion factors of 1, 1.5, and 2 (Fig. 19B). We intentionally do not regress through these data given the large uncertainty in converting knickpoint elevations to uplift rates. Particularly, we note that if knickpoints near the mountain front systematically underestimated uplift rates, whereas knickpoints farthest from the mountain front systematically overestimated uplift rates, a regression would yield a significant overestimate of the slope of the linear uplift field. These results do, however, demonstrate that the modern uplift field for the entire length of the Sierra is nonuniform and not zero (Fig. 19B).

We also used the longitudinal profile steepness below the mainstem tectonic knickpoints to independently estimate the average uplift rate experienced after the cessation of rapid tilting. We assumed that reaches downstream of the mainstem tectonic knickpoint are in approximate equilibrium with modern uplift rates such that the average channel steepness, k_{sn} , of each rock

type, should reflect the spatially averaged uplift rate divided by rock erodibility, K (Equation 3). Assuming segments flowing through Mesozoic plutonic rocks downstream of mainstem knickpoints have the same K value as the upland basins in Mesozoic plutonic rocks, we estimated a mean modern uplift rate of $98.0 \pm 21.7 \text{ m m.y.}^{-1}$ ($\pm \text{SE}$), which, considering the spatially averaged nature of this estimate, is consistent with the rates estimated from knickpoint elevations (Fig. 19B). We acknowledge that the slightly concave up nature of the equilibrium reaches, particularly in the southern Sierra, could further suggest ongoing nonuniform uplift in the form of a tilt. However, quantitative estimates from this slight curvature are difficult to make and interpret given the range of other processes such as drainage area exchange that can induce such curvature to the χ plot, and as such we simply report a single spatially averaged value.

IMPACT OF GEOMETRIC DISEQUILIBRIUM AND RIVER NETWORK REORGANIZATION ON THE TRANSIENT RESPONSE TO TILTING

We quantified how relatively recent, discrete increases in drainage area associated with re-establishment of the river network in the northern Sierra modify signatures of rapid tilting by reconstructing stream captures and recalculating χ with the proposed pre-capture distribution of drainage area. We found that for mid-sized captures, as thought to have occurred on the South Yuba River (Fig. 8), that the adjusted k_{sn} and τ values fell within the observed cross-basin variability (Fig. 13). For the largest captures, as proposed to have occurred on the North and Middle Fork Feather rivers, adjusted τ values similarly fell within the observed cross-basin variability, but adjusted k_{sn} took on values similar to neighboring basins as compared to being high local outliers before the area adjustment (Fig. 13A).

In addition to discrete increases in drainage area, we investigated how drainage area loss in general may impact signatures of tectonic forcing. The steady-state elevation of the modern river, and thus the amount of fluvial incision, depends on the geometry of the river basin and whether the river basin is exchanging drainage area with neighboring rivers. Basins that are losing drainage area will have higher steady-state elevation and thus generate less incision into basement rock than rivers that are either gaining drainage area or have stable divides (Willett et al., 2014). Many small basins that do not drain the Sierra crest have characteristics of persistent drainage area loss: they are narrower than adjacent basins, have high channel-head χ relative to nearby channel-head χ in adjacent basins,

and have topologic and topographic evidence of experiencing drainage area loss through stream capture (e.g., Beeson et al., 2017; Chen et al., 2021; Willett et al., 2014; Yang et al., 2015).

To investigate to what degree drainage area exchange might create variability in our estimates of tilt timing and magnitude beyond discrete increases in drainage area, we analyzed signatures of tilt in three of these smaller non-crest-draining basins—the Bear, Cosumnes, and Calaveras rivers—as it is in these basins that we should see the most extreme impact of drainage area loss (Fig. 20). We plotted longitudinal profiles for the Bear, Cosumnes, and Calaveras rivers with surface geology, maximum upland surface elevation, and minimum and maximum elevations of Mio-Pliocene volcanic deposits and Eocene-aged auriferous gravels that fell within a 15-km-wide swath perpendicular to each river node as described above in the subsection, Magnitude of Accumulated Tilt and Rock Uplift from Longitudinal Pattern of Incision into Basement Rocks. On top of these profiles we plotted longitudinal profiles for an adjacent, large, crest-draining basin. We also plotted χ profiles of each pair to allow comparison between basins.

We identified mainstem tectonic knickpoints in river profiles for these three smaller basins, but at locations much closer to the mountain front than in the adjacent crest-draining basins, even after correcting for their much smaller drainage area (Fig. 20). For example, in the large, crest-draining North Fork American River, the mainstem tectonic knickpoint occurs at a χ value of 4.2 m, whereas in the smaller non-crest draining Bear River that is adjacent to the North Fork American, the mainstem tectonic knickpoint occurs at a χ value of 1.5 m (Fig. 20A). In addition to anomalously slow knickpoint propagation, much less incision is observed upstream of the mainstem tectonic knickpoints in the Bear, Cosumnes, and Calaveras rivers compared with proximal crest-draining rivers (Fig. 20). The greatest differences in incision between basin pairs occur in the headwaters of the small basins and are coincident with the greatest difference in channel-head χ values across divides (Fig. 6). We interpret these observations as evidence that river basin reorganization can significantly, but locally, impact signatures of the transient response to tectonic forcing. Although we show that even large stream captures have a small impact on estimates of tilt timing in the Sierra, this is likely because capture points are far from the mainstem tectonic knickpoints and thus the fractional change in drainage area at mainstem tectonic knickpoints is small. Captures may have a larger impact in cases in which capture points are proximal to knickpoints or in which knickpoints have propagated farther from the channel

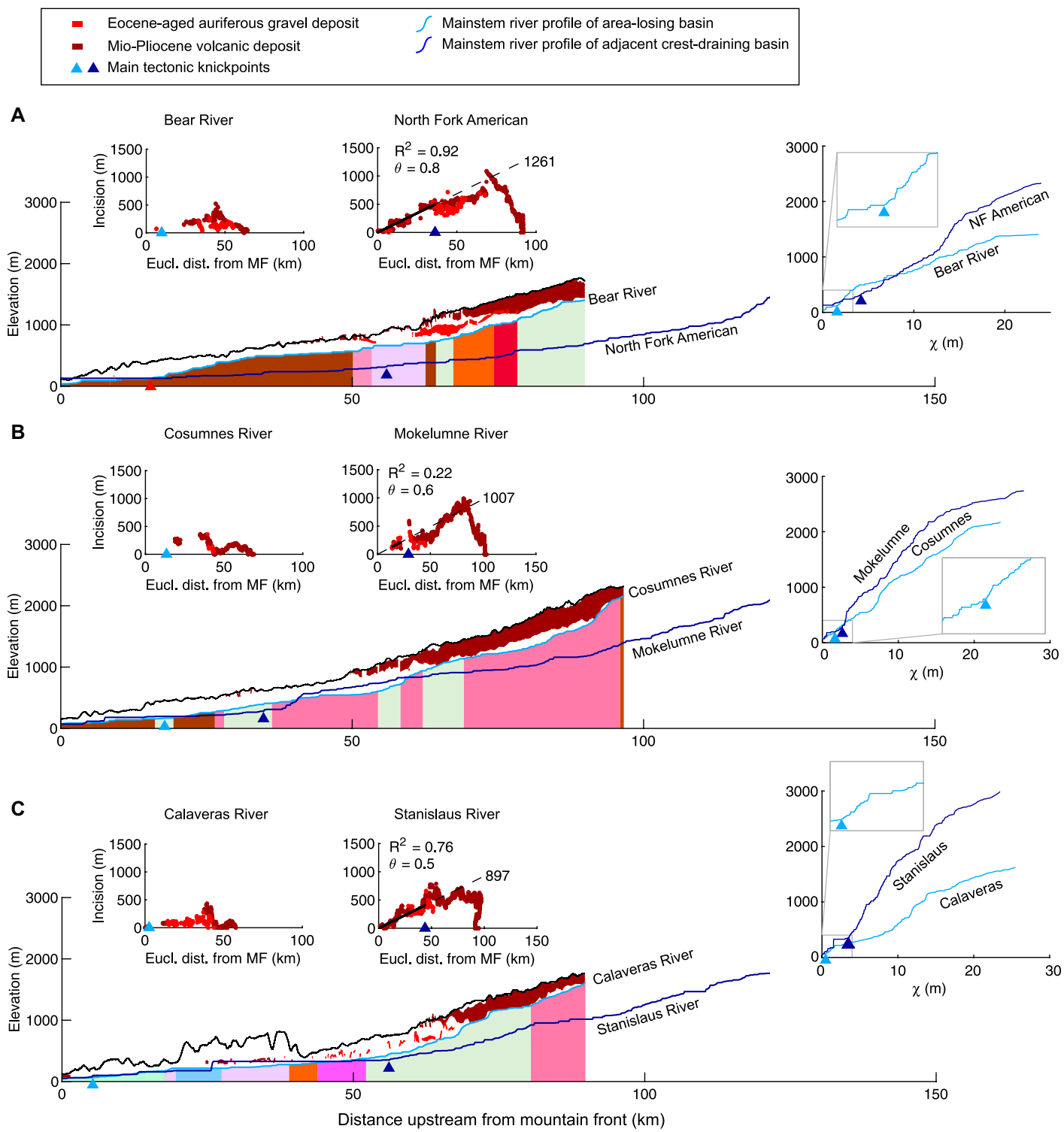


Figure 20. Impact of planform change in basin shape and size on tectonic signatures in the Sierra Nevada, California, USA. Longitudinal river profiles with surface geology and depth of river incision into basement rocks for the Bear (A), Cosumnes (B), and Calaveras (C) rivers compared to those of adjacent large, crest-draining basins. Line and symbology styles are the same as Figure 11. Insets on the right of the profile show χ plots of both mainstems and insets in plots show close-ups of the locations of mainstem tectonic knickpoints on χ plots in the smaller area-losing basins. Eucl. dist. from MF—Euclidean distance from mountain front; NF—North Fork.

outlet where similar-sized captures would create a larger fractional change in drainage area.

DISCUSSION

Late Cenozoic Tectonic History Recorded in Transient River Profiles of the Sierra Nevada

Our results show that all rivers draining the western slope of the Sierra Nevada are in a disequilibrium or transient state. With recognition of such transients comes the opportunity to extract tectonic history as well as to understand observations that may otherwise be difficult to reconcile. χ plots of Sierra river basins reveal nonuniform steepness in the entire river network upstream of positive-curvature slope-break knickpoints (“mainstem tectonic knickpoints”) in all mainstems from the Yuba River south through the Kings River, with significant but nonuniform steepness in both the mainstem just upstream of knickpoints and in tributary knickzones. We utilized the library of signatures of transient fluvial responses to perturbations created by Beeson and McCoy (2020) to identify that these disequilibrium forms are most consistent with a rapid tilting event of duration <5 m.y. downward toward the mountain front. Mainstem tectonic knickpoint locations indicate that this short-lived rapid tilting event slowed significantly at 4.1 ± 0.6 Ma. In addition to the common technique of extracting tectonic histories from mainstem knickpoints, we used the recently developed technique of extracting tilt timing from tributary knickzones (Beeson and McCoy, 2020). This method yielded a mean estimate of 2.6 ± 0.7 Ma for when the short-lived rapid tilting event in the Sierra slowed significantly. The relationships between channel gradient and azimuth that we document in the modern river network on three upland surfaces are further evidence of a young tilting event. In total, we find multiple independent lines of evidence that suggest a late Cenozoic tectonic perturbation occurred in the Sierra. Although a short-lived rapid tilting event that slowed between 2 and 6 Ma is our preferred interpretation, we recognize that the differences in signatures between this and late Cenozoic onset of rapid tilting are subtle and our ability to discern between the two may be impacted by reservoirs, heterogeneous lithology, and tributary versus mainstem azimuth. However, our estimates of the magnitude of surface uplift are unaffected by this uncertainty as is our ability to constrain the timing of this uplift to the late Cenozoic.

We used an ensemble of methods to estimate the magnitude of accumulated tilt and late Cenozoic surface uplift at the crest, including

two novel techniques—one based on the spatial gradient in tributary knickzone drop height and one based on the geometry of deeply incised segments of mainstems that run through more erodible rock. We expanded on previous efforts that used isolated measurements of mainstem incision into basement rock below the base of late Cenozoic deposits to estimate rock uplift by analyzing the spatial gradient in incision along mainstem profiles. Our estimates of tilt magnitude from the North Yuba River to the Stanislaus River range from 0.3 to 0.8° or ~ 500 – 1300 m surface uplift at the crest. Though this is a relatively large range, this is mostly a result of systematic variability among methods, rather than variability within estimates made using any particular method (Fig. 18). Furthermore, we observe no systematic trends of surface uplift along strike. Estimates of tilt magnitude are similar in the southern Sierra, once paleorelief is subtracted from measurements made from canyon relief, ranging from 0.6 to 0.9° or ~ 1000 – 1400 m surface uplift at the crest. Thus, we interpret this as evidence that the magnitude of late Cenozoic tilting was relatively uniform along strike such that the late Cenozoic period of tectonic activity constrained in this paper cannot explain the crest elevations that are 2000 m higher in the southern Sierra.

Our estimates of modern rock uplift rates made using the spatial pattern of mainstem tectonic knickpoint elevations, while quite uncertain, are relatively high (Fig. 19) in light of the total estimated late Cenozoic surface uplift at the crest (Fig. 18) and our observation that Sierra river profiles are more consistent with a rapid tilting event that has slowed rather than onset of continuous rapid tilting. We offer two possible explanations for this discrepancy: (1) the magnitude of late Cenozoic rock uplift at the crest is actually much higher than we estimate, allowing for significant uplift during a short-lived tilting event as well as significant uplift after rapid tilting ceased; or (2) cessation of rapid tilting was gradual such that some of the uplift rates associated with the short-lived rapid tilting event translated into the high knickpoint elevations we observe. We favor interpretation two given the lack of evidence for greater surface uplift.

The recognition that the Sierra Nevada is in a transient state of adjustment to a recent perturbation of significant magnitude allows us to interpret previous observations about Sierra geomorphology in this context. In particular, one of the most striking features of the modern western slope of the Sierra is the large variability in the depth of basement rock incision when moving upstream within a single basin as well as between adjacent basins (Fig. 11). Downstream of the mainstem tectonic knickpoints, river profiles have largely incised through uplifted rock to

reach an equilibrium grade and, in these reaches, basement incision depths show little variability between basins and follow a consistent linear trend that increases away from the mountain front. In contrast, upstream of the mainstem tectonic knickpoints where river profiles are still in a transient state, incision depths are variable owing to the varying degrees to which river profiles have incised through the rock uplifted in the late Cenozoic. Our results demonstrate that variations in longitudinal patterns of rock erodibility can largely explain the large variations in incision depth upstream of the mainstem tectonic knickpoint. Following a short-lived tilting event, the entire river profile begins to incise in response to being steeper than equilibrium grade, but river segments that travel through more erodible rock incise toward equilibrium at a faster rate relative to segments that travel through less erodible rock (Fig. 5). Additionally, variation in longitudinal patterns of rock erodibility influence propagation rates of the mainstem tectonic knickpoint. All together, this means that the unique path integrals of rock type in each mainstem river can result in large variability in the magnitude of incision at any given distance from the mountain front owing to variability in the position of the mainstem tectonic knickpoint and the transient response upstream.

Re-establishment of the River Network in the Northern Sierra Following Mio-Pliocene Volcanism

Mio-Pliocene volcanic flows from the ancestral Cascades arc filled and smoothed pre-existing topography on the western slope of the Sierra north of the Tuolumne River (Bateman and Wahrhaftig, 1966; Busby et al., 2008; Busby and Putirka, 2009; Christensen, 1966; Curtis, 1953; Durrell, 1966; Slemmons, 1966). Evidence that Mio-Pliocene volcanism effectively “repaved” the northern Sierra, such that re-establishment of the river network was required, lies in the fact that modern rivers are in a different configuration than the Eocene-Oligocene river network (Henry et al., 2012 and references therein). Furthermore, the geometric disequilibrium observed in the Sierra between large, crest-draining basins and smaller basins that do not drain the crest is analogous to other locations where incipient networks are evolving on inclined planar surfaces (Willett et al., 2018) and provides evidence that modern river canyons reflect tilting and are not simply incised into their Eocene-Oligocene canyons (Gabet, 2020a; Gabet and Miggins, 2020).

We investigated the degree to which geometric disequilibrium and associated river network reorganization resulting from re-establishment

of the river network may be impacting the transient fluvial response to tilting. We found that the estimates of tilt timing that were adjusted for discrete increases in drainage area caused by stream capture fell within the observed variability. This demonstrates that ongoing drainage area exchange in the northern Sierra has not obscured signatures of late Cenozoic tectonic forcing in the large, crest-draining basins. However, in the Bear, Cosumnes, and Calaveras rivers—all of which have evidence of persistent drainage area loss—less incision is observed and mainstem knickpoints are closer to the mountain front and at lower χ values than adjacent crest-draining basins (Fig. 20). These observations suggest that drainage area loss could perturb erosional processes away from detachment-limited stream power in a manner that could create deviations in signatures of perturbations and variability in estimates of perturbation timing and magnitude. Although we have interpreted these basins as having experienced the most extreme drainage area loss in the Sierra, with the possibility of both large headwater captures and lateral tributary captures, it is possible that less extreme area loss in other basins is responsible for some of the deviations in the observed signatures of tilt. Furthermore, regions of the Sierra Nevada with shrinking basins, such as the Bear, Cosumnes, and Calaveras rivers, are likely experiencing geometric reorganization rather than entrenchment of the existing river network following surface uplift. These results suggest that planform river basin dynamics may be as important in modulating signatures of tectonic forcing as lithology and, just as one would examine regional geologic maps, χ maps displaying regional geometric disequilibrium can provide an additional template on which to identify river basins that may best display signatures of external forcing.

Limitations of Simple Detachment-Limited Stream Power Model as an Interpretive Tool and Additional Sources of Unquantified Uncertainty

Our primary interpretive tool to reconstruct the late Cenozoic tectonic history of the Sierra Nevada from quantitative measures of river profile morphology was the simplest of bedrock river evolution models, the detachment-limited stream power model of bedrock incision (Whipple and Tucker 1999). We chose such a simple model because it appeared capable of creating the rich variety of forms present in the Sierra, but with simplicity there are limitations that result from the model lacking elements of reality. We argue that the ability of the model to reproduce the first-order characteristics of river profile

forms in the Sierra is strong evidence that the model does contain the necessary elements for this application. However, the range of profile forms observed in tributary knickzones, particularly the degree to which knickzones collapse with the mainstem, suggests that processes of bedrock incision at large slopes and/or small drainage areas may deviate from simple detachment-limited stream power. Quantifying how adding more elements of reality to models might change the transient response to tectonic perturbations such as tilting would be a useful trajectory for future studies (Scheingross et al., 2020).

Some well-known elements of complexity that are absent in simple detachment-limited stream power are sediment-flux dependency on bedrock erosion rates and sediment entrainment thresholds, which have both been suggested to be important for small upland basins as well as for Sierra mainstems (Callahan et al., 2019; Gabet, 2020b; Pelletier, 2007). If our estimates for channel head response time are correct, the inferred Eocene-aged surface of Clark et al. (2005) that comprises the foothills of many southern Sierra basins should not be preserved today or at least be of limited extent. While it is possible that these surfaces are younger, it is also possible that our values for channel head response time are underestimates and that other processes, such as sediment-flux dependent bedrock erosion, entrainment thresholds, or input of large blocks from hillslopes, may be responsible for slowing incision rates upstream in a way that simple detachment-limited stream power is completely blind to (Callahan et al., 2019; Pelletier, 2007; Shobe et al., 2016; Sklar and Dietrich, 2004, 2001). Another process absent from the simple stream power model is erosion related to waterfalls, which are known to be abundant in the Sierra. Recent work on waterfall erosion mechanics has shown that the presence of waterfalls can change stream power predictions for bedrock erosion rates by orders of magnitude in either direction (Scheingross and Lamb, 2017) and alter longitudinal profile forms (Scheingross et al., 2020). Tributaries with knickzones that do not collapse with the mainstem provide opportunities for identifying and studying processes such as waterfall formation and their influence on knickzone retreat rates (Scheingross and Lamb, 2017), as well as other sediment-flux dependent bedrock erosion processes that move the transient response away from simple detachment-limited stream power behavior (Scheingross et al., 2020). Our model also did not account for isostatic response to erosional unloading that could potentially create positive feedback with tilting (e.g., Ruetenik et al., 2018).

Two additional elements of complexity not explored herein are temporal and spatial variability in precipitation, including both orographic

precipitation and along-strike changes in rain and snow, as well as the impact of glaciation. River discharge is calculated using precipitation and surface drainage area, therefore when drainage area is used as a proxy for discharge in the stream power model, precipitation is encompassed in the coefficient of erodibility, K (Equation 1). Ferrier et al. (2013) showed that K varies nonlinearly with precipitation with an exponent of ~ 0.5 , though they note that the most accurate way to account for spatial variability in precipitation is to use discharge rather than drainage area. Modern precipitation increases northward and reaches a maximum at mid-elevations, but snow water equivalent increases southward and is highest at the crest, with the highest discharge events occurring as a result of rain on snow (Bales et al., 2006). Therefore, although these trends likely drive spatial variability in K , it is not clear how spatial variability in precipitation would translate to spatial variability in discharge or K over the last ~ 10 m.y., and it is unlikely to be one to one. The influence of climatic variability on K is muted, however, due to the exponent 0.5 (Ferrier et al., 2013). Furthermore, climatic fluctuations (e.g., glacial-interglacial cycles) and surface uplift of the Sierra crest in the late Cenozoic undoubtedly shifted precipitation patterns such that modern precipitation gradients are not necessarily representative of the past (Molnar, 2010). In addition to influencing K in the stream power model, orographically enhanced precipitation can influence river concavity by changing channel steepness downstream (Roe et al., 2002). Rainfall gradients on the order of those observed in the Sierra resulted in mean concavities of $\sim 0.4\text{--}0.6$ for an m/n input of 0.5. Non-uniformity in concavity of magnitude ~ 0.1 is unlikely to be observable in the Sierra Nevada owing to the disequilibrium state of Sierra river profiles. In summary, quantifying the role that spatial variability in precipitation has in shaping Sierra river networks would require more tailored methods than those employed herein.

At least eight glacial advances have been documented in the Sierra Nevada since the mid-Pleistocene (Gillespie and Clark, 2011 and references therein). Glacial deposits occur in stratigraphic sequences in alluvial fans in the eastern Great Valley (e.g., Cherven, 1984; Weissmann et al., 2002), with fan sequences even being linked to Pleistocene glacial cycles in the Kings River alluvial fan (Weissmann et al., 2002). Although both the mainstem tectonic knickpoints and the tributary knickzones that we analyzed occur far downstream of the Pleistocene glacial limit, channel profile form may still have been affected by the fluctuations in sediment flux associated with glacial cycles. Furthermore, fluctuations in climate and sediment

flux during the Pleistocene may have triggered temporal variability in K which would influence our estimates of tilt timing. These are all areas asking for further systematic study.

In the 1-D simulations of rapid tilting with $n = 1$, all three methods of estimating the cessation of tilt yield the elapsed time since the end of the perturbation (Beeson and McCoy, 2020) but to estimate cessation of tilting from a real landscape using these methods requires some assumptions. The two methods based on knickpoint τ values require that both rock erodibility, K , and the stream power slope exponent, n , can be constrained. The discrepancy between estimates based on the mainstem tectonic knickpoints (4.1 ± 0.6 Ma) versus tributary knickzones (2.6 ± 0.7 Ma) from Sierra rivers may thus be a result of differences in K between the mainstem and tributaries or systematic deviations in n between the mainstem and tributaries. Tributaries with smaller values for K (less erodible) or n as compared to mainstems would result in longer response times, which would result in underestimating the timing of cessation of tilt if changes in K or n are not accounted for. The surface geology is granite for many tributaries in all basins, whereas many mainstems flow through belts of metamorphic rock near the mountain front. The difference in lithology between mainstem and tributary channels could manifest as a change in n as it has been suggested that $n = 2/3$ in granitic landscapes (Larimer et al., 2019). In a 1-D model of a punctuated tilting event with parameters similar to those calculated herein for the Sierra, tilt timing is underestimated by a factor of ~ 2 when $n = 2/3$ is used in the model but $n = 1$ is assumed when calculating τ (Beeson and McCoy, 2020). Thus, deviation in n from unity in mainstem Sierra rivers to less than unity in tributaries would bring estimates of tilt timing made from tributary knickzones close to the 4.1 ± 0.6 Ma estimate from the mainstem tectonic knickpoints. Although n can in principle be estimated from erosion rates and k_{sn} , we were unable to estimate n with the existing data from upland granitic basins in the Sierra as the data did not span a large enough range in erosion rates.

The difference in lithology between mainstems and tributaries could also manifest as a change in K , with higher K in mainstems than our estimate of K based on small granitic basins. This seems possible given that many mainstems run through metamorphic belts near the mountain front, which have K values 1.2–1.9 times greater than the K value that we calculated from upland granitic basins and used to calculate τ . An increase in K of this factor would bring estimates of tilt timing made from mainstem knickpoints close to the 2.6 ± 0.7 Ma estimate from tributary knickzones. A larger data set of erosion rates,

that includes basins near the mountain front that are equilibrated to modern boundary conditions and in a range of lithologies, would be needed to better constrain both n and K values and hence the timing of rapid tilting in the Sierra.

We estimated the magnitude of surface uplift at the crest using three different methods (Fig. 18), all of which require two assumptions: (1) that the transient river profile is equilibrating to the same steepness and fluvial relief as the initial river profile, and (2) that the Sierra is behaving as a rigid block. With regard to the first assumption, a step increase in fluvial relief accompanying a tilt would result in underestimates of tilt magnitude and a simultaneous step decrease in fluvial relief would result in overestimates. However, even a twofold decrease in fluvial relief only results in projected incision depths that are $\sim 20\%$ greater than surface uplift at $t = 3$ Ma in simulations of tilt (for parameters similar to those of the Sierra) (Beeson and McCoy, 2020). Similarly, an increase in fluvial relief by a factor of two results in projected incision depths that are 90% of the magnitude of surface uplift. Our estimates of the modern uplift field (Fig. 19) and the similarity in k_{sn} between the equilibrium reaches and upland sub-basins (Fig. 13) suggest that the Sierra is either equilibrating to a similar or greater fluvial relief and thus, with regard to this assumption, these methods likely yield underestimates of tilt magnitude. With regard to the second assumption, although all of the observations made herein point to rigid block behavior, internal faulting since the Eocene has been suggested (Hudson, 1955). Additional work investigating and quantifying internal deformation would be required to constrain the impact this may have on our estimates of tilt magnitude.

In summary, uncertainty in our results stems from the use of the simplest detachment-limited stream power model and from assumptions in our methods that are difficult to constrain, largely relating to the pre-perturbation steepness of river channels and the amount of paleo-relief. Although clear evidence of deviation away from simple stream power with $n = 1$ exists in some tributary profiles in the Sierra, the striking resemblance between profile forms developed with this model and first-order disequilibrium forms in Sierra river profiles suggests that this model adequately captures the first-order dynamics of the transient response in the Sierra such that valid estimates of timing and magnitude can be made from profile forms. We attempted to mitigate the unknown degree of uncertainty resulting from our choice of model and assumptions inherent in the chosen methods by using three independent methods each with a suite of different assumptions. The consistency in the estimates of both timing and magnitude

across methods demonstrate that our conclusion that the Sierra experienced tilting of significant magnitude in the late Cenozoic is robust.

Comparison with Previous Work in the Sierra Nevada

Our interpretation that the range experienced a rapid westward tilting event in the last ~ 11 m.y. is consistent with previous work in the northern and central Sierra based on azimuth-gradient relationships in auriferous gravels (Hudson, 1955; Jones et al., 2004; Lindgren, 1911; Wakabayashi, 2013), tilted Cenozoic strata on the eastern side of the Great Valley (Unruh, 1991), tilt of the Lovejoy Basalt (Wakabayashi and Sawyer, 2001), and reconstruction of Eocene paleochannels compared to modern rivers (Wakabayashi and Sawyer, 2001). Many of these studies argue for progressive tilting or a step increase in uplift rates in the late Cenozoic, whereas the results we present point to a relatively short-lived (<5 m.y.) rapid tilting event, which then transitions to a lower-magnitude and likely ongoing rate of tilting. This interpretation is consistent with the significant body of literature that infers a late Cenozoic pulse of uplift in the southern Sierra based on stream incision rates (Stock et al., 2005, 2004), river profile analysis (Clark et al., 2005; Pelletier, 2007), tilted Cenozoic volcanic deposits (Huber, 1981), geophysical modeling (Ducea and Saleeby, 1996), and potassic volcanism in the southern Sierra that has been linked to eclogitic root delamination (Farmer et al., 2002). If our estimate of pulse duration is correct at <5 m.y., and the mechanism is indeed related to removal of more dense lower crust, our results would suggest that such removal occurred quite rapidly in the Sierra, with corresponding constraints on temperature and compositional gradients required to achieve such rates (Lee, 2014; Saleeby et al., 2013, 2012).

Seismic imaging suggests that eclogitic root delamination may be actively progressing from south to north and from east to west (Frassetto et al., 2011; Gilbert et al., 2012). Wakabayashi (2013) also interprets the uplift signal as younging toward the north based on rates of canyon relief production and the onset of incision below Mio-Pliocene volcanic deposits. Although our results do not have the resolution to discriminate along-strike differences in timing of initiation of rapid tilting, the better constrained time of cessation is similar from the North Yuba River south through the Kings River.

The only geochronologic evidence of a punctuated uplift event comes from dated tiered caves in the southern Sierra that show rapid incision rates between ca. 2.7 and 1 Ma, with each tiered cave exhibiting a short-lived peak in incision

rates and subsequent rapid reduction in rates (Fig. S11 [see footnote 1]; Stock et al., 2005, 2004). The spike in incision rates suggest that a knickzone reflecting a pulse of uplift propagated upstream past the caves, but the river profiles are inconsistent with that interpretation in that the mainstem tectonic knickpoints are still near the outlets in southern Sierra rivers (Fig. 10) and the dated caves are further upstream at higher elevations (Fig. S11 [see footnote 1]; Stock et al., 2005, 2004). The relatively similar timing between the peak in incision rates measured from the caves and the punctuated tilting event identified herein can be explained despite the upstream locations of the caves relative to the mainstem tectonic knickpoints in that these caves occur in thin bands of marble that are more erodible than the surrounding granodiorite (Despain and Stock, 2005). The spike in incision rates measured from these caves is consistent with incision observed in the bed of more erodible rock in the 1-D simulation of tilt with heterogeneous lithology described above. Immediately following simulated tilting, a knickpoint forms at the downstream end of the more erodible bed and rapidly propagates upstream. This results in rapid incision that lowers channel steepness to a quasi-equilibrium steepness that is maintained until the mainstem knickpoint propagates upstream (Fig. 5). In this simulation, knickzones form in tributaries with mainstem-tributary junctions in the bed of more erodible rock. In the South Fork Kings River, tributaries upstream and downstream of the band of metamorphic rock do not have large knickzones, whereas Boulder Creek, a tributary that joins the South Fork Kings in the middle of the band of marble just upstream of the cave, has a significant knickzone (Fig. S11; see footnote 1). We therefore interpret the pulse of incision recorded by the tiered caves as a signature of the transient response to rapid tilting modulated by a band of anomalously erodible rock (Fig. 5).

In rivers from the North Yuba south through the Stanislaus River, our estimates of late Cenozoic tilt magnitude (0.3–0.8°) and surface uplift at the crest (500–1300 m) are a little lower than previously published estimates, which range from 1 to 2° tilt and 1–2 km of surface uplift at the crest (Jones et al., 2004; Unruh, 1991; Wakabayashi and Sawyer, 2001). Previous work suggests that eclogitic root delamination would trigger more uplift in the southern Sierra than the northern Sierra owing to differences in root thickness (Cecil et al., 2012; Ducea and Saleeby, 1996; Jones et al., 2014). Without subtracting paleorelief, our upper estimates of tilt magnitude and surface uplift increase southward up to 2.7 km of surface uplift in the southern Sierra. However, subtracting estimated paleorelief

from these brings our estimates for the southern Sierra down to the lower end of published estimates that range from 1.5 to 2.5 km (Clark et al., 2005; Ducea and Saleeby, 1996; Huber, 1981; McPhillips and Brandon, 2012; Stock et al., 2005, 2004).

A significant body of literature based on stable isotope paleoaltimetry and paleobotany suggests that the Sierra was a topographic feature as high or higher as that of today throughout the Cenozoic (Cassel et al., 2014, 2012a, 2009b; Crowley et al., 2008; Hren et al., 2010; Mix et al., 2019, 2016; Mulch et al., 2008, 2006; Poage and Chamberlain, 2002; Wolfe et al., 1997). The lower half of our estimates of surface uplift are within that permitted by these geochemical data and as discussed in the introduction, these studies are based on methods and assumptions that have associated large uncertainties (Molnar, 2010). Our results also do not refute the idea that the Sierra was a high topographic feature in the Cretaceous (Clark et al., 2005; House et al., 2001, 1998; McPhillips and Brandon, 2012) that may have declined in elevation since the Cretaceous until a late Cenozoic uplift event (McPhillips and Brandon, 2012). Although thermochronology data indicates slow exhumation rates through the Cenozoic, it does not preclude the magnitude of surface uplift we observe in the late Cenozoic, only that <3 km has been eroded since the early Cenozoic (Cecil et al., 2006; House et al., 2001).

A detailed analysis of the lower sections of five rivers in the northern Sierra documented a correlation between channel steepness and underlying lithology (Gabet, 2020a). Our findings are in agreement with strong lithologic control of river channel steepness in the northern Sierra (Fig. 14). However, our interpretation differs in important ways from the interpretations in Gabet (2020a). The correlation between k_{sn} and rock type is interpreted by Gabet (2020a) as evidence that the Sierra is in a state of post-orogenic decay that is out of steady-state owing to differential erosion in rock types with variable erodibility. If this were the case, k_{sn} should only vary across rock types that have different erodibility. However, we observe systematic variability in k_{sn} even within the same rock type relative to the location of the mainstem tectonic knickpoints (Fig. 14). Even if our mainstem tectonic knickpoints occur near lithologic boundaries, the systematic differences in k_{sn} between segments downstream versus upstream of the knickpoints indicates that these knickpoints do not simply mark a change in erodibility, but rather a late Cenozoic change in the uplift field.

Most recently, a study using mining reports, high resolution geological maps, and newly mapped deposits documents careful measure-

ments of mainstem incision below Cenozoic deposits on the western slope of the northern Sierra at a handful of points along northern Sierra rivers (Gabet and Miggins, 2020). Similar to our results, their measurements of basement incision depth along each river transition from low values near the mountain front to high values at low to mid elevations before dropping again to low values at mid to high elevations. The low values of incision that they document occur just upstream of the locations of our mainstem tectonic knickpoints or in the upper reaches of the river network, consistent with our findings and the model of a transient response to rapid tilting. The authors interpret these measurements as evidence that the modern morphology of northern Sierra bedrock rivers reflects Eocene bedrock morphology that is simply being exhumed as Cenozoic deposits are eroded, with no need to appeal to late Cenozoic rock uplift. They argue that Eocene river deposits (and subsequently Oligocene ash-flow tuffs and Mio-Pliocene volcanics) buried a landscape that had been experiencing a propagating wave of bedrock incision that has resumed as the bedrock river network has been exposed in the late Cenozoic. However, we find that the mainstem tectonic knickpoints are at similar τ values throughout the range (Fig. 15), even though there is no evidence of widespread deposition of Cenozoic deposits in the southern Sierra. It is unlikely that other mechanisms that have been suggested to stall knickpoints in the southern Sierra, such as lack of tools (Callahan et al., 2019), would have stalled knickpoints at the same τ values as Gabet and Miggins (2020) suggest deposition did in the northern Sierra (Fig. 15). That said, our interpretations rely on topographic analysis and published erosion rates, of which few are from portions of the landscape downstream of our migrating knickpoints. Future work will seek to quantify erosion rates across these migrating knickpoints and in varying lithologies.

In the southernmost Sierra, we observe signatures of active tectonics in the Poso, Kern, and Tehachapi rivers. A knickzone with 325 m vertical offset occurs ~20 km upstream in the Poso River and a knickzone with a vertical offset of 580 m occurs also at ~20 km upstream in the Kern River (Fig. 10); the locations of these knickzones are coincident with the locations of the Pond-Poso and Kern Gorge Quaternary faults, respectively (Jennings, 1994; Mahéo et al., 2009). These knickzones likely reflect Quaternary northeast-side-up normal displacement on the linked Kern Gorge and Pond-Poso faults, which are estimated to have accumulated ~725 m of offset over the past ~1 m.y. (Mahéo et al., 2009). Farther south, in the Tehachapi River, a step-change in k_{sn} occurs at

~40 km upstream, with significantly higher k_{sn} downstream (Fig. 10). The recent increase in channel steepness likely reflects increased rock uplift rate in the Tehachapi Mountains and the onset of sinistral slip on the Garlock fault ca. 10 Ma (Blythe and Longinotti, 2013; Loomis and Burbank, 1988). We include these observations to demonstrate the marked difference in river profile forms between true slope-break knickpoints (step changes in otherwise uniform steepness) as observed in the Tehachapi River, vertical-step knickpoints as observed in the Kern and Poso rivers, and the slope-break knickpoints observed in the majority of Sierra rivers that separate a downstream section with relatively uniform steepness from an upstream section with nonuniform steepness. Although less research exists on the structures of the northern California shear zone that bounds the northern end of the range (Wesnousky, 2005), neotectonic activity related to the northwestward translation of the Sierra Nevada microplate (Unruh et al., 2003) is likely to have shaped the disequilibrium forms of the Feather River that we document.

Evidence from geochronology, geomorphology (Clark et al., 2005; Stock et al., 2005, 2004), and thermochronology (Sousa et al., 2016) suggests surface uplift in the southern Sierra may have occurred over two phases of uplift. As discussed above (see Mainstem and Tributary Longitudinal Profiles and χ Plots), secondary knickzones have larger variability in both presence and form in both mainstems and tributaries than the lower elevation mainstem tectonic knickpoints and tributary knickzones analyzed in this paper. Tributary profiles in the southern Sierra do have more complex transient forms containing multiple knickzones than do tributaries to rivers in the northern Sierra, which more consistently have one knickzone despite traveling through heterogeneous lithology. However, a recent tilting event would have partially obscured an earlier pulse of uplift, particularly if the earlier pulse of uplift were also a westward tilt (Fig. S12 [see footnote 1]; Beeson and McCoy, 2020). It is therefore difficult to use river profile morphology to quantify the nature of forcing that led the southern Sierra to have ~2000 m higher crest elevations than the northern Sierra. With higher resolution geologic maps and more careful investigation of erosion rates and processes, it may be possible to reconstruct what is clearly a more varied tectonic history in the southern Sierra than a single rigid-block tilting event in the late Cenozoic.

CONCLUSION

We analyzed river geomorphology in basins draining the western slope of the Sierra Nevada

from the Feather River south to the Tehachapi River and compared the results to published simulations of fluvial response to tectonic and non-tectonic perturbations in order to constrain the timing, magnitude, and spatial patterns in late Cenozoic uplift across the range. Disequilibrium forms in mainstem and tributary profiles from the Yuba River in the northern Sierra south through the Kings River are consistent with simulations of rapid tilting in the last ~11 m.y. Furthermore, elevations of mainstem knickpoints suggest that modern uplift rates increase linearly away from the mountain front and are still on the order of 100 m m.y.⁻¹. Estimates of surface uplift at the crest based on signatures identified in a 1-D model of a rapid pulse of tilt range from ~500 to 1300 m for the northern Sierra (0.3–0.8° tilt) and from ~1000 to 1400 m for the southern Sierra (0.6–0.9° tilt). Mainstem and tributary profile forms are most consistent with a short-lived (<5 m.y.) and rapid pulse of down-to-the-west tilting that began <11 Ma and slowed significantly between 2 and 6 Ma. However, the differences in profile signatures between a rapid punctuated tilt and onset of rapid tilting are subtle and we recognize that onset of rapid tilting in the last 5 m.y. is an alternative interpretation that cannot be ruled out based on river profile morphology alone. Disequilibrium river profile forms transition at the Kaweah River, which reflects a pulse of tilt in its mainstem but which has tributary profile forms inconsistent with a transient response to tilting. Basins south of the Kaweah River either reflect a pulse of uniform uplift or a step increase in uplift rates and the disequilibrium forms of all forks of the Feather River at the northern end of the Sierra have many secondary forms that likely reflect a more complex uplift field than simply a punctuated tilting event.

Beyond illustrating that late Cenozoic surface uplift of significant magnitude has occurred along the length of the Sierra, we demonstrate how geomorphic signatures described by simple numerical landscape evolution models can be used to help guide interpretations of similar forms found in real landscapes in order to reconstruct tectonic histories. We demonstrate that drainage area exchange between river basins can modulate the transient response to tectonic forcing in as substantial a manner as heterogeneous lithology, but that, once accounted for, disparate estimates of perturbation timing and magnitude from adjacent basins can be interpreted more clearly. Furthermore, we present evidence that portions of the Sierra are likely experiencing geometric reorganization rather than entrenchment of the existing river network. By limiting our analysis to major crest-draining river basins with minimal impact from geomet-

ric disequilibrium and by using multiple independent measures of timing and magnitude, we show that tectonic signatures can be recognized and quantified despite the presence of heterogeneous lithology, documented changes in the configuration of the river network, and the erosional dynamics associated with drainage area exchange between river basins.

ACKNOWLEDGEMENTS

This work was supported by the 2017 and 2018 Graduate Student Research Award from the Nevada Petroleum and Geothermal Society awarded to Helen Beeson. We thank two anonymous reviewers as well as Emmanuel Gabet for providing critical reviews that significantly strengthened the manuscript. Additionally, we thank Craig Jones and Greg Stock for many stimulating conversations and constructive feedback during the course of this work, Eric Deal for assisting with the analytical solutions for knickpoint location, and John Jansen for handling this paper as Associate Editor.

REFERENCES CITED

- Ague, J.J., 1997, Thermodynamic calculation of emplacement pressures for batholithic rocks, California: Implications for the aluminum-in-hornblende barometer: *Geology*, v. 25, p. 563–566, [https://doi.org/10.1130/0091-7613\(1997\)025<563:TCOEPF>2.3.CO;2](https://doi.org/10.1130/0091-7613(1997)025<563:TCOEPF>2.3.CO;2).
- Argus, D.F., and Gordon, R.G., 1991, Current Sierra Nevada–North America motion from very long baseline interferometry: Implications for the kinematics of the western United States: *Geology*, v. 19, p. 1085–1088, [https://doi.org/10.1130/0091-7613\(1991\)019<1085:CSNAM>2.3.CO;2](https://doi.org/10.1130/0091-7613(1991)019<1085:CSNAM>2.3.CO;2).
- Argus, D.F., and Gordon, R.G., 2001, Present tectonic motion across the Coast Ranges and San Andreas fault system in central California: *Geological Society of America Bulletin*, v. 113, p. 1580–1592, [https://doi.org/10.1130/0016-7606\(2001\)113<1580:PTMATIC>2.0.CO;2](https://doi.org/10.1130/0016-7606(2001)113<1580:PTMATIC>2.0.CO;2).
- Bales, R.C., Molotch, N.P., Painter, T.H., Dettinger, M.D., Rice, R., and Dozier, J., 2006, Mountain hydrology of the western United States: *Water Resources Research*, v. 42, <https://doi.org/10.1029/2005WR004387>.
- Bateman, P., and Wahrhaftig, C., 1966, Geology of the Sierra Nevada, in Bailey, E.H., eds., *Geology of Northern California: San Francisco, California*, U.S. Geological Survey Bulletin, California Division of Mines and Geology, v. 190, p. 107–172.
- Beeson, H.W., and McCoy, S.W., 2020, Geomorphic signatures of the transient fluvial response to tilting: *Earth Surface Dynamics*, v. 8, p. 123–159, <https://doi.org/10.5194/esurf-8-123-2020>.
- Beeson, H.W., McCoy, S.W., and Keen-Zebert, A., 2017, Geometric disequilibrium of river basins produces long-lived transient landscapes: *Earth and Planetary Science Letters*, v. 475, p. 34–43, <https://doi.org/10.1016/j.epsl.2017.07.010>.
- Berlin, M.M., and Anderson, R.S., 2007, Modeling of knickpoint retreat on the Roan Plateau, western Colorado: *Journal of Geophysical Research: Earth Surface*, v. 112, no. F3, <https://doi.org/10.1029/2006F000553>.
- Bernard, T., Sinclair, H.D., Gailleton, B., Mudd, S.M., and Ford, M., 2019, Lithological control on the post-orogenic topography and erosion history of the Pyrenees: *Earth and Planetary Science Letters*, v. 518, p. 53–66, <https://doi.org/10.1016/j.epsl.2019.04.034>.
- Blythe, A.E., and Longinotti, N., 2013, Exhumation of the southern Sierra Nevada–eastern Tehachapi Mountains constrained by low-temperature thermochronology: Implications for the initiation of the Garlock fault: *Lithosphere*, v. 5, p. 321–327, <https://doi.org/10.1130/L252.1>.
- Busby, C.J., and Putirka, K., 2009, Miocene evolution of the western edge of the Nevadaplano in the central

- and northern Sierra Nevada: Palaeocanyons, magmatism, and structure: International Geology Review, v. 51, p. 670–701, <https://doi.org/10.1080/00206810902978265>.
- Busby, C.J., Hagan, J.C., Putirka, K., Pluhar, C.J., Gans, P.B., Wagner, D.L., Rood, D., DeOreo, S.B., and Skilling, I., 2008, The ancestral Cascades arc: Cenozoic evolution of the central Sierra Nevada (California) and the birth of the new plate boundary, in Wright, J.E., and Shervais, J.W., eds., Ophiolites, Arcs, and Batholiths: A Tribute to Cliff Hopson: Geological Society of America Special Papers, v. 438, p. 331–378, [https://doi.org/10.1130/2008.2438\(12\)](https://doi.org/10.1130/2008.2438(12)).
- Callahan, R.P., Ferrier, K.L., Dixon, J., Dosseto, A., Hahm, W.J., Jessup, B.S., Miller, S.N., Hunsaker, C.T., Johnson, D.W., Sklar, L.S., and Riebe, C.S., 2019, Arrested development: Erosional equilibrium in the southern Sierra Nevada, California, maintained by feedbacks between channel incision and hillslope sediment production: Geological Society of America Bulletin, v. 131, p. 1179–1202, <https://doi.org/10.1130/B35006.1>.
- Carder, D.S., 1973, Trans-California seismic profile, Death Valley to Monterey Bay: Bulletin of the Seismological Society of America, v. 63, p. 571–586, <https://doi.org/10.1785/BSSA0630020571>.
- Cassel, E.J., and Graham, S.A., 2011, Paleovalley morphology and fluvial system evolution of Eocene–Oligocene sediments (“auriferous gravels”), northern Sierra Nevada, California: Implications for climate, tectonics, and topography: Geological Society of America Bulletin, v. 123, p. 1699–1719, <https://doi.org/10.1130/B30356.1>.
- Cassel, E.J., Calvert, A.T., and Graham, S.A., 2009a, Age, geochemical composition, and distribution of Oligocene ignimbrites in the northern Sierra Nevada, California: Implications for landscape morphology, elevation, and drainage divide geography of the Nevadaplano: International Geology Review, v. 51, p. 723–742, <https://doi.org/10.1080/00206810902880370>.
- Cassel, E.J., Graham, S.A., and Chamberlain, C.P., 2009b, Cenozoic tectonic and topographic evolution of the northern Sierra Nevada, California, through stable isotope paleoaltimetry in volcanic glass: Geology, v. 37, p. 547–550, <https://doi.org/10.1130/G25572A.1>.
- Cassel, E.J., Graham, S.A., Chamberlain, C.P., and Henry, C.D., 2012a, Early Cenozoic topography, morphology, and tectonics of the northern Sierra Nevada and western Basin and Range: Geosphere, v. 8, p. 229–249, <https://doi.org/10.1130/GES00671.1>.
- Cassel, E.J., Grove, M., and Graham, S.A., 2012b, Eocene drainage evolution and erosion of the Sierra Nevada batholith across northern California and Nevada: American Journal of Science, v. 312, p. 117–144, <https://doi.org/10.2475/02.2012.03>.
- Cassel, E.J., Breecker, D.O., Henry, C.D., Larson, T.E., and Stockli, D.F., 2014, Profile of a paleo-orogen: High topography across the present-day Basin and Range from 40 to 23 Ma: Geology, v. 42, p. 1007–1010, <https://doi.org/10.1130/G35924.1>.
- Cecil, M.R., Ducea, M.N., Reiners, P.W., and Chase, C.G., 2006, Cenozoic exhumation of the northern Sierra Nevada, California, from (U-Th)/He thermochronology: Geological Society of America Bulletin, v. 118, p. 1481–1488, <https://doi.org/10.1130/B25876.1>.
- Cecil, M.R., Rotberg, G.L., Ducea, M.N., Saleeby, J.B., and Gehrels, G.E., 2012, Magmatic growth and batholithic root development in the northern Sierra Nevada, California: Geosphere, v. 8, p. 592–606.
- Chen, C.-Y., Willett, S.D., Christl, M., and Shyu, J.B.H., 2021, Drainage basin dynamics during the transition from early to mature orogeny in Southern Taiwan: Earth and Planetary Science Letters, v. 562, <https://doi.org/10.1016/j.epsl.2021.116874>.
- Cherven, V.B., 1984, Early Pleistocene glacial outwash deposits in the eastern San Joaquin Valley, California: A model for humid-region alluvial fans: Sedimentology, v. 31, p. 823–836, <https://doi.org/10.1111/j.1365-3091.1984.tb00889.x>.
- Christensen, M.N., 1966, Late Cenozoic crustal movements in the Sierra Nevada of California: Geological Society of America Bulletin, v. 77, p. 163–182, [https://doi.org/10.1130/0016-7606\(1966\)77\[163:LCCMIT\]2.0.CO;2](https://doi.org/10.1130/0016-7606(1966)77[163:LCCMIT]2.0.CO;2).
- Clark, M.K., Maheo, G., Saleeby, J., and Farley, K.A., 2005, The non-equilibrium landscape of the southern Sierra Nevada, California: GSA Today, v. 15, p. 4–10, [https://doi.org/10.1130/1052-5173\(2005\)015<4:TNELOT>2.0.CO;2](https://doi.org/10.1130/1052-5173(2005)015<4:TNELOT>2.0.CO;2).
- Colgan, J.P., and Henry, C.D., 2009, Rapid middle Miocene collapse of the Mesozoic orogenic plateau in north-central Nevada: International Geology Review, v. 51, p. 920–961, <https://doi.org/10.1080/00206810903056731>.
- Colgan, J.P., John, D.A., Henry, C.D., and Fleck, R.J., 2008, Large-magnitude Miocene extension of the Eocene Caetano caldera, Shoshone and Toiyabe Ranges, Nevada: Geosphere, v. 4, p. 107–130, <https://doi.org/10.1130/GES00115.1>.
- Colgan, J.P., Howard, K.A., Fleck, R.J., and Wooden, J.L., 2010, Rapid middle Miocene extension and unroofing of the southern Ruby Mountains, Nevada: Tectonics, v. 29, no. 6, <https://doi.org/10.1029/2009TC002655>.
- Crowley, B.E., Koch, P.L., and Davis, E.B., 2008, Stable isotope constraints on the elevation history of the Sierra Nevada Mountains, California: Geological Society of America Bulletin, v. 120, p. 588–598, <https://doi.org/10.1130/B26254.1>.
- Curtis, G.H., 1953, Mode of origin of pyroclastic debris in the Mehrten formation of the Sierra Nevada: Berkeley, California, USA, University of California Press, 501 p.
- DeCelles, P.G., 2004, Late Jurassic to Eocene evolution of the Cordilleran thrust belt and foreland basin system, western USA: American Journal of Science, v. 304, p. 105–168, <https://doi.org/10.2475/ajs.304.2.105>.
- Despain, J.D., and Stock, G.M., 2005, Geomorphic history of Crystal Cave, southern Sierra Nevada, California: Journal of Caves and Karst Studies, v. 67, p. 92–102.
- DiBiase, R.A., and Whipple, K.X., 2011, The influence of erosion thresholds and runoff variability on the relationships among topography, climate, and erosion rate: Journal of Geophysical Research. Earth Surface, v. 116, no. F4, <https://doi.org/10.1029/2011JF002095>.
- DiBiase, R.A., Whipple, K.X., Heimsath, A.M., and Ouimet, W.B., 2010, Landscape form and millennial erosion rates in the San Gabriel Mountains, CA: Earth and Planetary Science Letters, v. 289, p. 134–144, <https://doi.org/10.1016/j.epsl.2009.10.036>.
- DiBiase, R.A., Heimsath, A.M., and Whipple, K.X., 2012, Hillslope response to tectonic forcing in threshold landscapes: Earth Surface Processes and Landforms, v. 37, p. 855–865, <https://doi.org/10.1002/esp.3205>.
- Dixon, T.H., Miller, M., Farina, F., Wang, H., and Johnson, D., 2000, Present-day motion of the Sierra Nevada block and some tectonic implications for the Basin and Range province, North American Cordillera: Tectonics, v. 19, p. 1–24, <https://doi.org/10.1029/1998TC001088>.
- Dokka, R.K., and Travis, C.J., 1990a, Late Cenozoic strike-slip faulting in the Mojave Desert, California: Tectonics, v. 9, p. 311–340, <https://doi.org/10.1029/TC009i002p00311>.
- Dokka, R.K., and Travis, C.J., 1990b, Role of the Eastern California shear zone in accommodating Pacific-North American plate motion: Geophysical Research Letters, v. 17, p. 1323–1326, <https://doi.org/10.1029/GL017i009p01323>.
- Ducea, M., and Saleeby, J., 1998, A case for delamination of the deep batholithic crust beneath the Sierra Nevada, California: International Geology Review, v. 40, p. 78–93, <https://doi.org/10.1080/00206819809465199>.
- Ducea, M.N., and Saleeby, J.B., 1996, Buoyancy sources for a large, unrooted mountain range, the Sierra Nevada, California: Evidence from xenolith thermobarometry: Journal of Geophysical Research. Solid Earth, v. 101, p. 8229–8244, <https://doi.org/10.1029/95JB03452>.
- Durrell, C., 1966, Tertiary and Quaternary geology of the northern Sierra Nevada, in Bailey, E.H., ed., Geology of Northern California: San Francisco, California, U.S. Geological Survey Bulletin, California Division of Mines and Geology, v. 190, p. 185–197.
- Duvall, A., Kirby, E., and Burbank, D., 2004, Tectonic and lithologic controls on bedrock channel profiles and processes in coastal California: Journal of Geophysical Research. Earth Surface, v. 109, no. F3, <https://doi.org/10.1029/2003JF000086>.
- England, P., and Molnar, P., 1990, Surface uplift, uplift of rocks, and exhumation of rocks: Geology, v. 18, p. 1173–1177, [https://doi.org/10.1130/0091-7613\(1990\)018<1173:SUUORA>2.3.CO;2](https://doi.org/10.1130/0091-7613(1990)018<1173:SUUORA>2.3.CO;2).
- Farmer, G.L., Glazner, A.F., and Manley, C.R., 2002, Did lithospheric delamination trigger late Cenozoic potassio volcanism in the southern Sierra Nevada, California?: Geological Society of America Bulletin, v. 114, p. 754–768, [https://doi.org/10.1130/0016-7606\(2002\)114<754:DLDLTC>2.0.CO;2](https://doi.org/10.1130/0016-7606(2002)114<754:DLDLTC>2.0.CO;2).
- Ferrier, K.L., Perron, J.T., Mukhopadhyay, S., Rosener, M., Stock, J.D., Huppert, K.L., and Slosberg, M., 2013, Co-variation of climate and long-term erosion rates across a steep rainfall gradient on the Hawaiian island of Kauai: Geological Society of America Bulletin, v. 125, p. 1146–1163, <https://doi.org/10.1130/B30726.1>.
- Flint, J.J., 1974, Stream gradient as a function of order, magnitude, and discharge: Water Resources Research, v. 10, p. 969–973, <https://doi.org/10.1029/WR010i005p00969>.
- Forte, A.M., and Whipple, K.X., 2018, Criteria and tools for determining drainage divide stability: Earth and Planetary Science Letters, v. 493, p. 102–117, <https://doi.org/10.1016/j.epsl.2018.04.026>.
- Forte, A.M., Yanites, B.J., and Whipple, K.X., 2016, Complexities of landscape evolution during incision through layered stratigraphy with contrasts in rock strength: Earth Surface Processes and Landforms, v. 41, p. 1736–1757, <https://doi.org/10.1002/esp.3947>.
- Frassetto, A.M., Zandt, G., Gilbert, H., Owens, T.J., and Jones, C.H., 2011, Structure of the Sierra Nevada from receiver functions and implications for lithospheric foundering: Geosphere, v. 7, p. 898–921, <https://doi.org/10.1130/GES00570.1>.
- Gabet, E.J., 2014, Late Cenozoic uplift of the Sierra Nevada, California? A critical analysis of the geomorphic evidence: American Journal of Science, v. 314, p. 1224–1257, <https://doi.org/10.2475/08.2014.03>.
- Gabet, E.J., 2020a, Lithological and structural controls on river profiles and networks in the northern Sierra Nevada (California, USA): Geological Society of America Bulletin, v. 132, p. 655–667, <https://doi.org/10.1130/B35128.1>.
- Gabet, E.J., 2020b, River profile evolution by plucking in lithologically heterogeneous landscapes: Uniform uplift vs. tilting: Earth Surface Processes and Landforms, v. 45, p. 1579–1588, <https://doi.org/10.1002/esp.4832>.
- Gabet, E.J., and Miggins, D.P., 2020, Minimal net incision of the northern Sierra Nevada (California, USA) since the Eocene–early Oligocene: Geology, <https://doi.org/10.1130/G47902.1>.
- Gailleton, B., Sinclair, H.D., Mudd, S.M., Graf, E.L.S., Matenco, L.C., 2021, Isolating lithologic versus tectonic signals of river profiles to test orogenic models for the eastern and southeastern Carpathians: Journal of Geophysical Research. Earth Surface, v. 126, no. 8, <https://doi.org/10.1029/2020JF005970>.
- Galewsky, J., 2009a, Orographic precipitation isotopic ratios in stratified atmospheric flows: Implications for paleoelevation studies: Geology, v. 37, p. 791–794, <https://doi.org/10.1130/G30008A.1>.
- Galewsky, J., 2009b, Rain shadow development during the growth of mountain ranges: An atmospheric dynamics perspective: Journal of Geophysical Research. Earth Surface, v. 114, no. F1, <https://doi.org/10.1029/2008JF001085>.
- Garside, L.J., Henry, C.D., Faulds, J.E., and Hinz, N.H., 2005, The upper reaches of the Sierra Nevada auriferous gold channels, California and Nevada, in Rhoden, H.N., Steininger, R.C., and Vikre, P.G., eds., Geological Society of Nevada Symposium: Window to the World, Reno, Nevada, May, p. 209–235.
- Gilbert, G.K., 1883, Peneplain on western slope of Sierra: Science, v. 1, p. 194–195.
- Gilbert, H., Yang, Y., Forsyth, D.W., Jones, C.H., Owens, T.J., Zandt, G., Stachnik, J.C., 2012, Imaging lithospheric foundering in the structure of the Sierra Nevada: Geosphere, v. 8, no. 6, <https://doi.org/10.1130/GES00790.1>.
- Gillespie, A.R., and Clark, D.H., 2011, Glaciations of the Sierra Nevada, California, USA, in Ehlers, J., Gibbard, P.L., and Hughes, P.D., eds., Developments in Quaternary Sciences: Quaternary Glaciations - Extent and Chronology: A Closer Look: Oxford, UK, Elsevier, v. 15, p. 447–462, <https://doi.org/10.1016/B978-0-444-53447-7.00034-9>.

- Granger, D.E., Kirchner, J.W., and Finkel, R., 1996, Spatially averaged long-term erosion rates measured from in situ-produced cosmogenic nuclides in alluvial sediment: *The Journal of Geology*, v. 104, p. 249–257, <https://doi.org/10.1086/629823>.
- Hack, J.T., 1957, Studies of longitudinal stream profiles in Virginia and Maryland: U.S. Geological Survey Professional Paper, v. 294-B, 59 p.
- Hack, J.T., 1973, Stream profile analysis and stream-gradient index: *Journal of Research of the U.S. Geological Survey*, v. 1, p. 421–429.
- Harel, M.-A., Mudd, S.M., and Attal, M., 2016, Global analysis of the stream power law parameters based on worldwide ^{10}Be denudation rates: *Geomorphology*, v. 268, p. 184–196, <https://doi.org/10.1016/j.geomorph.2016.05.035>.
- Harkins, N., Kirby, E., Heimsath, A., Robinson, R., and Reiser, U., 2007, Transient fluvial incision in the headwaters of the Yellow River, northeastern Tibet, China: *Journal of Geophysical Research*, v. 112, no. F3, <https://doi.org/10.1029/2006JF000570>.
- Haviv, I., Enzel, Y., Whipple, K.X., Zilberman, E., Matmon, A., Stone, J., and Fifield, K.L., 2010, Evolution of vertical knickpoints (waterfalls) with resistant caprock: Insights from numerical modeling: *Journal of Geophysical Research. Earth Surface*, v. 115, no. F3, <https://doi.org/10.1029/2008JF001187>.
- Hayakawa, Y., and Matsukura, Y., 2003, Recession rates of waterfalls in Boso Peninsula, Japan, and a predictive equation: *Earth Surface Processes and Landforms*, v. 28, p. 675–684, <https://doi.org/10.1002/esp.519>.
- Henry, C.D., 2008, Ash-flow tuffs and paleovalleys in north-eastern Nevada: Implications for Eocene paleogeography and extension in the Sevier hinterland, northern Great Basin: *Geosphere*, v. 4, p. 1–35, <https://doi.org/10.1130/GES00122.1>.
- Henry, C.D., 2009, Uplift of the Sierra Nevada, California: *Geology*, v. 37, p. 575–576, <https://doi.org/10.1130/focus062009.1>.
- Henry, C.D., and Faulds, J.E., 2010, Ash-flow tuffs in the Nine Mile, Nevada, paleovalley and implications for tectonism and volcanism of the western Great Basin, USA: *Geosphere*, v. 6, p. 339–369, <https://doi.org/10.1130/GES00548.1>.
- Henry, C.D., Hinz, N.H., Faulds, J.E., Colgan, J.P., John, D.A., Brooks, E.R., Cassel, E.J., Garside, L.J., Davis, D.A., and Castor, S.B., 2012, Eocene-Early Miocene paleotopography of the Sierra Nevada-Great Basin-Nevadaplano based on widespread ash-flow tuffs and paleovalleys: *Geosphere*, v. 8, p. 1–27, <https://doi.org/10.1130/GES00727.1>.
- House, M.A., Wernicke, B.P., and Farley, K.A., 1998, Dating topography of the Sierra Nevada, California, using apatite (U-Th)/He ages: *Nature*, v. 396, p. 66–69, <https://doi.org/10.1038/23926>.
- House, M.A., Wernicke, B.P., and Farley, K.A., 2001, Paleo-geomorphology of the Sierra Nevada, California, from (U-Th)/He ages in apatite: *American Journal of Science*, v. 301, p. 77–102, <https://doi.org/10.2475/ajs.301.2.77>.
- Howard, A.D., 1994, A detachment-limited model of drainage basin evolution: *Water Resources Research*, v. 30, p. 2261–2285, <https://doi.org/10.1029/94WR00757>.
- Howard, A.D., and Kerby, G., 1983, Channel changes in badlands: *Geological Society of America Bulletin*, v. 94, p. 739–752, [https://doi.org/10.1130/0016-7606\(1983\)94<739:CCIB>2.0.CO;2](https://doi.org/10.1130/0016-7606(1983)94<739:CCIB>2.0.CO;2).
- Hren, M.T., Pagani, M., Erwin, D.M., and Brandon, M., 2010, Biomarker reconstruction of the early Eocene paleotopography and paleoclimate of the northern Sierra Nevada: *Geology*, v. 38, p. 7–10, <https://doi.org/10.1130/G30215.1>.
- Hu, K., Fang, X., Ferrier, K.L., Granger, D.E., Zhao, Z., and Ruetenik, G.A., 2021, Covariation of cross-divide differences in denudation rate and χ : Implications for drainage basin reorganization in the Qilian Shan, northeast Tibet: *Earth and Planetary Science Letters*, v. 562, <https://doi.org/10.1016/j.epsl.2021.116812>.
- Huber, N.K., 1981, Amount and timing of late Cenozoic uplift and tilt of the central Sierra Nevada, California: evidence from the upper San Joaquin River basin: U.S. Geological Survey Professional Paper, 28 p., <https://pubs.er.usgs.gov/publication/pp1197>.
- Hudson, F.S., 1955, Measurement of the deformation of the Sierra Nevada, California, since middle Eocene: *Geological Society of America Bulletin*, v. 66, p. 835–870, [https://doi.org/10.1130/0016-7606\(1955\)66\[835:MOTD\]2.0.CO;2](https://doi.org/10.1130/0016-7606(1955)66[835:MOTD]2.0.CO;2).
- Hurst, M.D., Mudd, S.M., Walcott, R., Attal, M., and Yoo, K., 2012, Using hilltop curvature to derive the spatial distribution of erosion rates: *Journal of Geophysical Research. Earth Surface*, v. 117, no. F2, <https://doi.org/10.1029/2011JF002057>.
- Jansen, J.D., Codilean, A.T., Bishop, P., and Hoey, T.B., 2010, Scale dependence of lithological control on topography: Bedrock channel geometry and catchment morphometry in western Scotland: *The Journal of Geology*, v. 118, p. 223–246, <https://doi.org/10.1086/651273>.
- Jansen, J.D., Fabel, D., Bishop, P., Xu, S., Schnabel, C., and Codilean, A.T., 2011, Does decreasing paraglacial sediment supply slow knickpoint retreat?: *Geology*, v. 39, p. 543–546, <https://doi.org/10.1130/G32018.1>.
- Jennings, C.W., 1994, Fault activity map of California and adjacent areas, with locations and ages of recent volcanic eruptions: Sacramento, California, USA, California Division of Mines and Geology, California Geologic Data Map Series, no. 6, 92 p.
- Jones, C.H., Kanamori, H., and Roecker, S.W., 1994, Missing roots and mantle “drips”: Regional P_n and teleseismic arrival times in the southern Sierra Nevada and vicinity, California: *Journal of Geophysical Research. Solid Earth*, v. 99, p. 4567–4601, <https://doi.org/10.1029/93JB01232>.
- Jones, C.H., Farmer, G.L., and Unruh, J., 2004, Tectonics of Pliocene removal of lithosphere of the Sierra Nevada, California: *Geological Society of America Bulletin*, v. 116, p. 1408–1422, <https://doi.org/10.1130/B25397.1>.
- Jones, C.H., Reeg, H., Zandt, G., Gilbert, H., Owens, T.J., and Stachnik, J., 2014, P-wave tomography of potential convective downwellings and their source regions, Sierra Nevada, California: *Geosphere*, v. 10, p. 505–533, <https://doi.org/10.1130/GES00961.1>.
- Kirby, E., and Whipple, K., 2001, Quantifying differential rock-uplift rates via stream profile analysis: *Geology*, v. 29, p. 415–418, [https://doi.org/10.1130/0091-7613\(2001\)029<0415:QDRURV>2.0.CO;2](https://doi.org/10.1130/0091-7613(2001)029<0415:QDRURV>2.0.CO;2).
- Kirby, E., and Whipple, K.X., 2012, Expression of active tectonics in erosional landscapes: *Journal of Structural Geology*, v. 44, p. 54–75, <https://doi.org/10.1016/j.jsg.2012.07.009>.
- Kreemer, C., Blewitt, G., and Klein, E.C., 2014, A geodetic plate motion and Global Strain Rate Model: *Geochemistry, Geophysics, Geosystems*, v. 15, p. 3849–3889, <https://doi.org/10.1002/2014GC005407>.
- Lague, D., 2014, The stream power river incision model: Evidence, theory and beyond: *Earth Surface Processes and Landforms*, v. 39, p. 38–61, <https://doi.org/10.1002/esp.3462>.
- Lal, D., 1991, Cosmic ray labeling of erosion surfaces: In situ nuclide production rates and erosion models: *Earth and Planetary Science Letters*, v. 104, p. 424–439, [https://doi.org/10.1016/0012-821X\(91\)90220-C](https://doi.org/10.1016/0012-821X(91)90220-C).
- Larimer, J.E., Yanites, B.J., Phillips, W., and Mittelstaedt, E., 2019, Late Miocene rejuvenation of central Idaho landscape evolution: A case for surface processes driven by plume-lithosphere interaction: *Lithosphere*, v. 11, p. 59–72, <https://doi.org/10.1130/L746.1>.
- Lavé, J., and Avouac, J.P., 2000, Active folding of fluvial terraces across the Siwaliks Hills, Himalayas of central Nepal: *Journal of Geophysical Research. Solid Earth*, v. 105, p. 5735–5770, <https://doi.org/10.1029/1999JB900292>.
- Lechler, A.R., and Galewsky, J., 2013, Refining paleoaltimetry reconstructions of the Sierra Nevada, California, using air parcel trajectories: *Geology*, v. 41, p. 259–262, <https://doi.org/10.1130/G33553.1>.
- Lechler, A.R., and Niemi, N.A., 2011, Controls on the spatial variability of modern meteoric ^{18}O : Empirical constraints from the western U.S. and east Asia and implications for stable isotope studies: *American Journal of Science*, v. 311, p. 664–700, <https://doi.org/10.2475/08.2011.02>.
- Le Conte, J., 1886, Post-Tertiary elevation of the Sierra Nevada shown by the river beds: *American Journal of Science*, v. 32, p. 167–181.
- Lee, C.-T.A., 2014, Physics and chemistry of deep continental crust recycling, in Holland, H.D., and Turekian, K.K. eds., *Treatise on Geochemistry* (Second Edition): Amsterdam, Netherlands, Elsevier, v. 4, p. 423–456, <https://doi.org/10.1016/B978-0-08-095975-7.00314-4>.
- Lindgren, W., 1911, The Tertiary gravels of the Sierra Nevada of California: U.S. Geological Survey Professional Paper, v. 73, 226 p., <https://doi.org/10.3133/pp73>.
- Loget, N., and Van Den Driessche, J., 2009, Wave train model for knickpoint migration: *Geomorphology*, v. 106, p. 376–382, <https://doi.org/10.1016/j.geomorph.2008.10.017>.
- Loomis, D.P., and Burbank, D.W., 1988, The stratigraphic evolution of the El Paso basin, southern California: Implications for the Miocene development of the Garlock fault and uplift of the Sierra Nevada: *Geological Society of America Bulletin*, v. 100, p. 12–28, [https://doi.org/10.1130/0016-7606\(1988\)100<0012:TSEOTE>2.3.CO;2](https://doi.org/10.1130/0016-7606(1988)100<0012:TSEOTE>2.3.CO;2).
- Ludington, S., Moring, B.C., Miller, R.J., Stone, P.A., Bookstrom, A.A., Bedford, D.R., Evans, J.G., Hazel, G.A., Nutt, C.J., Flynn, K.S., and Hopkins, M.J., 2005, Preliminary integrated geologic map databases for the United States: Western states: California, Nevada, Arizona, Washington, Idaho, and Utah: U.S. Geological Survey, Open-File Report no. 1305, <http://pubs.usgs.gov/of/2005/1305/index.htm>.
- Mackin, J.H., 1948, Concept of the graded river: *Geological Society of America Bulletin*, v. 59, p. 463–512, [https://doi.org/10.1130/0016-7606\(1948\)59\[463:COTGR\]2.0.CO;2](https://doi.org/10.1130/0016-7606(1948)59[463:COTGR]2.0.CO;2).
- Mahéo, G., Saleeby, J., Saleeby, Z., and Farley, K.A., 2009, Tectonic control on southern Sierra Nevada topography, California: *Tectonics*, v. 28, <https://doi.org/10.1029/2008TC002340>.
- Manley, C.R., Glazner, A.F., and Farmer, G.L., 2000, Timing of volcanism in the Sierra Nevada of California: Evidence for Pliocene delamination of the batholith root?: *Geology*, v. 28, p. 811–814, [https://doi.org/10.1130/0091-7613\(2000\)28<811:TOVITS>2.0.CO;2](https://doi.org/10.1130/0091-7613(2000)28<811:TOVITS>2.0.CO;2).
- Martel, S.J., Stock, G.M., and Ito, G., 2014, Mechanics of relative and absolute displacements across normal faults, and implications for uplift and subsidence along the eastern escarpment of the Sierra Nevada, California: *Geosphere*, v. 10, p. 243–263, <https://doi.org/10.1130/GES00968.1>.
- Matthes, F., 1930, Geologic history of Yosemite Valley: U.S. Geological Survey Professional Paper, v. 160, 137 p., <https://pubs.er.usgs.gov/publication/pp160>.
- McPhillips, D., and Brandon, M.T., 2012, Topographic evolution of the Sierra Nevada measured directly by inversion of low-temperature thermochronology: *American Journal of Science*, v. 312, p. 90–116, <https://doi.org/10.2475/02.2012.02>.
- Mitchell, N., and Yanites, B., 2019a, Spatially variable increase in rock uplift in the northern U.S. Cordillera recorded in the distribution of river knickpoints and incision depths: *Journal of Geophysical Research. Earth Surface*, v. 124, p. 1238–1260, <https://doi.org/10.1029/2018JF004880>.
- Mitchell, N.A., and Yanites, B.J., 2019b, Spatially variable increase in rock uplift in the northern U.S. Cordillera recorded in the distribution of river knickpoints and incision depths: *Journal of Geophysical Research. Earth Surface*, v. 124, p. 1238–1260, <https://doi.org/10.1029/2018JF004880>.
- Mix, H.T., Ibarra, D.E., Mulch, A., Graham, S.A., and Chamberlain, C.P., 2016, A hot and high Eocene Sierra Nevada: *Geological Society of America Bulletin*, v. 128, p. 531–542, <https://doi.org/10.1130/B31294.1>.
- Mix, H.T., Caves Rugenstein, J.K., Reilly, S.P., Ritch, A.J., Winnick, M.J., Kukla, T., and Chamberlain, C.P., 2019, Atmospheric flow deflection in the late Cenozoic Sierra Nevada: *Earth and Planetary Science Letters*, v. 518, p. 76–85, <https://doi.org/10.1016/j.epsl.2019.04.050>.
- Molnar, P., 2010, Deuterium and oxygen isotopes, paleoelevations of the Sierra Nevada, and Cenozoic climate:

- Geological Society of America Bulletin, v. 122, p. 1106–1115, <https://doi.org/10.1130/B30001.1>.
- Morisawa, M., 1964, Development of drainage systems on an upraised lake floor: American Journal of Science, v. 262, p. 340–354, <https://doi.org/10.2475/ajs.262.3.340>.
- Mudd, S.M., Clubb, F.J., Gailleton, B., and Hurst, M.D., 2018, How concave are river channels?: Earth Surface Dynamics, v. 6, p. 505–523, <https://doi.org/10.5194/esurf-6-505-2018>.
- Mulch, A., Graham, S.A., and Chamberlain, C.P., 2006, Hydrogen isotopes in Eocene River Gravels and Paleoelevation of the Sierra Nevada: Science, v. 313, p. 87–89, <https://doi.org/10.1126/science.1125986>.
- Mulch, A., Sarna-Wojcicki, A.M., Perkins, M.E., and Chamberlain, C.P., 2008, A Miocene to Pleistocene climate and elevation record of the Sierra Nevada (California): Proceedings of the National Academy of Sciences of the United States of America, v. 105, p. 6819–6824, <https://doi.org/10.1073/pnas.0708811105>.
- Nadin, E.S., Saleeby, J., and Wong, M., 2016, Thermal evolution of the Sierra Nevada batholith, California, and implications for strain localization: Geosphere, v. 12, p. 377–399, <https://doi.org/10.1130/GES01224.1>.
- Namson, J.S., and Davis, T.L., 1988, Seismically active fold and thrust belt in the San Joaquin Valley, central California: Geological Society of America Bulletin, v. 100, p. 257–273, [https://doi.org/10.1130/0016-7606\(1988\)100<0257:SAFATB>2.3.CO;2](https://doi.org/10.1130/0016-7606(1988)100<0257:SAFATB>2.3.CO;2).
- Namson, J., and Davis, T.L., 1990, Late Cenozoic fold and thrust belt of the southern Coast Ranges and Santa Maria Basin, California: AAPG Bulletin, v. 74, p. 467–492.
- Niemann, J.D., Gasparini, N.M., Tucker, G.E., and Bras, R.L., 2001, A quantitative evaluation of Playfair's law and its use in testing long-term stream erosion models: Earth Surface Processes and Landforms, v. 26, p. 1317–1332, <https://doi.org/10.1002/esp.272>.
- Ouimet, W.B., Whipple, K.X., and Granger, D.E., 2009, Beyond threshold hillslopes: Channel adjustment to base-level fall in tectonically active mountain ranges: Geology, v. 37, p. 579–582, <https://doi.org/10.1130/G30013A.1>.
- Pelletier, J.D., 2007, Numerical modeling of the Cenozoic geomorphic evolution of the southern Sierra Nevada, California: Earth and Planetary Science Letters, v. 259, p. 85–96, <https://doi.org/10.1016/j.epsl.2007.04.030>.
- Perron, J.T., and Royden, L., 2013, An integral approach to bedrock river profile analysis: Earth Surface Processes and Landforms, v. 38, p. 570–576, <https://doi.org/10.1002/esp.3302>.
- Pickett, D.A., and Saleeby, J.B., 1993, Thermobarometric constraints on the depth of exposure and conditions of plutonism and metamorphism at deep levels of the Sierra Nevada Batholith, Tehachapi Mountains, California: Journal of Geophysical Research. Solid Earth, v. 98, p. 609–629, <https://doi.org/10.1029/92JB01889>.
- Poage, M.A., and Chamberlain, C.P., 2002, Stable isotopic evidence for a Pre-Middle Miocene rain shadow in the western Basin and Range: Implications for the paleotopography of the Sierra Nevada: Tectonics, v. 21, no. 4, <https://doi.org/10.1029/2001TC001303>.
- Portenga, E.W., and Bierman, P.R., 2011, Understanding Earth's eroding surface with ^{10}Be : GSA Today, v. 21, p. 4–10, <https://doi.org/10.1130/G111A.1>.
- Riebe, C.S., Kirchner, J.W., Granger, D.E., and Finkel, R.C., 2000, Erosional equilibrium and disequilibrium in the Sierra Nevada, inferred from cosmogenic ^{26}Al and ^{10}Be in alluvial sediment: Geology, v. 28, p. 803–806, [https://doi.org/10.1130/0091-7613\(2000\)28<803:EEADIT>2.0.CO;2](https://doi.org/10.1130/0091-7613(2000)28<803:EEADIT>2.0.CO;2).
- Roe, G.H., Montgomery, D.R., and Hallet, B., 2002, Effects of orographic precipitation variations on the concavity of steady-state river profiles: Geology, v. 30, p. 143–146, [https://doi.org/10.1130/0091-7613\(2002\)030<0143:EOOPVO>2.0.CO;2](https://doi.org/10.1130/0091-7613(2002)030<0143:EOOPVO>2.0.CO;2).
- Royden, L., and Perron, J.T., 2013, Solutions of the stream power equation and application to the evolution of river longitudinal profiles: Journal of Geophysical Research. Earth Surface, v. 118, p. 497–518, <https://doi.org/10.1002/jgrf.20031>.
- Rosenbloom, N.A., and Anderson, R.S., 1994, Hillslope and channel evolution in a marine terraced landscape, San-ta Cruz, California: Journal of Geophysical Research. Solid Earth, v. 99, p. 14013–14029, <https://doi.org/10.1029/94JB00048>.
- Ruetenik, G.A., Hoke, G.D., Moucha, R., and Val, P., 2018, Regional landscape response to thrust belt dynamics: The Iglesias basin, Argentina: Basin Research, v. 30, p. 1141–1154, <https://doi.org/10.1111/bre.12295>.
- Saleeby, J., Pourhiet, L.L., Saleeby, Z., and Gurnis, M., 2012, Epeirogenic transients related to mantle lithosphere removal in the southern Sierra Nevada region, California, part I: Implications of thermomechanical modeling: Geosphere, v. 8, p. 1286–1309, <https://doi.org/10.1130/GES00746.1>.
- Saleeby, J., Saleeby, Z., and Pourhiet, L.L., 2013, Epeirogenic transients related to mantle lithosphere removal in the southern Sierra Nevada region, California: Part II: Implications of rock uplift and basin subsidence relations: Geosphere, v. 9, p. 394–425, <https://doi.org/10.1130/GES00816.1>.
- Saucedo, G.J., and Wagner, D.L., 1992, Geologic map of the Chico quadrangle: Sacramento, California, USA, California Division of Mines and Geology, Regional Geologic Map 7A, scale 1:250,000, https://ngmdb.usgs.gov/ProdDesc/proddesc_63087.htm.
- Scheingross, J.S., and Lamb, M.P., 2017, A mechanistic model of waterfall plunge pool erosion into bedrock: Journal of Geophysical Research. Earth Surface, v. 122, p. 2079–2104, <https://doi.org/10.1002/2017JF004195>.
- Scheingross, J.S., Limaye, A.B., McCoy, S.W., and Whitaker, A.C., 2020, The shaping of erosional landscapes by internal dynamics: Nature Reviews Earth & Environment, v. 1, p. 661–676, <https://doi.org/10.1038/s43017-020-0096-0>.
- Schwanaghart, W., and Scherler, D., 2014, Short Communication: TopoToolbox 2 - MATLAB-based software for topographic analysis and modeling in Earth surface sciences: Earth Surface Dynamics, v. 2, p. 1–7, <https://doi.org/10.5194/esurf-2-1-2014>.
- Shobe, C.M., Tucker, G.E., Anderson, R.S., 2016, Hillslope-derived blocks retard river incision: Geophysical Research Letters, v. 43, p. 5070–5078, <https://doi.org/10.1002/2016GL069262>.
- Siedl, M.A., and Dietrich, W.E., 1992, The problem of channel erosion into bedrock, in Schmidt, K.-H., De Ploey, J., eds., Functional Geomorphology: Landform Analysis and Models: Cremlingen, Germany, Catena-Verlag, Catena Supplement, v. 23, p. 101–124.
- Sklar, L.S., and Dietrich, W.E., 2001, Sediment and rock strength controls on river incision into bedrock: Geology, v. 29, p. 1087–1090, [https://doi.org/10.1130/0091-7613\(2001\)029<1087:SARSCO>2.0.CO;2](https://doi.org/10.1130/0091-7613(2001)029<1087:SARSCO>2.0.CO;2).
- Sklar, L.S., and Dietrich, W.E., 2004, A mechanistic model for river incision into bedrock by saltating bed load: Water Resources Research, v. 40, no. 6, <https://doi.org/10.1029/2003WR002496>.
- Slemmons, D.B., 1966, Cenozoic volcanism of the central Sierra Nevada, California, in Bailey, E.H., ed., Geology of Northern California: San Francisco, California, U.S. Geological Survey Bulletin, California Division of Mines and Geology, v. 190, p. 199–208.
- Small, E.E., and Anderson, R.S., 1995, Geomorphically driven late Cenozoic rock uplift in the Sierra Nevada, California: Science, v. 270, p. 277–281, <https://doi.org/10.1126/science.270.5234.277>.
- Small, E.E., Anderson, R.S., Repka, J.L., and Finkel, R., 1997, Erosion rates of alpine bedrock summit surfaces deduced from in situ ^{10}Be and ^{26}Al : Earth and Planetary Science Letters, v. 150, p. 413–425, [https://doi.org/10.1016/S0012-821X\(97\)00092-7](https://doi.org/10.1016/S0012-821X(97)00092-7).
- Snyder, N.P., Whipple, K.X., Tucker, G.E., and Merritts, D.J., 2000, Landscape response to tectonic forcing: Digital elevation model analysis of stream profiles in the Mendocino triple junction region, northern California: Geological Society of America Bulletin, v. 112, p. 1250–1263, [https://doi.org/10.1130/0016-7606\(2000\)112<1250:LRTTFD>2.0.CO;2](https://doi.org/10.1130/0016-7606(2000)112<1250:LRTTFD>2.0.CO;2).
- Sousa, F.J., Farley, K.A., Saleeby, J., and Clark, M., 2016, Eocene activity on the Western Sierra Fault System and its role incising Kings Canyon, California: Earth and Planetary Science Letters, v. 439, p. 29–38, <https://doi.org/10.1016/j.epsl.2016.01.020>.
- Stock, G.M., Anderson, R.S., and Finkel, R.C., 2004, Pace of landscape evolution in the Sierra Nevada, California, revealed by cosmogenic dating of cave sediments: Geology, v. 32, p. 193–196, <https://doi.org/10.1130/G20197.1>.
- Stock, G.M., Anderson, R.S., and Finkel, R.C., 2005, Rates of erosion and topographic evolution of the Sierra Nevada, California, inferred from cosmogenic ^{26}Al and ^{10}Be concentrations: Earth Surface Processes and Landforms, v. 30, p. 985–1006, <https://doi.org/10.1002/esp.1258>.
- Stock, J., and Dietrich, W.E., 2003, Valley incision by debris flows: Evidence of a topographic signature: Water Resources Research, v. 39, no. 4, <https://doi.org/10.1029/2001WR001057>.
- Stock, J.D., and Montgomery, D.R., 1999, Geologic constraints on bedrock river incision using the stream power law: Journal of Geophysical Research. Solid Earth, v. 104, p. 4983–4993, <https://doi.org/10.1029/98JB02139>.
- Thompson, G.A., and Parsons, T., 2009, Can footwall unloading explain late Cenozoic uplift of the Sierra Nevada crest?: International Geology Review, v. 51, p. 986–993, <https://doi.org/10.1080/00206810903059156>.
- Tucker, G.E., and Whipple, K.X., 2002, Topographic outcomes predicted by stream erosion models: Sensitivity analysis and intermodel comparison: Journal of Geophysical Research. Solid Earth, v. 107, no. B9, <https://doi.org/10.1029/2001JB000162>.
- Unruh, J.R., 1991, The uplift of the Sierra Nevada and implications for late Cenozoic epeirogeny in the western Cordilleran: Geological Society of America Bulletin, v. 103, p. 1395–1404, [https://doi.org/10.1130/0016-7606\(1991\)103<1395:TUOTSN>2.3.CO;2](https://doi.org/10.1130/0016-7606(1991)103<1395:TUOTSN>2.3.CO;2).
- Unruh, J., Humphrey, J., and Barron, A., 2003, Transtensional model for the Sierra Nevada frontal fault system, eastern California: Geology, v. 31, p. 327–330, [https://doi.org/10.1130/0091-7613\(2003\)031<0327:TMFTSN>2.0.CO;2](https://doi.org/10.1130/0091-7613(2003)031<0327:TMFTSN>2.0.CO;2).
- USGS, 1916, Historical quadrangle for Copperopolis, California: U.S. Department of the Interior, U.S. Geological Survey, scale 1:62,500.
- Wagner, D.L., Jennings, C.W., Bedrossian, T.L., Bortugno, E.J., 1981, Geologic map of the Sacramento quadrangle, California: Sacramento, California, USA, California Division of Mines and Geology, Regional Geologic Map 1A, scale 1:250,000, https://ngmdb.usgs.gov/ProdDesc/proddesc_520.htm.
- Wahrhaftig, C., 1965, Stepped topography of the southern Sierra Nevada, California: Geological Society of America Bulletin, v. 76, p. 1165–1190, [https://doi.org/10.1130/0016-7606\(1965\)76\[1165:STOTSS\]2.0.CO;2](https://doi.org/10.1130/0016-7606(1965)76[1165:STOTSS]2.0.CO;2).
- Wakabayashi, J., 2013, Paleochannels, stream incision, erosion, topographic evolution, and alternative explanations of paleoaltimetry, Sierra Nevada, California: Geosphere, v. 9, p. 191–215, <https://doi.org/10.1130/GES00814.1>.
- Wakabayashi, J., and Sawyer, T.L., 2001, Stream incision, tectonics, uplift, and evolution of topography of the Sierra Nevada, California: The Journal of Geology, v. 109, p. 539–562, <https://doi.org/10.1086/321962>.
- Weissmann, G.S., Mount, J.F., and Fogg, G.E., 2002, Glacially driven cycles in accumulation space and sequence stratigraphy of a stream-dominated alluvial fan, San Joaquin Valley, California, U.S.A.: Journal of Sedimentary Research, v. 72, p. 240–251, <https://doi.org/10.1306/062201720240>.
- Wentworth, C.M., and Zoback, M.D., 1989, The style of Late Cenozoic deformation at the eastern front of the California Coast Ranges: Tectonics, v. 8, p. 237–246, <https://doi.org/10.1029/TC008i002p00237>.
- Wernicke, B., and Snow, J.K., 1998, Cenozoic tectonism in the central Basin and Range: Motion of the Sierran-Great Valley Block: International Geology Review, v. 40, p. 403–410, <https://doi.org/10.1080/00206819809465217>.
- Wesnousky, S.G., 2005, Active faulting in the Walker Lane: Tectonics, v. 24, no. 3, <https://doi.org/10.1029/2004TC001645>.
- Whipple, K.X., 2004, Bedrock rivers and the geomorphology of active orogens: Annual Review of Earth and Planetary Sciences, v. 32, p. 151–185, <https://doi.org/10.1146/annurev.earth.32.101802.120356>.
- Whipple, K.X., and Tucker, G.E., 1999, Dynamics of the stream-power river incision model: Implications for height limits of mountain ranges, landscape response timescales, and research needs: Journal of Geophysical

Sierra Nevada river networks record late Cenozoic tilting

- Research. Solid Earth, v. 104, p. 17661–17674, <https://doi.org/10.1029/1999JB900120>.
- Whipple, K.X., DiBiase, R.A., and Crosby, B.T., 2013, Bedrock rivers, in Shroder, J.F., ed., Treatise on Geomorphology: San Diego, California, USA, Academic Press, v. 9, p. 550–573, <https://doi.org/10.1016/B978-0-12-374739-6.00254-2>.
- Whipple, K.X., Hancock, G.S., and Anderson, R.S., 2000, River incision into bedrock: Mechanics and relative efficacy of plucking, abrasion, and cavitation: Bulletin of the Geological Society of America, v. 112, p. 490–503, [https://doi.org/10.1130/0016-7606\(2000\)112<490:RIIBMA>2.0.CO;2](https://doi.org/10.1130/0016-7606(2000)112<490:RIIBMA>2.0.CO;2).
- Willett, S.D., McCoy, S.W., Perron, J.T., Goren, L., and Chen, C.-Y., 2014, Dynamic reorganization of river basins: Science, v. 343, <https://doi.org/10.1126/science.1248765>.
- Willett, S.D., McCoy, S.W., and Beeson, H.W., 2018, Transience of the North American High Plains landscape and its impact on surface water: Nature, v. 561, p. 528–532, <https://doi.org/10.1038/s41586-018-0532-1>.
- Wobus, C., Whipple, K.X., Kirby, E., Snyder, N., Johnson, J., Spyropoulou, K., Crosby, B., and Sheehan, D., 2006, Tectonics from topography: Procedures, promise, and pitfalls, in Tectonics, Climate, and Landscape Evolution: Geological Society of America Special Papers, v. 398, p. 55–74, [https://doi.org/10.1130/2006.2398\(04\)](https://doi.org/10.1130/2006.2398(04)).
- Wolfe, J.A., Schorn, H.E., Forest, C.E., and Molnar, P., 1997, Paleobotanical evidence for high altitudes in Nevada during the Miocene: Science, v. 276, p. 1672–1675, <https://doi.org/10.1126/science.276.5319.1672>.
- Yang, R., Willett, S.D., and Goren, L., 2015, In situ low-relief landscape formation as a result of river network disruption: Nature, v. 520, p. 526–529, <https://doi.org/10.1038/nature14354>.
- Yanites, B.J., Becker, J.K., Madritsch, H., Schnellmann, M., and Ehlers, T.A., 2017, Lithologic effects on landscape response to base level changes: A modeling study in the context of the eastern Jura Mountains, Switzerland: Journal of Geophysical Research. Earth Surface, v. 122, p. 2196–2222, <https://doi.org/10.1002/2016JF004101>.
- Yeend, W.E., 1974, Gold-bearing gravel of the ancestral Yuba River, Sierra Nevada, California: U.S. Geological Survey Professional Paper, v. 772, 44 p., <https://doi.org/10.3133/pp772>.
- Zandt, G., Gilbert, H., Owens, T.J., Ducea, M., Saleeby, J., and Jones, C.H., 2004, Active foundering of a continental arc root beneath the southern Sierra Nevada in California: Nature, v. 431, p. 41–46, <https://doi.org/10.1038/nature02847>.

SCIENCE EDITOR: BRAD S. SINGER
ASSOCIATE EDITOR: JOHN JANSEN

MANUSCRIPT RECEIVED 16 AUGUST 2019
REVISED MANUSCRIPT RECEIVED 17 SEPTEMBER 2021
MANUSCRIPT ACCEPTED 22 NOVEMBER 2021

Printed in the USA